Michael Pamminger

Experimental Investigations on an Engine with Extended Expansion

Master Thesis

Master's Degree Mechanical Engineering

Institute for Internal Combustion Engines and Thermodynamics
Graz, University of Technology

Head of Institute:
Univ.-Prof. Dr.techn. Helmut Eichlseder

Supervisor:
Dipl.-Ing. Ortwin Dumböck
Dipl.-Ing. Dr.techn. Eberhard Schutting

Graz, 2014

Affidavit

I declare that I have authored this thesis independently, that I have not used other than the declared sources/resources, and that I have explicitly marked all material which has been quoted either literally or by content from the used sources.

Ich erkläre an Eides statt, dass ich die vorliegende Arbeit selbstständig verfasst, andere als die angegebenen Quellen/Hilfsmittel nicht benutzt, und die den benutzten Quellen wörtlich und inhaltlich entnommenen Stellen als solche kenntlich gemacht habe.

Graz, August 27, 2014

Michael Pamminger

Preface

I have been interested in the mechanics of vehicles and engines since my early childhood and have continued to pursue this passion and refine the skills required with a proactive approach to study. At a young age I was more interested in the operation of these vehicles and motorcycles. In the course of my education not only the operation but more the operating principle was interesting for me. With the help of my lectures at the university and many internship programs, focusing on engine development and automotive engineering, my knowledge in the subject has been increase exponentially.

The present thesis arose at the Institute for *Internal Combustion Engines and Thermodynamics* in Graz, University of Technology. The execution of this scientific work took place in cooperation with a client.

I would like to thank Mister Univ.-Prof. Dipl.-Ing. Dr.techn. Helmut Eichlseder, Head of the institute, for the enabling of this project and the answering of numerous of my questions.

I would like to express the deepest thank to my supervisor, Mister Dipl.-Ing. Ortwin Dumböck, who has answered numerous of my questions concerning not only the operation of internal combustion engines but also general relationships in the field of thermodynamics. Due to the large number of discussions with Mr. Dumböck my comprehension in terms of the operation of engines in theory and practice and also fundamental relationships in thermodynamics grew rapidly. Due to my huge interest in this field I would like to explicitly thank him for his patience and endurance.

My sincere thanks also goes to Mister Dipl.-Ing. Dr.techn. Eberhard Schutting, how has also answered many of my questions and for his technical advices. It is also thanks to him for the excellent organisation and management of this project.

A great thank is dedicated to my parents who has supported me not only during the five years of my study in financial as well as in psychological terms.
A far greater thank is dedicated to my future wife Anita who gave birth to our daughter Melanie at the end of January 2014 and is bringing her up in the most loving way.

Graz, August 27, 2014

Abstract

The reduction of fuel consumption as well as meeting current and future emission standards become a primary requirement. Since the efficiency of the conventional engine can only slightly be increased with current approaches, the time has come to investigate concepts which differs from common once. One approach in order to rise the efficiency of an internal combustion engine is using the residual pressure energy at the end of the conventional expansion by means of an elongated expansion stroke.

Since the expansion stroke is extended compared to a conventional engine, the engine is called extended expansion engine. The content of this thesis includes an investigation of an extended expansion engine on the test bench in order to determine the potential of this concept. The engine operates according to the Otto cycle and is fitted with manifold injection. The engine expands to a volume twice the intake volume ($\gamma = 2$) by using a revised crank train. The cylinder head as well as the valve train was adopted from a reference engine. The reference engine is a 2 cylinder in-line engine, which is also used in mass production with a total cylinder volume of $800\,\mathrm{cm}^3$. A further part of this thesis contains the analysis of the measured data.

Since extended expansion can also be realised by means of shifted valve timing, which is also well known as Miller or Atkinson strategy an engine was fitted with valve timing which ensures a Miller strategy. This concept was also investigated on the test bench. Also the behaviour of an engine with extended expansion and Miller strategy in terms of mechanical supercharging was investigated.

With the aid of these measurements a big part of the simulated potential could be shown. These investigations showed that the difference between a conventional engine (γ=1) and an extended expansion engine with a γ of 2 is about 6 %Points.

Furthermore the potential of the Miller strategy within low load operating points compared to the throttled operation could be demonstrated.

The potential of the Miller strategy as extended expansion could not be shown since the valve train was inappropriate for these investigations.

Tasks and procedure

This section should give an introduction about the procedure and the progress of this project.

The project has been started one and a half years ago before I became a part of it. Fundamental thermodynamic investigations and simulations had been done during this period of time. Also the design and the manufacturing of the engine was performed parallel to the theoretic investigations.

One of the first tasks at the beginning of the Master Thesis was the assistance of the test bench design. The design of the test bench and the measurement equipment are described in chapter 5.

Firstly the test bench was designed for the reference engine which is described in section 4.1. Parallel to the measurement series of the reference engine the technology carrier was assembled. The fundamental operation of the technology carrier is described in section 4.2. After completing the measurement series of the reference engine the test bench was designed for the technology carrier. Afterwards the measurement series of the technology carrier was carried out. The results of the measurements are described in chapter 7.

During the first measurements with the technology carrier a lot of additional work, concerning the data analysis was done. Due to the unconventional volume course it was necessary to develop several additional routines. Some of them are described in section 6.4.

Because of my own interest the theoretical processes was programmed in Matlab. I decided to do this additional work in order to gain a better comprehension of the processes which occur within an internal combustion engine. Furthermore I was particularity interested in a more detailed calculation of the fuel-air cycle. Therefore I divided the compression as well as the expansion in 200 steps. The calculation of the engine processes at different configurations are described in chapter 3.

At the beginning of the measurement series with the technology carrier, problems with oscillations occurred and at the beginning it was not clear by what was it triggered. This forced me to theoretically describe the problem, which is explained in section 5.5. After the treatment of this problem I was very interested in the movement of the additional parts at the extended expansion engine. This further forced me to program a routine in Matlab which was able to show the movement of the additional parts. This is described in section 4.3. Every single part was described by vectors related to the angle of the crank shaft. This was followed by a simplification of all parts by single mass points and the calculation of the free mass moments and

forces. At a further exact determination of the free mass moments and forces it would have been necessary to consider several other effects e.g. the piston force due to the compression and combustion. Since the effort for a more detailed description would have been to great the apparent courses in section 4.3.1 of free mass moments and forces were delivered form the division Design and Construction.

In addition, to author this thesis in English was also a wish of me, in order to improve me linguistic skills.

Contents

List of abbrevations and symbols

Abbrevations

aTDC	after Top Dead Centre
BDC	Bottom Dead Centre
$BMEP$	Brake Mean Effective Pressure
$FMEP$	Friction Mean Effective Pressure
$IMEP$	Indicated Mean Effective Pressure
NEDC	New European Driving Cycle
RDE	Real driving emission
$ROHR$	Rate of heat release
TDC	Top Dead Centre
TT	Technology carrier

Symbols

c_p	$\frac{\mathrm{J}}{\mathrm{gK}}$	Heat capacity (constant pressure)
c_v	$\frac{\mathrm{J}}{\mathrm{gK}}$	Heat capacity (constant volume)
c_{mv}	$\frac{\mathrm{J}}{\mathrm{molK}}$	Heat capacity (constant volume)
c_m	-	Mass fraction of carbon
C	-	Carbon
CO_{ppm}	J	Volume fraction of carbon
ε	-	compression ratio
ε_c	-	compression ratio at compression
ε_{ex}	-	compression ratio at expansion
γ	-	Volume Ratio
h_m	-	Mass fraction of hydrogen
H	-	Hydrogen
κ	-	Isentropic exponent
λ	-	air-to-fuel ratio
$L_{\mathrm{min}}^{\mathrm{mol}}$	-	Minimum amount of air
M	Nm	Torque
M_x	$\frac{\mathrm{g}}{\mathrm{mol}}$	Molar mass of a species
MR	-	Measurement series
MFB_{50}	°CA	Mass fraction burned

o_{m}	-	Mass fraction of oxygen
O	-	Oxygen
Q	J	Heat
R	$\frac{\mathrm{J}}{\mathrm{molK}}$	Gas constant
rpm	$\frac{1}{\mathrm{min}}$	revolutions per minute
U	J	Inner energy
W	J	Work

Indices

1-6	state points
ae	air excess
air	related to air
asp	aspiration
c	compression
C, c	carbon
CO_2	carbon dioxide
cc	combustion chamber volume
cf	conversion factor
comp	related to compression
corr	corrected
cs	total swept volume at compression
cyl	refered to cylinder
e	effective
ex	expansion
ex_m	exhaust gas refered to mol
exg	exhaust gas
exg_d	dry exhaust gas
exg_m	moist exhaust gas
exh	exhausting
fuel	related to fuel
H, h	hydrogen
H_2O	water
HPC	high pressure cycle
i	current step
i+1	next step
ic	indicated incl. compressor
int	intake volume
ind	indicated
LPC	low pressure cycle
N_2	nitrogen
min	required minimum
O, o	oxygen
p	pressure
ppm	parts per million
sc	isentropic compressor efficiency
t	technical
t_c	total compression volume
t_{ex}	total expansion volume
v	volume

1 Introduction

Since the invention of the spark ignition engine in 1876 by Nicolaus Otto the four-stroke process has been enhanced and the efficiency rose steadily over years. At the end of the 19^{th} century engines operated with efficiencies in single figures. Due to crucial improvements of the engineers the indicated efficiency which can be reached nowadays is about 40% and beyond. The reduction of engine fuel consumption as well as meeting current and future emission standards become a primary requirement. Especially CO_2 emissions which will be stricter regulated once every few years have to be reduced. This fact is apparent in figure 1.1.

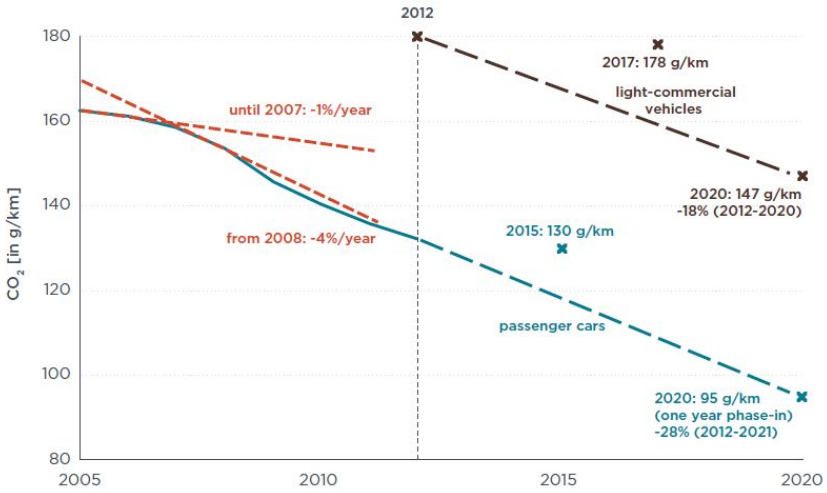

Figure 1.1: Historical development and future targets for CO_2 emission levels of new passenger cars and light-commercial vehicles in the EU. Effects of phase-in, super-credits and eco-innovations not shown here [1]

As CO_2 is a product of complete combustion it is necessary to reduce the fuel consumption. In last decades tremendous development expenses were undertaken in order to raise the efficiency moderately, especially in low load regions of the engine map where it is operated in the New European Driving Cycle (NEDC). Techniques which were introduced in mass production lately are variable valve technology, direct injection, turbo charging and of course downsizing and some other techniques which causes load point shifting like cylinder deactivation and hybridisation.

As mentioned before in order to be within the current and future emission standards the development of more efficient engines constantly continues. Thus, techniques

which are currently investigated, among other topics, are variable compression ratio and energy recovery systems by means of utilisation of the exhaust gas energy. Furthermore, special attention is dedicated to the operation with different fuels. The development has now reached a point where the efficiency can not be increased significantly. A further possibility to decrease the CO_2 emissions is to reduce the vehicle mass. The ongoing flattening course of the curves is in favour of lighter vehicles - apparent in figure 1.2. However a significant mass reduction can not be expected due to the political attitude. Furthermore OEM's have to significantly reduce their average fleet consumption in order to meet the ambitious targets in the future. Since the main target in engine development is to achieve the emission standards, whereby not only CO_2 but also many other fractions in the exhaust gas are strictly regulated, it is necessary to make compromises in order to achieve all targets. However, many of these measures can negatively affect the efficiency.

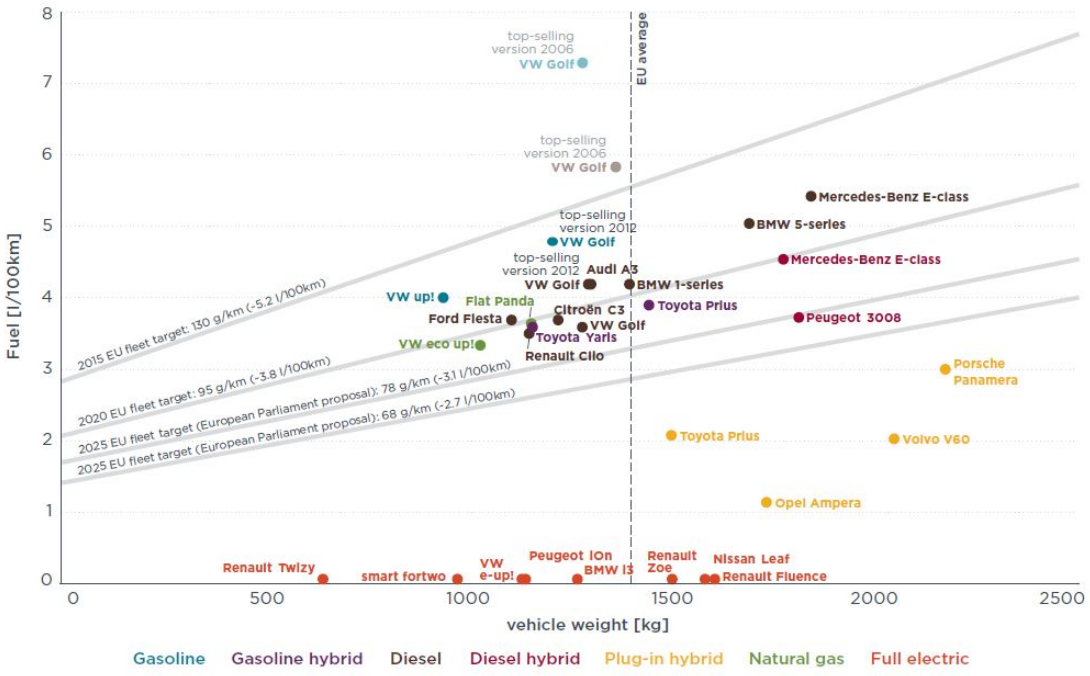

Figure 1.2: CO_2 emissions of selected commercially available passenger car models in the EU in 2013 [1]

Since EURO 6, which regulates the current emission output for light duty vehicles in the EU has been introduced in 2014 not only CO_2 emissions but also particles and NO_x emissions have been again significantly reduced. However, the today's emission output is determined by the NEDC which covers only the low load and low speed regions of the engine map. Another topic which should be considered in order to be within future emission standards are the driving cycles which will be introduced in

the near future. They measure the emission output not only in the low load and low speed regions as up to now but also at higher load points and probably full load. These driving cycles are called Real driving emission (RDE). As a consequence it is necessary to operate the engine most of the time near the most efficient operating point. Hence, widen up the area with the highest efficiency will help to reduce the emission output. Therefore engines have to be optimised towards the most efficient area within the engine map, despite the compliance of all emission limit values.

This reasons have been the motivation for the investigation of an unconventional engine concept in order to make this ambitious target come true. The aim in near future will be to reduce the average fleet consumption until 90 g/km by 2020. However, this equates an average fuel consumption of approximately 3.8 litre of petrol as it is apparent in figure 1.2. A CO_2 emission standard of about 78 g/km or even 68 g/km in 2025 are discussed currently, also visual in figure 1.2.

The operation of an average passenger car with a fuel consumption of 3.1 litre, as it would be with an average fleet consumption of 78 g/km, is only possible with extreme downsized engines or in combination with hybridisation in order to ensure high load points and high efficiency of the engine. Another scenario would be the operation with different kinds of fuel, which could be a medium-term solution.

Since one borderline condition of our client was the operation with petrol, the rise in efficiency due to an elongated expansion stroke has proved as the most appropriate approach after time-consuming fundamental investigations.

2 Extended Expansion

In case of a conventional internal combustion engine the blow down process is initiated with the exhaust valve opening. The pressure within the cylinder at the beginning of the exhaust valve opening is higher than the pressure in the exhaust system and due to this fact useful energy escapes unused through the exhaust system and dissipates. When an exhaust gas supercharger is applied a part of the exhaust gas enthalpy is used for the pre-compression of the charge mass. Moreover the exergy within the exhaust gas could be converted into mechanical or electrical energy through other technical processes, like a steam engine or a thermoelectric element. If the overall efficiency by means of recuperation is considered, it is more efficient to convert the fuel into mechanical energy by an additional expansion. It is obvious that this unused energy could be converted for the most part into mechanical power within the cylinder if the power stroke is elongated and is therefore longer than the intake stroke.

Extended expansion can be basically realised by two different types. Firstly, through changed valve timing which offers the possibility to implement the approach on a conventional engine or secondly by a revised crank train. Both of these concepts have advantages and disadvantages. The main aim of this thesis is the comparison of this two concepts and a fundamental investigation of the extended expansion engine.

2.1 Principles

Figure 2.1 shows the process in the pressure-volume diagram. Firstly the process starts with the compression of the charge mass, which takes place from point 1 to 2. Secondly the isochoric combustion occurs until point 3 is reached. In a conventional combustion engine the expansion proceeds until 4, since the intake volume as well as the expansion volume are equal. A conventional internal combustion engine provides the work which is equal to the enclosed area 1-2-3-4-1 (see figure 2.1). Since the cylinder volume V_{cyl} is equal to each cycle it is not possible to use the residual pressure-energy in point 4 which is higher than the pressure in the exhaust system. Due to this fact a big part of exergy leaves the engine through the exhaust system.

Because of the elongated expansion stroke the expansion can continue beyond 4 up to 4'. At the same total added fuel energy the indicated work and also the efficiency can be increased since the enclosed area (1-2-3-4-4'-5-1) compared to a conventional engine is enlarged. The additional indicated work compared to a conventional engine which would be the benefit of this concept can be seen as the grey area in figure

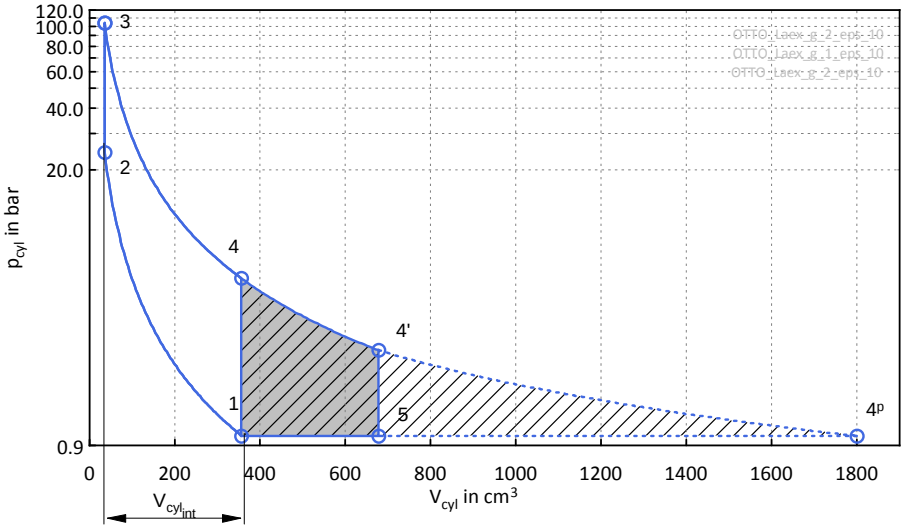

Figure 2.1: pV-diagram of a conventional and extended expansion engine

2.1. The expansion until ambient pressure, respectively the pressure in the exhaust system offers the maximum work which could be done on the piston. In figure 2.1 the maximum possible additional work of the concept can be seen by the hatched area. The enclosed are 1-2-3-4-4'-4^p-1 would deliver the highest possible work and efficiency of an extended expansion engine.

The entire indicated work which is done on the piston can be calculated by equation 2.1.

$$W_{\text{ind}} = \oint_{CA=0}^{CA=720} p_{\text{cyl}} \mathrm{d}V_{\text{cyl}} \tag{2.1}$$

In equation 2.1, p_{cyl} defines the pressure within the cylinder which is crank-angle-dependent. $\mathrm{d}V_{\text{cyl}}$ defines the differential change in volume between two infinite decimal points. By using the following quantity Volume Ratio (γ) an extended expansion engine can be described.

$$\gamma = \frac{V_{\text{t}_{\text{ex}}}}{V_{\text{t}_{\text{c}}}} = \frac{\frac{V_{\text{cc}}+V_{cs}}{V_{\text{cc}}}}{\frac{V_{\text{cc}}+V_{exs}}{V_{\text{cc}}}} = \frac{\varepsilon_{\text{ex}}}{\varepsilon_{\text{c}}} \tag{2.2}$$

In equation 2.2 $\mathrm{V_{t_c}}$ defines the total cylinder volume at Bottom Dead Centre (BDC) after the intake stroke and $\mathrm{V_{t_{ex}}}$ defines the total cylinder volume at BDC after the expansion stroke. The equation can be extended by $\mathrm{V_{cc}}$ which describes the combustion

chamber volume and makes it furthermore possible to describe γ by the compression ratios.

A quantity of particular interest, related to internal combustion engines is the work done on the piston divided by the displacement, which is called Indicated Mean Effective Pressure ($IMEP$). This quantity has the dimension of pressure and would yield the same work on an engine with a constant pressure difference between compression and expansion stroke. This means an engine with an $IMEP$ of 10 bar is equal to an engine with a constant pressure of 1 bar during compression and 11 bar during expansion. The justification of the $IMEP$ is the comparability of different engine types. Due to the unconventional concept some discrepancies of definition appear. Due to two different cylinder volumes at BDC within one engine cycle a clear definition in order to determine the $IMEP$ is difficult.

The power output of an engine is mostly influenced by the charge mass, point of ignition and air-to-fuel ratio (λ). At conventional engines the determining factor for the charge mass is of course the intake volume. For the same reason the intake volume was chosen as basis for the following definitions. From the foregoing definitions the $IMEP$ is defined as:

$$IMEP_{\mathrm{c}} = \frac{W_{\mathrm{ind}}}{V_{\mathrm{int}}} \tag{2.3}$$

A further quantity of particular interest is the Brake Mean Effective Pressure ($BMEP$). This quantity defines the torque output of an engine divided by the displacement.

$$BMEP_{\mathrm{c}} = \frac{W_{\mathrm{e}}}{V_{\mathrm{int}}} = \frac{M \cdot 4\pi}{V_{\mathrm{int}}} \tag{2.4}$$

2.2 Extended expansion through valve timing - Miller- and Atkinson-Cycle

In mass production Miller and Atkinson-Cycle have been proposed in order to reduce NO_x emissions while maintaining a high engine efficiency [2]. Miller-Cycle and Atkinson-Cycle are also used to decrease gas exchange losses during part load.

Most of the gasoline engines operate quantity controlled by generating a pressure gradient between the ambient pressure and the pressure within the cylinder during the intake. The charge mass is reduced within the cylinder due to the decreasing density. As the most gasoline engines operate stoichiometric the load is mostly determined by the charge mass and the point of ignition, whereas the variation of the point of ignition allows only a little variation of load points. Therefore the charge mass must be reduced in order to ensure an operation in low load ranges.

If one of the processes as mentioned before is used, the load control can be put into action through an earlier (Miller-Cycle) or later (Atkinson-Cycle) inlet valve closure. Since the valves do not close at BDC the charge mass but also the effective compression ratio depend on the current piston position, respectively the current cylinder volume at intake valve closing. This approach is used to de-throttle during part-load [3], which goes along with reduced fuel consumption due to the wide open throttle. With both the processes it is able to make the expansion stroke shorter, compared to the effective compression stroke by suitable shifting of the inlet valve timing. [4] Basically, both of the strategies are extended expansion. The overall efficiency does not rise during part load since the increasing γ is overcompensated due to the decreasing effective compression ratio at compression (ε_c).

2.2.1 Miller strategy

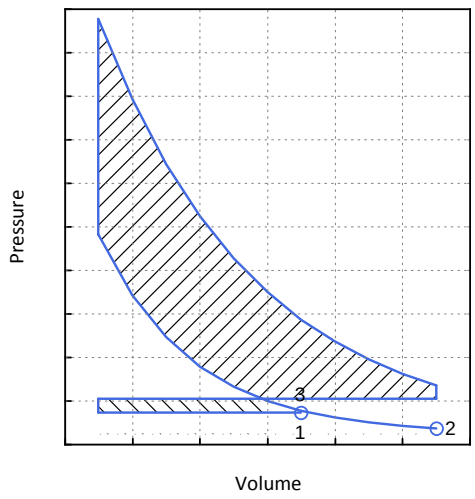

(a) pV-diagram of a Miller strategy

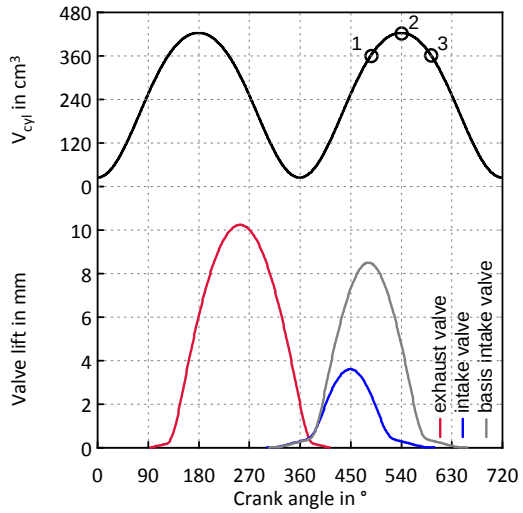

(b) Valve timing at Miller strategy

Figure 2.2: pV-diagram and valve timing at Miller strategy

The Miller strategy was originally purposed with the main objective to increase the power density of engines without exceeding their mechanical and thermal limits at supercharged engines. For the last decades the Miller strategy was mainly used within supercharged engines, in order to reduce the temperature at the beginning of the compression which go along with reduced peak temperatures at a constant power output. Moreover reduced peak temperatures go along with reduced NO_x emissions. In case of gas engines the indicated efficiency which are achieved nowadays are slightly under 50%. This high efficiencies are able, among other things due to the Miller strategy which allows a less tendency for knocking. [4]

As mentioned before, Miller-Cycle is called a strategy in which the intake valve closes before the piston reaches BDC. An exemplary valve lift curve is apparent in figure 2.2b. Due to the early inlet valve closure, which is apparent as point 1 in figure 2.2a the gas expands at the subsequent expansion and cooled off until the piston reaches point 2, respectively BDC. Afterwards, the charge mass is compressed and in the idealised process the intake conditions are reached at the same cylinder volume where the intake valve has closed before. This fact is shown in figure 2.2a since point 1 and 3 are equal. Beyond this point, the actual compression begins. During the power stroke the overall geometric cylinder volume is used for expansion.

By shifting the intake valve closure to earlier piston positions, the charge mass and also the effective compression ratio decrease. Using the advantage of the Miller-/Atkinson strategy but also making a full load operation possible, the charge mass has to be increased e.g. by supercharger. However, a higher charging pressure goes along with a higher intake temperature. Due to that Miller and Atkinson strategy can only bring a decrease of intake temperature, at supercharged engines, when a charge air cooler is applied. [5]

2.2.2 Atkinson strategy

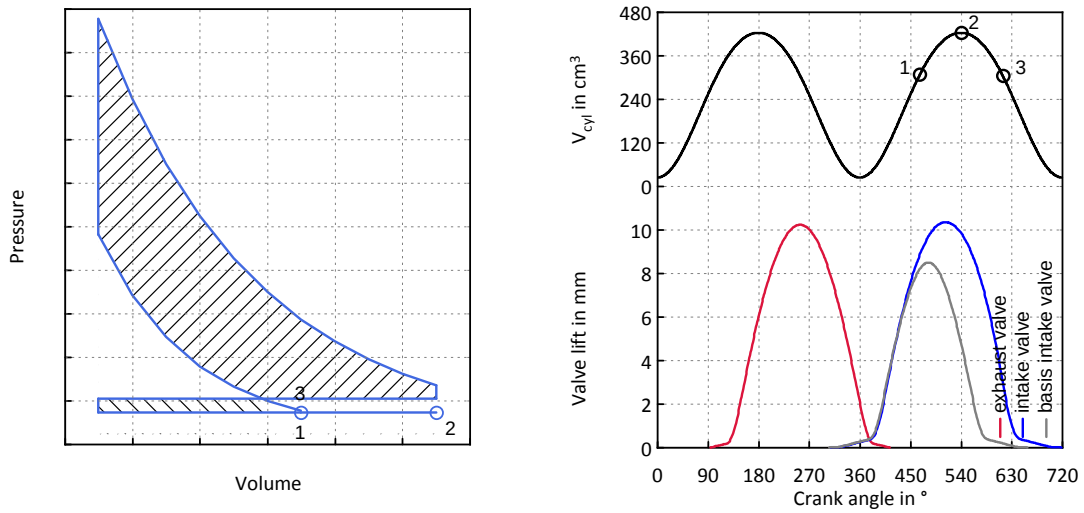

(a) pV-diagram of an Atkinson strategy

(b) Valve timing at Atkinson strategy

Figure 2.3: pV-diagram and valve timing at Atkinson strategy

With the Atkinson strategy the cylinder is filled with charge mass until the piston reaches BDC. Afterwards the charge mass is expelled back into the intake port and the inlet valve close at point 3 during the piston moves upwards. However, if the charge mass which is enclosed within the cylinder at BDC is burned stoichiometric,

the load point rises to full load. Therefore a part of the charge mass has to be expelled back into the intake system, in order to ensure a lower load point.

Whether the Miller strategy or the Atkinson strategy is applied on a real engine depends on the boundary conditions.

For example, at the Miller strategy the flow losses are higher compared to the Atkinson strategy due to the little valve port, which further reduce the amount of charge mass. This effect rises further at rising speeds.

At the Atkinson strategy the flow losses which occur during the intake and the expelling phase and in addition the warm cylinder walls heat up the charge mass which is expelled back into the inlet port. The pre-heated gas which flows into the cylinder during the cycle rises the likelihood for knocking, and as a result limits the possible compression ratio.

2.2.3 Advantages and Disadvantages of Miller -/Atkinson strategy

Using these techniques contains disadvantages, for instance the reduced volumetric efficiency due to the flow losses during the finite valve closing period. The inlet valve closes at positions with high piston speeds which rises the flow losses during the finite valve closure.

The load control at the Miller strategy is determined by the earlier inlet valve closure and therefore lower charge mass.

In figure 2.4 is assumed that the load control which is carried out through an earlier intake closure can also be put into action through a smaller cylinder volume while the throttle flap is wide open. In the idealised process it does not influence the efficiency.

In figure 2.4 the fact which was mentioned before can be seen. Because of the reduced intake volume at the same expansion volume the γ increases. However the compression ratio ε_c decreases with decreasing load and as a result both effects theoretically offset each other at higher loads. In low load regions the decreasing compression ratio has a greater influence on the efficiency and therefore the efficiency decreases.

In order to exploit the maximum potential of the Miller-/Atkinson strategy, the geometric compression ratio has to be increased at higher Miller-/Atkinson levels, respectively earlier intake valve closure and therefore lower load point.

At the real cycle the charge mass absorbs heat from the cylinder walls during the expansion phase which is between inlet valve closing and BDC. Due to the heat flow the charge mass features a higher temperature at the cylinder volume where the inlet valve has closed before. This means that point 3 in figure 2.2a as well as in 2.3a is above point 1. This fact rises also the combustion peak temperature and the likelihood for knocking. The mechanical issue limits the Miller strategy because the valve opening time decreases with rising γ. In order to minimise the flow losses the

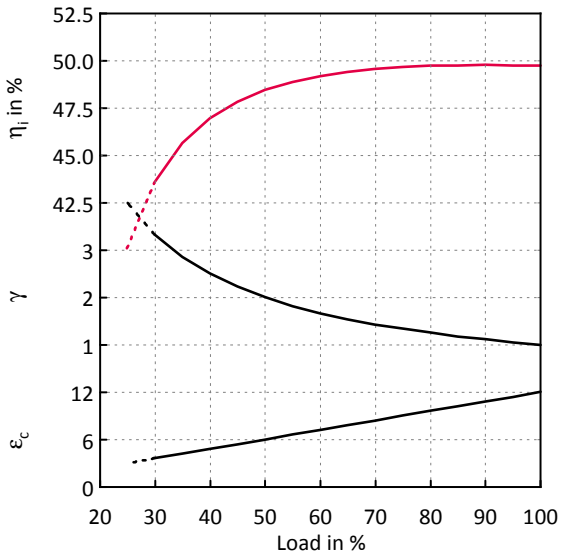

Figure 2.4: Influence of Miller on engine efficiency by equal compression volume

valve flanks have to be steep to ensure a rapid valve opening and closing. However, the mechanical limitations for valve acceleration can be exceeded in high speed engines. In summary can be said that the limiting size for the Miller strategy are the valve accelerations, respectively the valve train forces and surface pressure at high γ.

2.3 Extended expansion by means of a revised crank train

One approach in order to ensure an elongated expansion stroke compared to the intake stroke is to overlap the oscillation of the conventional crank journal with an oscillation with half the frequency. This could be ensured by using a second shaft which influences the movement of the piston. Figure 2.5 shows an example which could be applied on a four stroke engine.

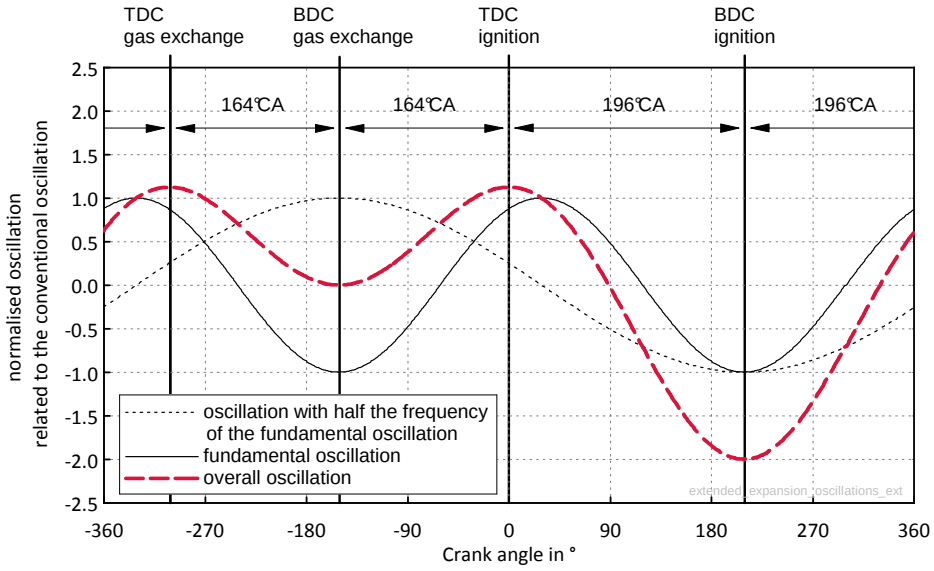

Figure 2.5: Superposed oscillations

The continuous black line is the fundamental oscillation, the black doted line represents the oscillation with half the frequency of the fundamental oscillation and an angular phase shift of $\pi/4$. The red dashed line shows the summation of both oscillations. With this measure the position of Top Dead Centre (TDC) for the piston is in identical position during TDC at gas exchange as well as during TDC at ignition.

Within the division Design and Construction at the *Institute for Internal Combustion Engines and Thermodynamics* in Graz, University of Technology a concept was designed which is similar to the approach as mentioned before. This design was patented in 1985 by Carl Nelson and can be seen in figure 2.6.

On the eccentric *Crank shaft* journal is an additional component rotary mounted which is called *Triangle*. The *Triangle* consists out of a upper part and and lower part which are held together by bolts. The upper part of the triangle has two extensions. The left extension is connected with the *Connecting rod* which furthermore connects

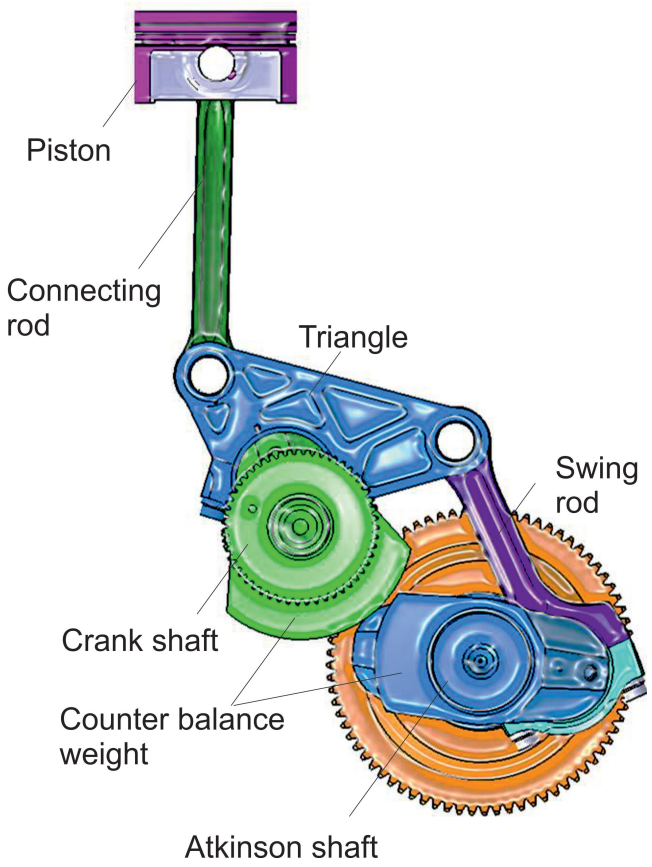

Figure 2.6: According to the patent of Carl Nelson [6]

the *Piston*. The right extension is connected with the *Swing rod*. A second shaft which is called *Atkinson shaft* is also rotary mounted within the crankcase and is spaced from the *Crank shaft* but parallel therewith. The *Atkinson shaft* and the *Crank shaft* are connected by intermeshing gears for mutual rotation. The gear which is mounted on the *Atkinson shaft* has the double number of teeth, which goes along with half the speed compared to the *Crank shaft*. On an eccentric journal at the *Atkinson shaft* is a *Swing rod* mounted which regulates the movement of the *Triangle*. The movement of the *Piston* is determined by the interrelationship of the *Atkinson shaft*, *Swing rod*, *Triangle*, *Crank shaft* and the *Connecting rod*. [6]

Due to this design it is able to elongate the power and exhaust stroke compared to the intake and compression stroke.

The illustrations in 2.7 and 2.8 shows the sequences of an engine with extended expansion. Figure 2.7a displays the piston at TDC which corresponds to 0 °CA in

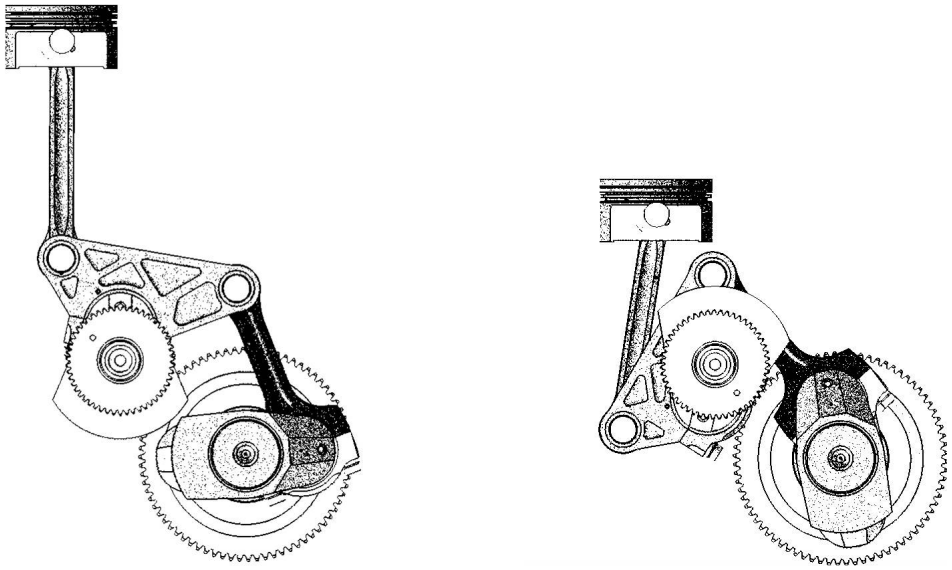

(a) **TDC ignition, 0**°CA (b) **BDC ignition, 196**°CA

Figure 2.7: Crank train mechanism I

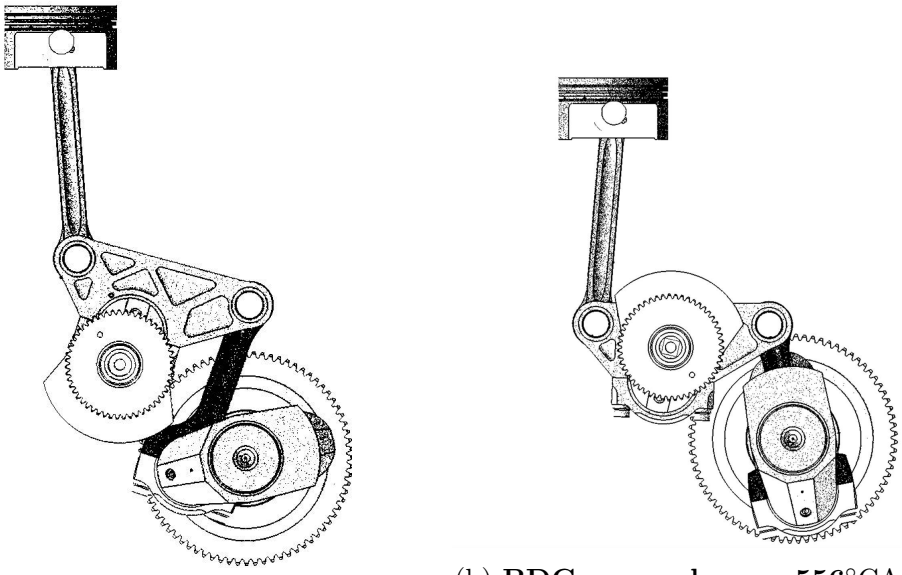

(a) **TDC gas exchange, 392**°CA (b) **BDC gas exchange, 556**°CA

Figure 2.8: Crank train mechanism II

figure 2.5. After the combustion the *Piston* reaches BDC. The *Crank shaft* has rotated 196 °CA, the *Atkinson shaft* half the angle, which corresponds to an angle of 98 degree due to the gear ratio.

Figure 2.8a displays the *Piston* at TDC after the *Crank shaft* has rotated 392 °CA. The Atkinson shaft has rotated 196 °CA and the *Piston* is in the equal position like in figure 2.7a.

Figure 2.8b shows the *Piston* in BDC after the intake stroke at 556 °CA.

2.3.1 Executed projects and other ideas for the realisation of extended expansion

2.3.1.1 Extended expansion through revised crank train

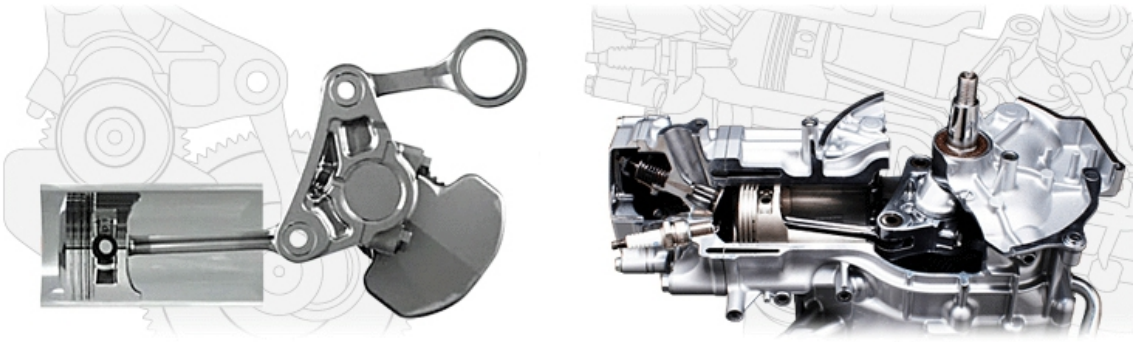

Figure 2.9: Honda Exlink; Adopted from [7]

The only available engine on the market which operates with an elongated power stroke is a combined heat and power plant of Honda and is designed for private households; the design is similar to the concept which was mentioned before. The engine operates according to the Otto cycle and has an intake volume of 110 cm^3, the ε_c is specified with 12.2. The expansion volume is about 163 cm^3 and the compression ratio at expansion (ε_{ex}) is specified with 17.6. ε_{ex} and ε_c together result in a γ of 1.44. The electrical nominal power of 1 kW is reached at 1950 rpm. [8] The engine is operated with CH_4 which allows higher compression ratios due to the less tendency for knocking. Honda also states that the higher friction is compensated due to the less piston forces because of the little deflection of the connecting rod.[7] Nowhere the indicated efficiency is mentioned - only the rise in electrical efficiency from 22.5 % to 26.3 % compared to a conventional engine.

2.3.1.2 Extended expansion through gear set

An another approach to realise an extended expansion can be seen in figure 2.10. On the eccentric journal of the crank shaft is a rotatable extender mounted which turns

with half the speed compared to the crank shaft. The extender rotates due to the annulus gear. This concept also ensures equal positions at TDC. At this design the annulus gear is the determining part for the size of this concept. The determining factor for higher values of γ is the eccentricity from the central axis of the crank shaft to the central axis to the crank shaft journal - apparent by e. As a consequence the friction radius increases and produces additional mechanical losses.

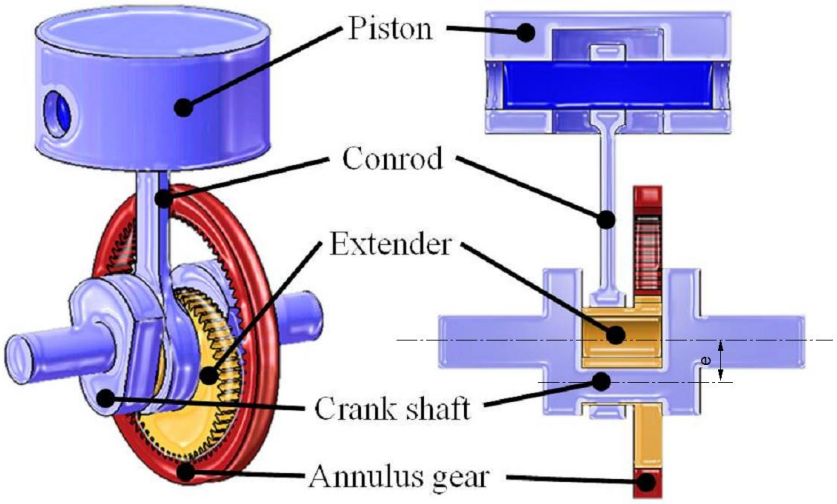

Figure 2.10: Extended expansion with a planetary gear [9]

In 1918 Walter M. Austin patented a mechanism which is similar to the one above. It comprises an additional mechanism on the crank shaft. Due to this planetary gear set an elongated power stroke compared to the intake stroke can be ensured.

A big disadvantage of this concept are the possible values of γ. The determining factor for the γ is the diameter of the connecting rod eye, apparent by 5. Since the cross-sectional area of the planetary gear (6) determines the maximum of load little values of γ are only possible at large-displacement engines.

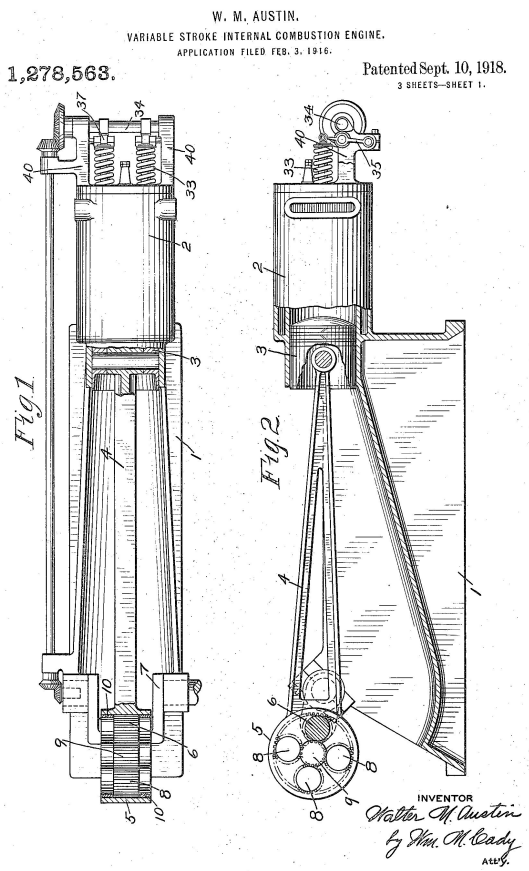

Figure 2.11: Extended expansion with a planetary gear [10]

2.4 Extended expansion by means of an expansion cylinder

The idea behind this concept is also using the residual energy within the exhaust gas. In cylinder 2 and 3 the common process of a four stroke engine, which is shown in figure 2.12 takes place. After the power stroke the combustion gases are not removed through the exhaust system; the expanded gas is pushed over through the decanting channel into the expansion cylinder (1). Within the expansion cylinder (1) which has about twice the volume of each of the fired cylinders the combustion gases run through an additional expansion. The expansion cylinder (1) works in a two stroke mode.

Afterwards the two-times expanded exhaust gas is removed through the exhaust port (19). This concept was patented in 1999 by Gerhard Schmitz [11]. The company which

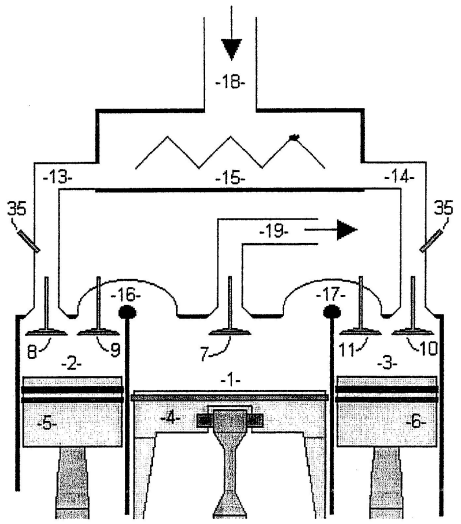

Figure 2.12: 5 stroke engine [11]

came first up with this concept was Ilmor Engineering Limited. Since 2007 the engine has been used within motor sport applications. It is a three cylinder in-line engine with a displacement of 1.478 cm^3. The power is about 130 bhp at 7000 rpm and a maximal torque of 166 Nm at 5000 rpm. The specific fuel consumption is stated with 226 g/kWh.[12] [13]

Due to the fact that Ilmor has not published detailed test results and findings the following section is dedicated to the investigation of AUDI's additional expansion cylinder which was published recently [14]. AUDI pursues the same idea but a different configuration. This investigation was conducted on a 4 cylinder in-line engine where both the outer cylinders 1 and 4 are the fired once and both the inner cylinders 2 and 3 are the expansion cylinders. In figure 2.13 the used concept of AUDI is shown. The blue channels are the intake channels for the fired cylinders. After the power stroke in the fired cylinders the gas is transported to the inner cylinder through the red channels. In cylinder 2 and 3 the gas is expanded again and afterwards the gas is expelled through the yellow channel to the atmosphere.

A crucial criterion to reach high efficiency at this concept are the heat and flow losses which occur during the transport from the fired cylinder into the expansion cylinder. Furthermore at the exhaust valve opening of the fired cylinders the gas is expanded without any work done on the piston due to the additional volume of the decanting channels. This means that the detrimental space within the expansion cylinder together with the volume within the decanting channel has to be minimised, in order to ensure high efficiency compared to conventional concepts. By reducing the volume of the decanting channels the heat and flow losses rise. The simulation of

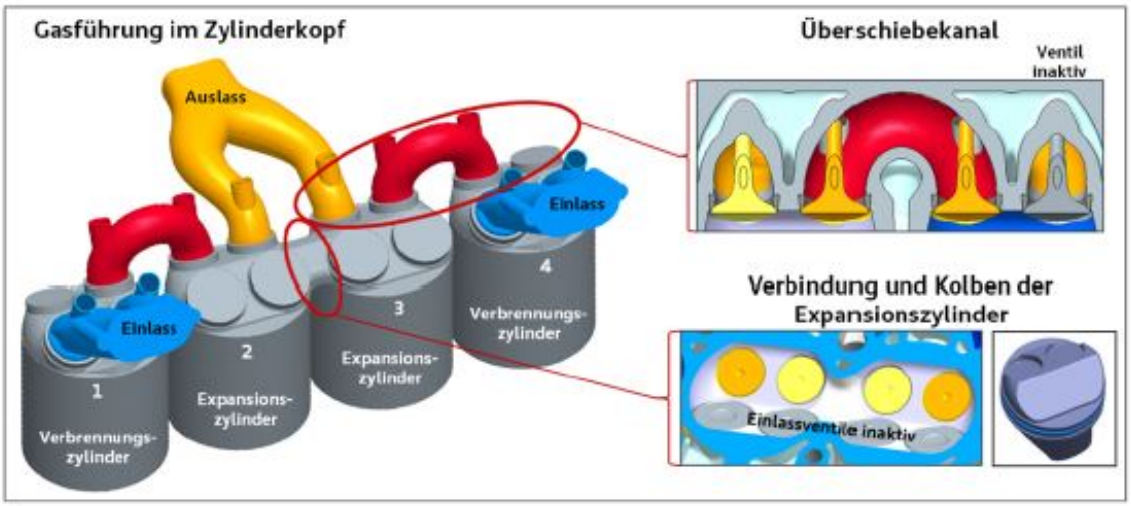

Figure 2.13: Extended expansion concept of AUDI [14]

AUDI showed that the theoretical rise of indicated efficiency amounts 18 % compared to a conventional concept. AUDI published that only 2.5 % of the theoretical 18 % can be achieved at the real engine due to the heat and flow losses as mentioned before. AUDI also states that this concept applied on stationary engines could enhance the efficiency by 8.4 % compared to conventional engines.

2.5 Using the residual exhaust gas energy by means of a power turbine

A further possibility using the residual gas energy is to use a power turbine within the exhaust gas system. The additional energy which is provided by the turbine can be directly used due to a mechanical connection with the crank shaft. A so-called "turbo-compound" system is apparent in figure 2.14.

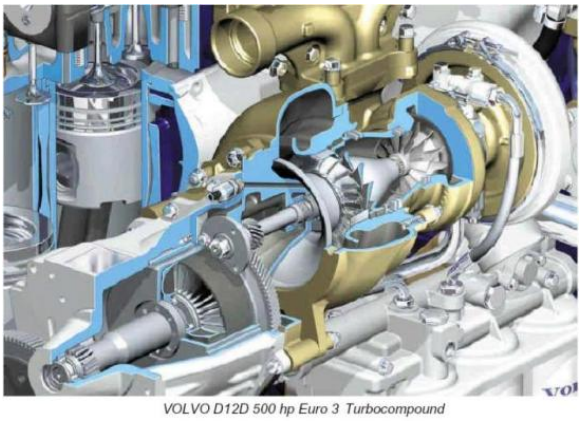

Figure 2.14: Turbo compound concept of Volvo [15]

Another possibility to convert the exhaust gas enthalpy into usable energy is an additional generator on the turbine which converts the exhaust gas energy into electrical energy.

3 Idealised process - fuel-air cycle

The operation cycle of an internal combustion engine is very complex. In a simplified method the processes which occur within the engine can be broken down into a sequence of separate processes: intake, compression, expansion and exhaust. [16] This approach can provide a fundamental insight of the processes within an engine. The processes proceed differently to the real engine but within the idealised process the maximum theoretical potential of a concept can be shown. This approach uses a couple of assumptions which are listed below. (according to DIN 1940)

- charge without residual gas
- without any flow losses
- without any pumping work
- without any blow-by gas
- the same air-to-fuel ratio as the real engine
- isentropic compression and expansion
- complete combustion
- combustion occurs at constant volume
- consideration of gas properties and composition

In the idealised process is assumed that atmospheric air is aspirated and compressed. This assumption differs to the real cycle of the used engines due to the fact that the engines are fitted with manifold injection. As the determination of the composition of the charge mass during the compression is a formidable task it is assumed that atmospheric air is aspirated and compressed.

The following section contains the calculation which was executed in *Matlab*. In order to determine the gas properties during the compression the properties, respectively the isentropic exponent and heat capacities were constantly calculated at little steps of volume and pressure. The gas properties were calculated at every step according to the equations of *NIST*. Compression and expansion are divided in several steps and the calculated efficiency depends on the step size. The efficiencies within this thesis are calculated by the division in 200 steps.

It is assumed that the compression as well as the expansion occur isentropic. Equation 3.1 describes the temperature change during compression. By using the ideal gas equation 6.5 other physical quantities, e.g. pressure can be calculated.

$$T_{\mathrm{i}+1} = T_{\mathrm{i}} \cdot \left(\frac{v_{\mathrm{i}}}{v_{\mathrm{i}+1}} \right)^{\kappa - 1} \tag{3.1}$$

A further assumption is that the combustion, which runs completely, is an isochoric process and takes place at TDC. While the piston is in TDC the amount of air is replaced by the combustion products according to the chemical equation 3.2. The left side of the equation 3.2 represents the chemical fraction of fuel and the required amount of air which is necessary for the stoichiometric combustion. The right side of equation 3.2 represents the combustion products at a complete combustion.

$$C_x H_y O_z + O_2 \cdot \left(x + \frac{y}{4} - \frac{z}{2} \right) = x \cdot CO_2 + \frac{y}{2} \cdot H_2O \tag{3.2}$$

The combustion temperature is calculated according to the first law of thermodynamics. The conversion from chemical energy is replaced by an added heat across the system boundaries. Wall heat losses are neglected.

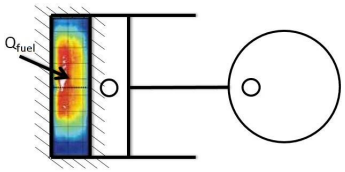

Figure 3.1: Added fuel heat at TDC

Since the process occurs isochoric the first law of thermodynamics can be written as follows:

$$dQ_{\mathrm{fuel}} = dU \tag{3.3}$$

After consideration of all species before and after the combustion, the equation can be transformed in order to calculate the combustion temperature T_3.

$$\begin{aligned} n_{\mathrm{fuel}} \cdot M_{\mathrm{fuel}} \cdot H_{\mathrm{fuel}} = \\ n_{\mathrm{exg}} \cdot \mathrm{c}_{mv_{\mathrm{exg}}} \cdot (T_3 - T_0) - n_{\mathrm{air}} \cdot \mathrm{c}_{mv_{\mathrm{air}}} \cdot (T_2 - T_0) - n_{\mathrm{fuel}} \cdot c_{\mathrm{fuel}} \cdot M_{\mathrm{fuel}} \cdot (T_{\mathrm{fuel}} - T_0) \end{aligned}$$

$$T_3 = T_0 + \frac{n_{\mathrm{fuel}} \cdot M_{\mathrm{fuel}} \cdot H_{\mathrm{fuel}} + n_{\mathrm{air}} \cdot \mathrm{c}_{mv_{\mathrm{air}}} \cdot (T_2 - T_0) + n_{\mathrm{fuel}} \cdot c_{\mathrm{fuel}} \cdot M_{\mathrm{fuel}} \cdot (T_{\mathrm{fuel}} - T_0)}{n_{\mathrm{exg}} \cdot \mathrm{c}_{mv_{\mathrm{exg}}}} \tag{3.4}$$

The overall efficiency is calculated with the aid of the energy which is necessary for the aspiration, compression and expelling of the charge mass and the energy which is provided during the expansion stroke. All these processes related to the added fuel heat equates the efficiency.

$$\eta_{\mathrm{i}} = -\frac{w_{\mathrm{ex}} + w_{\mathrm{comp}} + w_{\mathrm{asp}} + w_{\mathrm{exh}}}{n_{\mathrm{fuel}} \cdot M_{\mathrm{fuel}} \cdot H_{\mathrm{u}}} \tag{3.5}$$

3.1 Naturally aspirated engine

The process in an internal combustion engine starts with the isentropic compression of the charge mass from 1 to 2 - apparent in figure 3.2a. The conditions in point 1 represent the intake conditions. After the compression the process continues with the isochoric combustion until point 3 is reached. Afterwards the isochoric expansion occurs until point 4. The gas exchange is replaced by a heat removal from 4 up to 1 which occurs isochoric. At extended expansion engines the expansion takes place beyond 4 to 4'. The conditions within the cylinder at the end of the expansion, apparent by 4', depend on γ (see figure 3.2b).

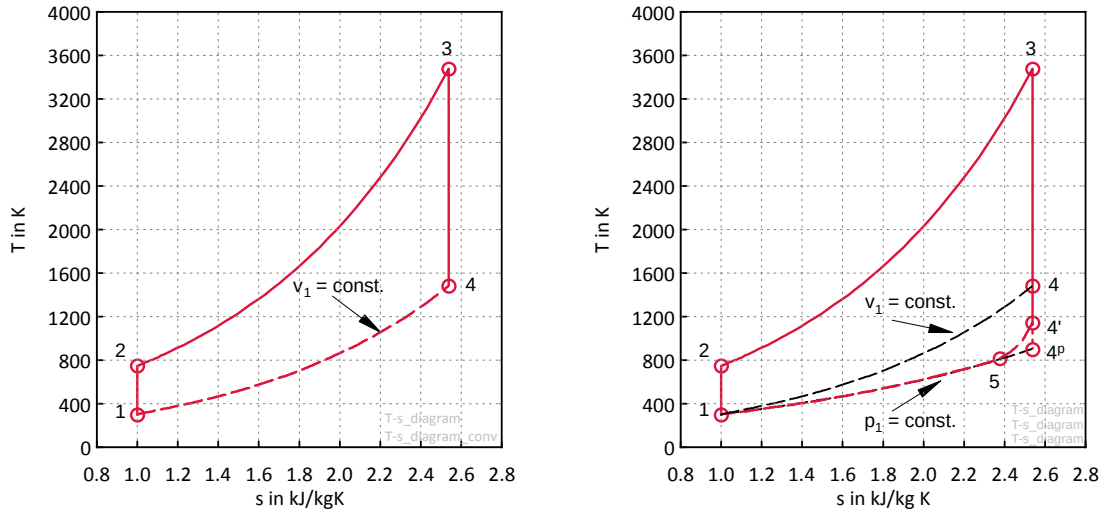

(a) Ts-diagram of a conventional engine

(b) Ts-diagram of an ext. exp. engine

Figure 3.2: Ts-diagram of conventional engine and an engine with extended expansion

The process from the end of the expansion until 1 is not isochoric as at conventional engines. At the beginning the process is isochoric from 4' to 5 until the intake pressure is reached (4^{p}), as it is apparent in figure 3.2b. Afterwards the process occurs isobar until the initial conditions are reached.

In borderline case the expansion occurs until the intake pressure is reached.

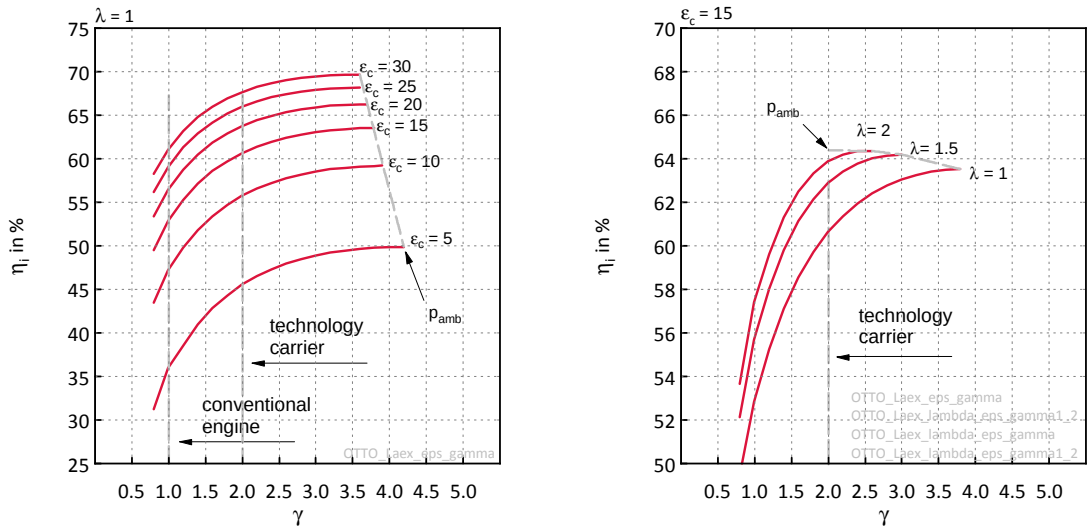

(a) Efficiency vs. gamma and ε_c

(b) Efficiency vs. gamma and λ

Figure 3.3: Different influences on the efficiency at varying γ

A conventional engine would reach an indicated efficiency of 47.2 % at a compression ratio (ε) of 10 and stoichiometric operation. In the idealised process the extended expansion features an efficiency of 55.8 % at an ε_c of 10 and a γ of 2 and also stoichiometric operation. This results in a difference of 8.6 %Points [1] efficiency compared to a conventional engine.

The maximum efficiency which can be reached in the idealised process by changing values of γ and ε_c can be seen in figure 3.3a. At first the efficiency increases steeply, especially at low values of ε_c, after that the efficiency flattens out until the maximum is reached. At this calculation an exhaust back pressure of 1 bar is assumed. It is also clearly apparent that the potential of the extended expansion decreases with rising ε_c. This means that the increase of efficiency due to extended expansion at e.g. diesel engines remains less.

In order to ensure part load at quality controlled engines the fraction of air is increased at the combustion. As it is apparent in figure 3.3b, the point with the maximum of efficiency is reached at lower values of γ. An expansion beyond this point would cause a pressure at the end of the expansion which is lower than the ambient pressure (p_{amb}), respectively the exhaust back pressure. This approach would decrease the efficiency.

This issue is apparent in figure 3.4a. The process until 3 is equal to 3.2b but the expansion takes place until 4' where the pressure is under ambient pressure, respectively under the pressure in the exhaust gas system.

[1] %Points defines the absolute difference, e.g the difference between an η_i of 40 and 44 are 10 % and 4 %Points, %Points is further abbreviated by %PT

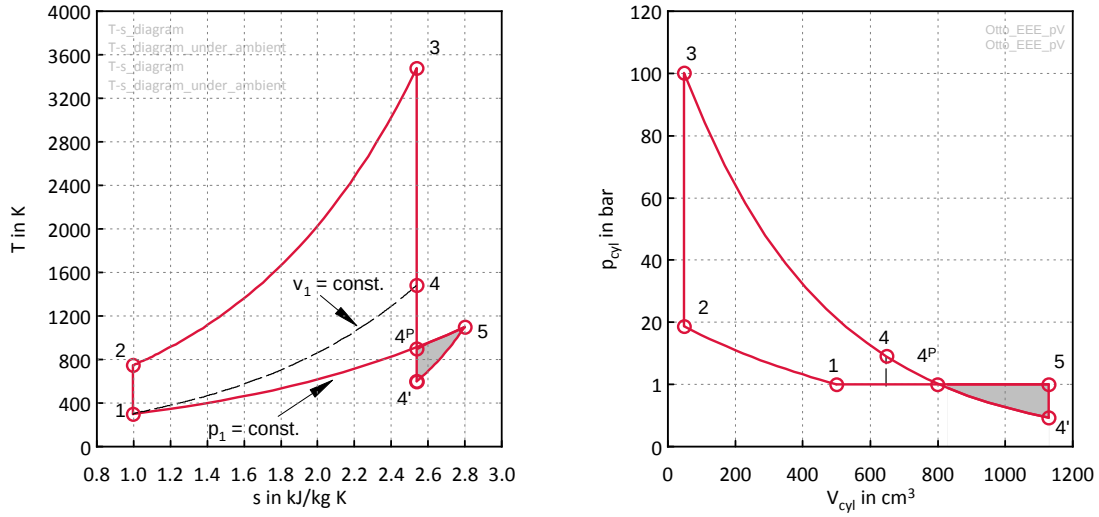

(a) Ts-diagram of an expansion below ambient pressure

(b) pV-diagram of an expansion below ambient pressure

Figure 3.4: Expansion below ambient pressure

When the exhaust valve opens and the current pressure in the cylinder is lower than the pressure in the exhaust system (visual by 4') a particular amount of exhaust gas flows back into the cylinder due to the pressure difference.

This issue can appear, depending on the γ in lower load regions and causes a decrease in efficiency.

In figure 3.4a as well as in figure 3.4b is apparent that the delivered work through the expansion beyond 4' is lower than the work for the expelling of the gas and therefore the efficiency decreases.

The rising γ at decreasing load can easily and clearly be explained by a non throttled engine which is able to realise a variable intake stroke.

Rather than a throttle flap at the conventional engine the charge mass can be reduced by means of a shorter intake stroke at full load. The effective γ rises at low load compared to the γ at full load. It is obvious that the pressure at the end of the expansion can easily drop under the pressure in the exhaust gas system.

In order to avoid this problem the engine could be fitted with a variable valve timing. By using this measure the effective γ can be influenced due to the exhaust valve opening. In case of figure 3.4 the exhaust valve could open in 4^{p} in order to avoid the expansion under exhaust back pressure. The process would occur from 4^{p} to 5 and back to 4^{p} without any losses.

The second possibility would be to keep the exhaust valve closed. The process would continue beyond 4^{p} up to $4'$ and afterwards back to 4^{p}. In theory both processes would not produce any losses.

3.2 Supercharged engine

3.2.1 Supercharging by means of mechanical supercharger

Supercharging is an appropriate measure to increase the power density of engines. The compressor between 0 and 1' in figure 3.5a is driven by the crank shaft in order to pre-compress the charge mass. By using an intercooler (from 1' to 1) the temperature of the pre-compressed charge mass can be reduced in order to rise the charge mass and decrease the tendency for knocking.

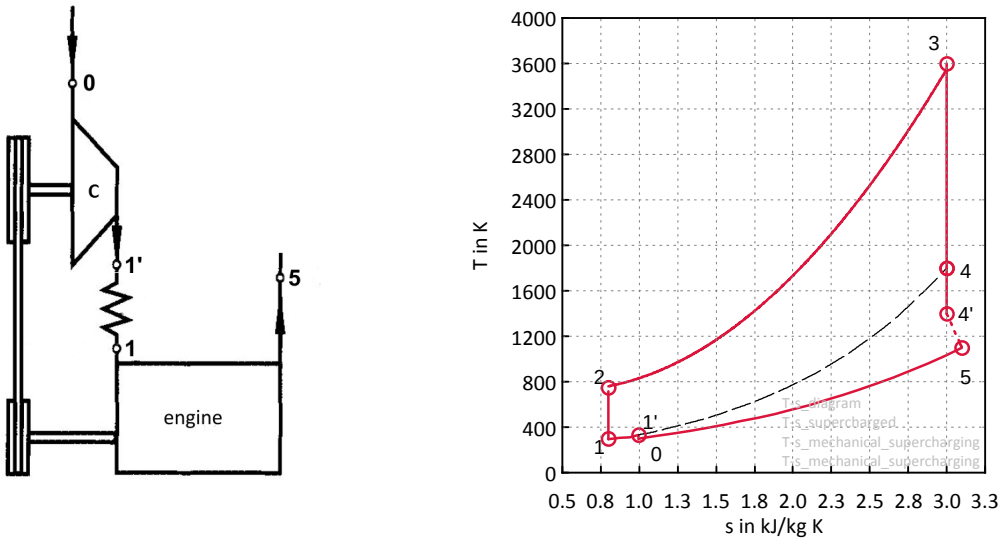

(a) Layout of a mechanical supercharged engine with a charge air cooler [17]

(b) Ts-diagram of a mechanical supercharged engine with charge air cooler

Figure 3.5: Viewing of a mechanical supercharger engine

The process starts with the compression of air with ambient conditions, from 0 to 1'. From 1 to 1' the compressed charge mass is then cooled down until ambient temperature is reached. This process occurs isobar. Afterwards the isentropic compression within the engine occurs form 1 to 2. Then the combustion at constant volume takes place, which rises pressure and temperature until 3 is reached. Reversible adiabatic expansion takes place until the original volume at point 4, or beyond up to 4' in case of an extended expansion engine.

Applied on conventional engines the main aim is to increase the power density. However the efficiency can not be increased at conventional engines since the overall γ becomes less. The following view should better explain this fact.

The rise of charge mass can also be realised through a greater intake volume instead of the pre-compression, by using a mechanical supercharger. In this case the effective γ decreases with rising boost pressure since ε_{ex} remains constant. At this consideration

a rising boost pressure is equal to a rising intake volume and according to equation 2.2 the γ decreases under 1.

Therefore a big part of the total added fuel heat can not be used due to the high pressure at the end of the expansion - respectively the decreasing γ.

The efficiency η_{ic} in the following figures contains the efficiency of the engine work by subtraction of the compressor work and this value related to the total added fuel heat. An isentropic compressor efficiency of 0.7 is assumed.

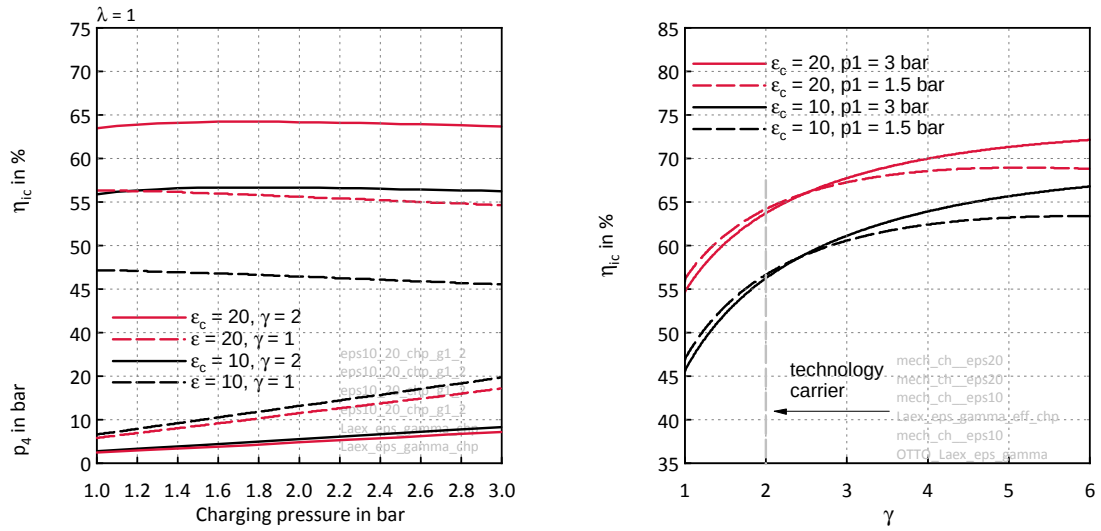

(a) Efficiency and p_4 vs. charging pressure

(b) Efficiency vs. γ

Figure 3.6: Influence of the charging pressure and γ on the efficiency

Figure 3.6a shows the influence of mechanical supercharging in terms of an engine with an elongated expansion stroke with an geometric γ of 2 and a conventional engine (γ of 1). The efficiency decreases at a conventional engine with rising charging pressure due to the decreasing effective γ, as mentioned before.

In operating regions with high charging pressure the work for the compression of the charge mass is higher than the gain due to the positive pressure gradient during the gas exchange. Therefore the efficiency slightly decreases with rising charging pressure. Also visual in figure 3.6a is the rising pressure at the end of the expansion at rising charging pressure which is also attributable to the decreasing effective γ.

At higher values of ε_c the pressure at the end of the expansion is basically lower. This can be seen by the difference of the red and the black line in figure 3.6a. At rising γ the difference between the pressure at the end of the expansion of different ε_c becomes reduced - apparent by the continuous red and black line in 3.6a.

The difference in efficiency between the conventional concept and the engine with an extended expansion stroke at an ε_c of 10 is about 12.7 %PT at 3 bar charging pressure - apparent by the difference of the black dashed and black continuous line.

The difference between an extended expansion engine with an ε_c of 10 and 20 is about 7.6 %PT at 3 bar charging pressure - apparent by the difference of the red dashed and red continuous line.

Figure 3.6b shows the efficiency at rising γ and two different charging pressures. An interesting fact is the intersection of the curves which is described in section 3.2.3.

The efficiency decreases with rising charging pressure at conventional engines. This fact is also visible in figure 3.6a by the difference of the dashed and the continous lines at a γ of 1. Therefore at a higher charging pressure the efficiency starts at a lower value at a γ of 1.

The higher the charging pressure the higher the γ where the pressure at the end of the expansion reaches the exhaust back pressure.

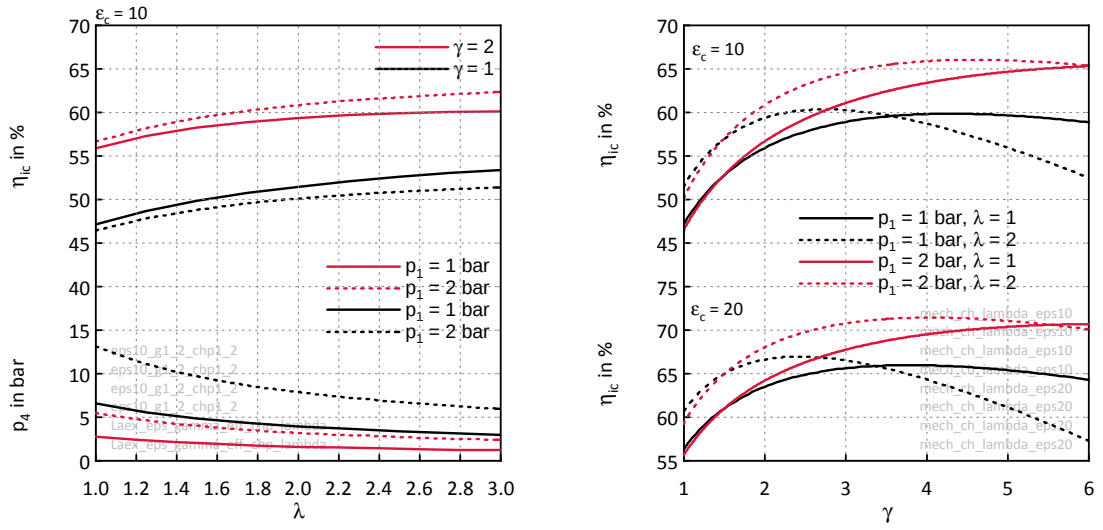

(a) Efficiency and p_4 vs. λ

(b) Efficiency vs. γ

Figure 3.7: Influence of λ on the efficiency

Figures 3.7 provide a fundamental insight into the influence on the efficiency of varying λ at conventional engines and engines with extended expansion.

At conventional engines with mechanical supercharging the efficiency decreases with rising charging pressure since the work for the compression rises and also the effective γ decreases - apparent by the difference in efficiency of the continuous lines and the dashed lines at a γ of 1.

Figure 3.7b shows the course of the efficiency at different values of γ, ε_c and λ. When the engine operates with a λ higher than 1 the highest efficiency is reached at earlier values of γ since the pressure at the end of the expansion drops under exhaust back pressure.

If an extended expansion engine is operated with lean combustion and supercharging the point with the highest efficiency can be shifted to higher values of γ - apparent by the difference of the dashed lines in figure 3.7b.

3.2.2 Turbocharging by means of utilisation of exhaust gas energy - exhaust gas turbocharger

Another possibility to increase the power density is turbocharging. In this case the exhaust gas enthalpy powers the turbine - apparent by T in figure 3.8a. The turbine is connected with a compressor in order to pre-compress the charge mass. By using an intercooler it is possible to further increase the charge mass and reduce the tendency for knocking. The vessel before the turbine reduces pressure fluctuations and make the use of steady-state equations possible.

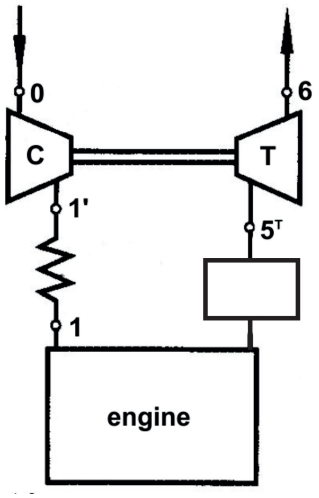

(a) Layout of a turbocharged engine with charge air cooler [17]

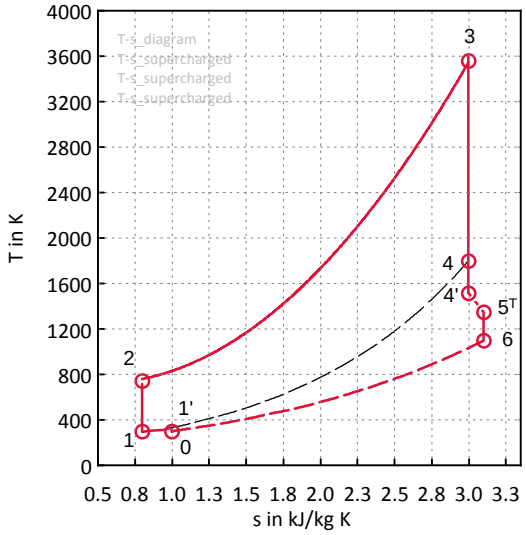

(b) Ts-diagram of a turbocharged engine with charge air cooler

Figure 3.8: Viewing of an exhaust gas turbocharged engine

An exhaust gas turbocharger is used at conventional engine concepts in order to increase not only the power density but also the efficiency. The available amount of enthalpy at the end of the expansion stroke is used to pre-compress the work medium before the intake. A positive pressure gradient can only be reached at operating points with high exhaust gas enthalpy and delivers positive work done on the piston during gas exchange.

Therefore an exhaust gas turbocharger can only increase the overall efficiency in operating regions where the charging pressure is higher than the exhaust back pressure.

Whether the pressure gradient is positive between the outlet of the compressor and the inlet of the turbine depends on the amount of enthalpy before the turbine and of course it depends on the efficiency of the turbocharger at the specific operating point.

In figure 3.8b the process of a turbocharged engine is apparent. After the compression from 0 to 1', the isobar heat removal from 1' to 1 takes place. The piston is then moved inwards by an external force and the gas is compressed reversibly and adiabatically until point 2. Afterwards heat is added to rise temperature and pressure at constant volume. Reversible adiabatic expansion takes place until the original volume at point 4, or beyond up to 4' in case of an extended expansion engine. After the exhaust valve opening, pressure and temperature drops down due to the rising volume which exists between the exhaust valve and the turbocharger. 5^{T} to 6 contains the expansion within the turbine which delivers the energy to compress the atmospheric air [18].

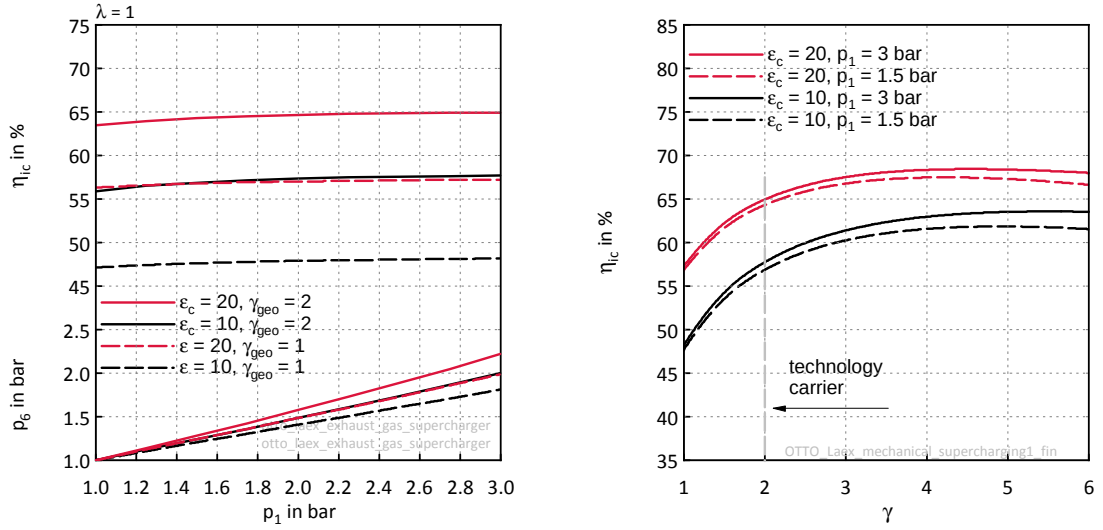

(a) Efficiency and p_4 vs. charging pressure

(b) Efficiency vs. γ

Figure 3.9: Influence of the charging pressure and γ on the efficiency

The available amount of enthalpy at extended expansion engines is lower compared to conventional engines. In figure 3.8b is this fact visual since point 4' is under 4. Therefore at extended expansion engines the required work for the compression of the charge mass entails a higher exhaust back pressure. Since the enthalpy becomes lower at rising values of γ the exhaust back pressure becomes disproportionate higher - apparent by the difference of the continuous and dashed lines in figure 3.9a. Furthermore this is the reason for the flat course of the efficiency at high values of γ in figure 3.9b.

At higher ε_c the exhaust gas enthalpy is basically lower and the higher rise of exhaust back pressure causes the decreasing efficiency of the red lines in figure 3.9b.

The vessel before the turbine allows the use of the steady-state equations for the calculation of the exhaust back pressure. In case of a conventional engine the efficiency can be slightly increased, apparent by the broken lines in figure 3.9a. An extended expansion engine with an exhaust gas supercharger has to expel against the exhaust back pressure with the entire expansion volume. This approach produces much gas exchange work which is furthermore the reason for the lower increase in efficiency compared to the mechanical supercharged extended expansion engine. In figure 3.9b the influence of the efficiency at rising γ is visual.

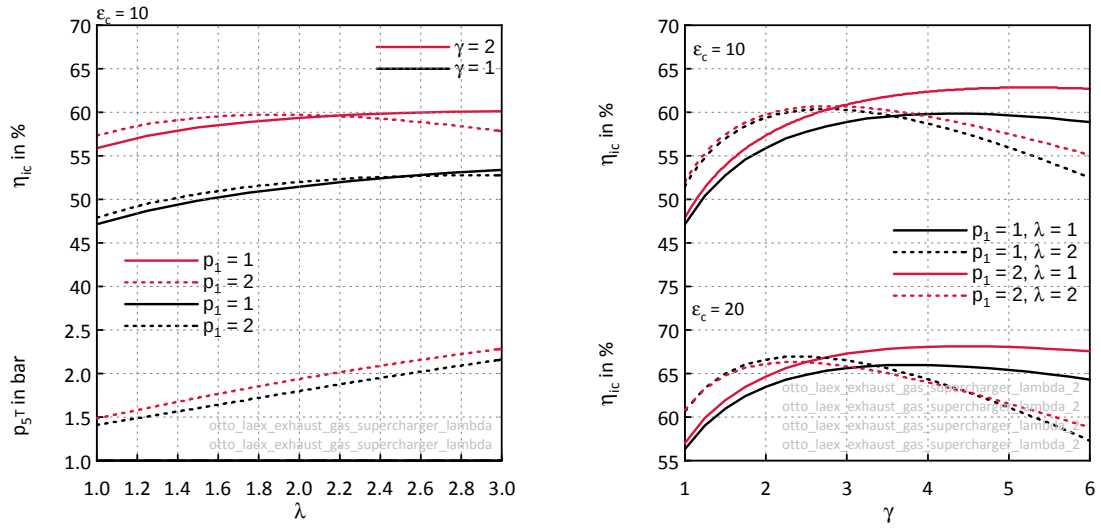

(a) Efficiency and p_4 vs. λ

(b) Efficiency vs. γ

Figure 3.10: Influence of λ on the efficiency

Figures 3.10 provide a fundamental insight into the influence of operating points with a λ higher than 1 and turbocharged operation.

Due to the decreasing pressure at the end of expansion at rising λ an expansion under the exhaust back pressure occurs. This fact causes the steep decrease in efficiency of the dashed lines in figure 3.10b.

Between a γ of 1.5 and 4.5 the black dashed line is above the red dashed line, at an ε_c of 20. In this area the rising exhaust back pressure delivers lower efficiencies. After a γ of 4.5 the higher charging pressure overcompensates the lower efficiency due to the lean combustion.

This section reveals that the gas exchange work has a significant influence on the overall efficiency at engines with extended expansion. Thus means that the difference of efficiency between a supercharged and a turbocharged engine decreases with rising values of γ.

3.2.3 Comparison of supercharging and turbocharging

After the very detailed description of supercharging and turbocharging in the foregoing sections, this section should give a basic impression how supercharging or turbocharging influences the efficiency.

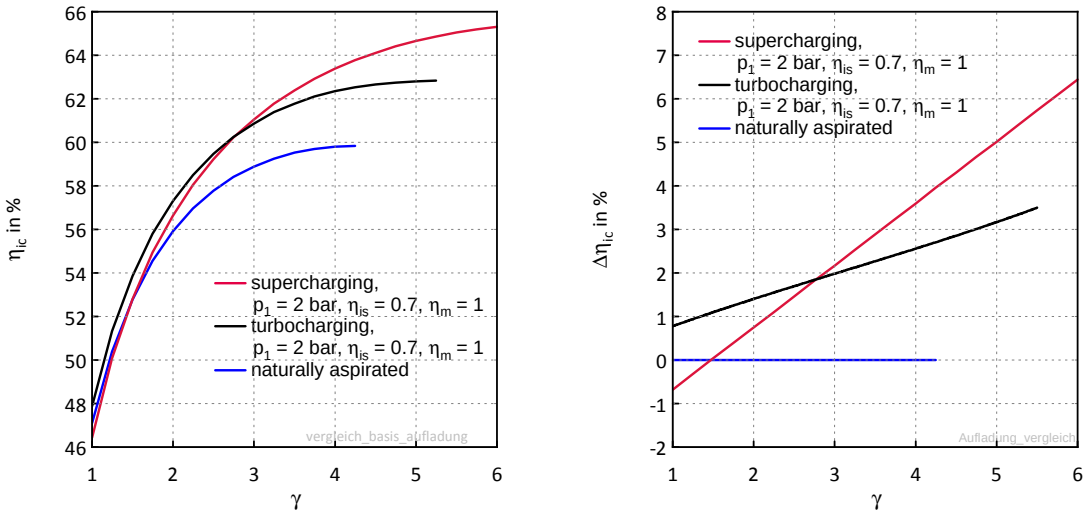

(a) η_{ic} vs. γ of different configurations

(b) $\Delta\eta_{ic}$ vs. γ of different configurations

Figure 3.11: Influence on the efficiency at supercharging and turbocharging related to γ

Figure 3.11a shows the efficiency vs. γ. The blue line describes the efficiency related to γ at a naturally aspirated engine. The black line represents a turbocharged engine and the red line an engine with mechanical charging. Figure 3.11b shows the difference of the efficiency related to the naturally aspirated engine. It is clearly apparent that it is not possible to increase the efficiency by using a mechanical supercharger at a conventional engine. By using an exhaust gas turbocharger the efficiency can be increased at conventional engines as well as at engines with extended expansion. The difference of the efficiency between the approach with supercharging and turbocharging is reduced with rising values of γ. At high values of γ the use of a mechanical supercharger delivers a higher efficiency compared to the exhaust gas turbocharger since the exhaust back pressure rises steeply due to the decreasing exhaust gas enthalpy at high values of γ.

4 Engines

4.1 Reference engine

Figure 4.1: BMW F800

The reference engine is a two cylinder in-line engine with an overall displacement of 798 cm^3. The maximal power of 64 kW is reached at 8000 revolutions per minute (rpm). The maximal torque of 86 Nm is reached at 6000 rpm. The engine operates according to the Otto cycle and the load control occurs quantity controlled. The mixture formation takes place in the intake path after the throttle flap by two injection valves. One for each cylinder. The gas exchange is determined by two overhead cam shafts which actuate four valves at every cylinder. The valve actuation is put into action by finger rocker arms. The cam shafts and the crank shaft are connected with a timing chain. The crank pin offset is 360 degrees and as a result the piston stroke is performed parallel. This ignition sequence is used in order to ensure a balanced gas exchange with high torque utilisation. This gives rise to an available torque which is 90 % of the maximum torque at 5000 rpm. [19]

(a) F800 mass balancing I

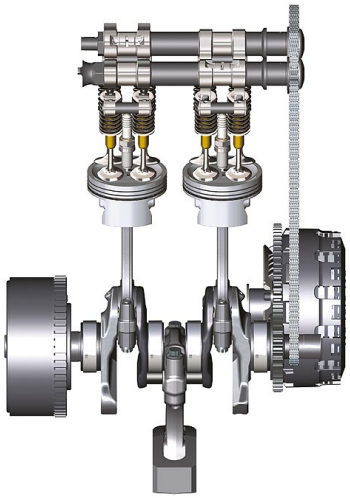

(b) F800 mass balancing II

Figure 4.2: Technical description of the engine

Unlike to conventional mass balance mechanism the F800 uses a system which works like an opposed piston. The crank shaft of the F800 carries three crank pins. On the outer crank pins there are the connecting rods mounted. The third crank pin in the middle is connected with a counterweight mass which is furthermore connected with a swinging-arm. The balance mass moves up and down countering the movement of the two piston. The overall oscillating mass of the swinging-arm and the counterweight virtually compensate the mass forces at all positions. [20] Due to the finite length of the swinging-arm the direction of motion of the counterweight is not exactly parallel to the cylinder axis and furthermore the compensation of the first and second order of inertia forces can not achieve 100 %.

The required lubrication is put into action through a gear-wheel pump which is driven by the gearbox input shaft. In order to minimise churning losses the engine is fitted with a semi-dry sump lubrication. Below the balance mechanism is an isolated duct, which is utilised as an integrated oil tank. The oil is drawn off from the isolated duct and all bearings within the gearbox as well as the cylinder head and the main bearings are supplied with oil. The water pump which is driven through the intake cam is installed at the cylinder head.

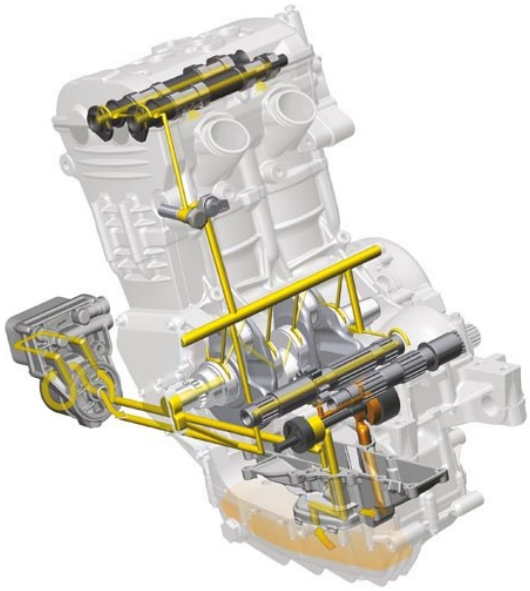

Figure 4.3: Oil circuit

4.1.1 Adopted parts for further investigations

For the investigation of the Miller strategy three different pistons were manufactured. The first piston is equal to the original piston, but forged in order to resist the forces during the supercharged operation. This configuration should ensure a similar combustion chamber shape at the technology carrier compared to the reference engine. The second piston should ensure a similar compression ratio between the original configuration of the reference engine and the technology carrier. The third piston was used for the Miller investigations. Furthermore special cam shafts was manufactured for the Miller investigations. In addition cam shafts were manufactured which were adjusted to the gas dynamics at 3000 rpm in order to ensure a maximum of charge mass. The different configurations are apparent in table 4.1.

Table 4.1: Different pistons

Pos.	ε at F800	ε_c at TT	Description
1	11.9	9.7	similar combustion chamber at F800 and TT
2	14.5	12.45	similar ε as at F800
3	17.7	14.3	Miller investigations at F800

The lower ε_c at the technology carrier is due to the shorter intake stroke compared to the reference engine.

4.2 Technology carrier (TT)

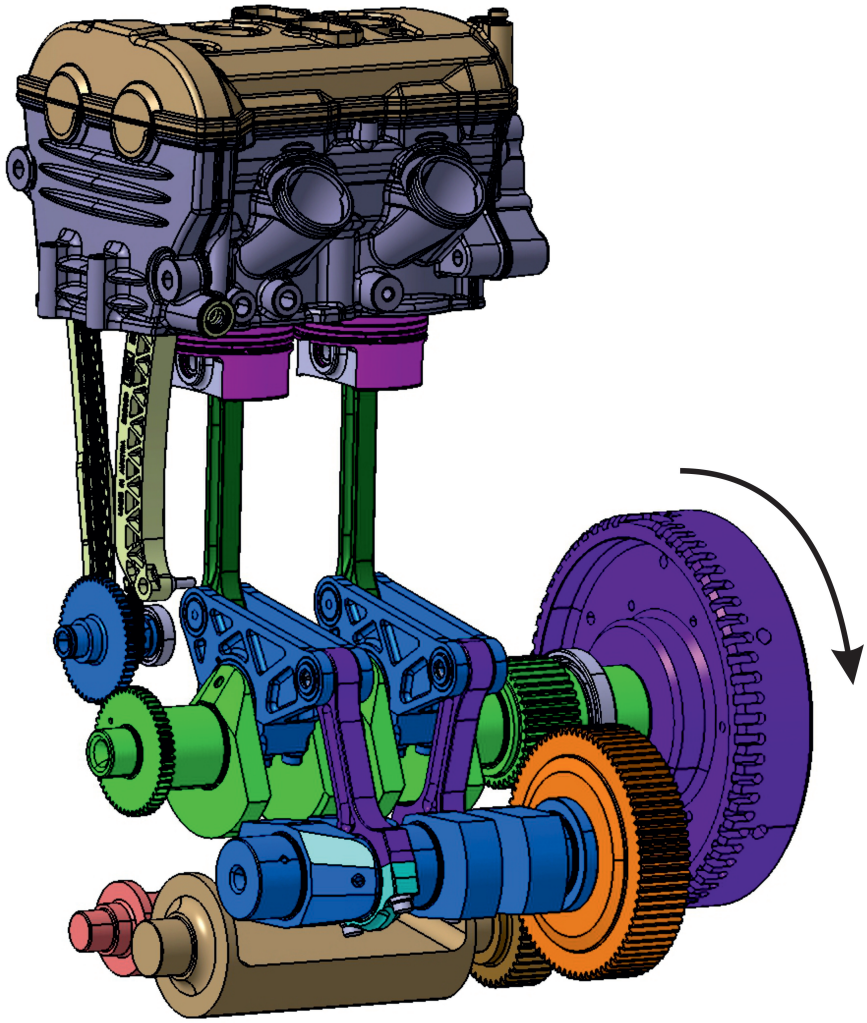

Figure 4.4: CAD-model of the TT

In figure 4.4 a CAD-model of the technology carrier is apparent. The visual engine is a 2 cylinder in-line engine with an intake volume of 321.15 cm^3 per cylinder. This engine operates according to the Otto cycle. The cylinder head and the valve train is adopted from the reference engine which is used in mass production. The actuation of the valves occur similar to the reference engine by finger rocker arms. In order to connect the crank shaft with the valve train a changed timing chain would be necessary. In order to avoid a modified valve train chain an intermediate shaft was designed which is driven by the crank shaft. Unlike the reference engine which is

fitted with a oil pump the oil supply is executed by an external oil pump. Pressure and temperature can be adjusted from the test bench cell.

Due to the different intake volume and the shifted TDC position between gas exchange and combustion special cam shafts were made. Due to the modified cam shaft gears, the valve timing can be changed in steps of 1 degree of cam angle, which is equal to 2 °CA.

The crank shaft drives the *Atkinson shaft* which turns with half the speed in the opposite direction. The mounting points of the *Swing rod* at the *Atkinson shaft* are arranged at an angle of 180 degrees to the other one due to the firing order which is also shifted at 360 degrees. Both oscillations together with these dimension results in a volume course which is shown in figure 4.5.

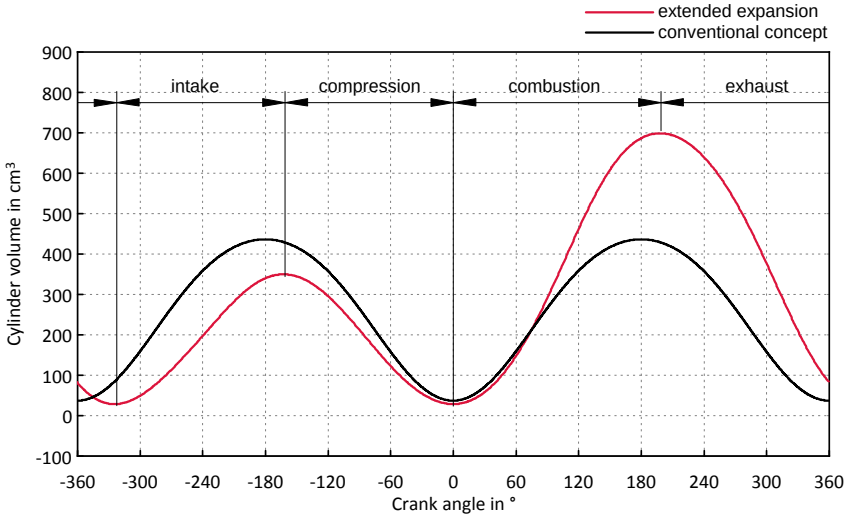

Figure 4.5: Cylinder volume vs. crank angle of both the concepts

Figure 4.5 shows the volume course of the technology carrier as well as the volume course of the reference engine. The red line represents the cylinder volume course of the unconventional concept with a γ of 2. The black line represents the volume course of the conventional engine.

The combustion stroke takes place from 0 °CA until 196 °CA, afterwards the exhaust stroke takes place from 196 °CA to - 328 °CA. The intake stroke starts at - 328 °CA and ends at -164 °CA. The charge mass is compressed during the compression stroke which takes place form -164 °CA to 0 °CA.

4.3 Kinematics of the crank train

In order to show the movement of the additional parts at the extended expansion engine the parts were described at every single crank shaft position. The course of the connecting points was calculated in Matlab. The determination of the connection points was made by means of the intersection of two circles. The moveable parts were simplified with few mass points allowing for the free mass forces of every part. The course of the movement was derived twice related to time. The acceleration multiplied with the mass points equates the forces.

Under consideration of the forces which occur due to the compression, combustion and expansion the free mass forces and moments can be calculated. The results are visible in figure 4.7b.

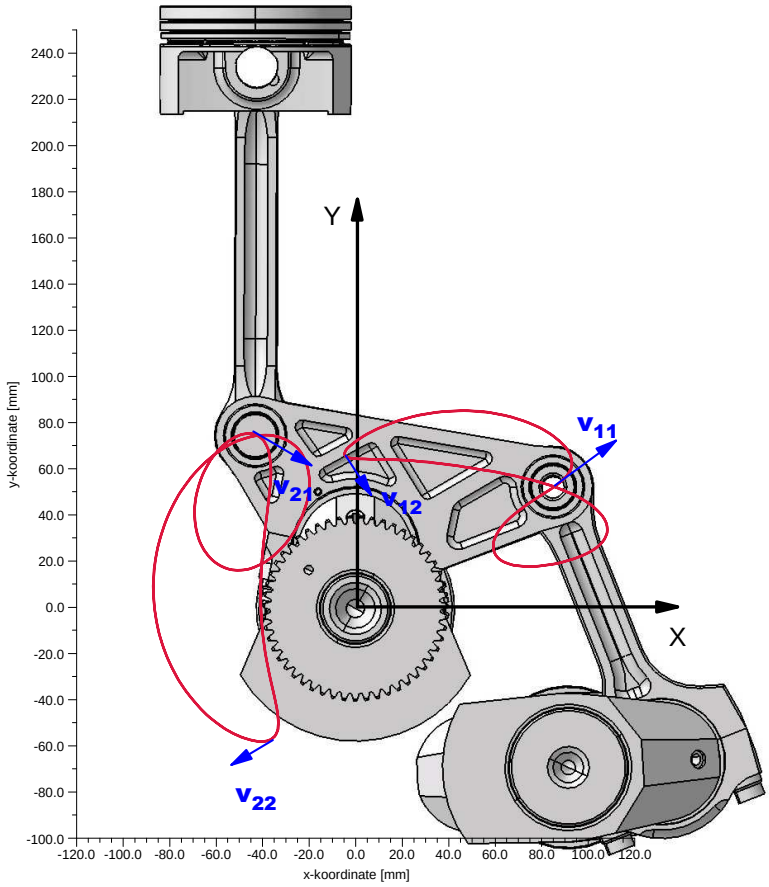

Figure 4.6: Movement of the Triangle

Figure 4.6 shows the movement of the connecting points of the *Triangle*. Figure 4.6 shows the configuration while the piston is at TDC before the expansion stroke takes place. The *Crank shaft* turns into the right direction and the *Atkinson shaft* turns half the revolution in the opposite direction. The blue vectors shows the velocity and the direction in which the points are moving. During the expansion the left end of the *Triangle* covers the path from vector v_{21} to vector v_{22} which is equal to the movement of the big con rod eye.

4.3.1 Mass balance

The motion of all the components lead to free mass forces which are uncommon compared to conventional engines. In order to reduce the free mass forces the division Construction and Design investigated the mass balance for this engine. The following figures shows the free mass forces of the entire crank assembly at different configurations.

The *Atkinson shaft* turns both shafts which are responsible for the mass balance - apparent on the bottom portion of figure 4.4. Figure 4.7 shows the results regarding to the mass balance of the technology carrier. The point of origin is the centre of the *Crank shaft* and the vertical axis is parallel to the cylinder axis.

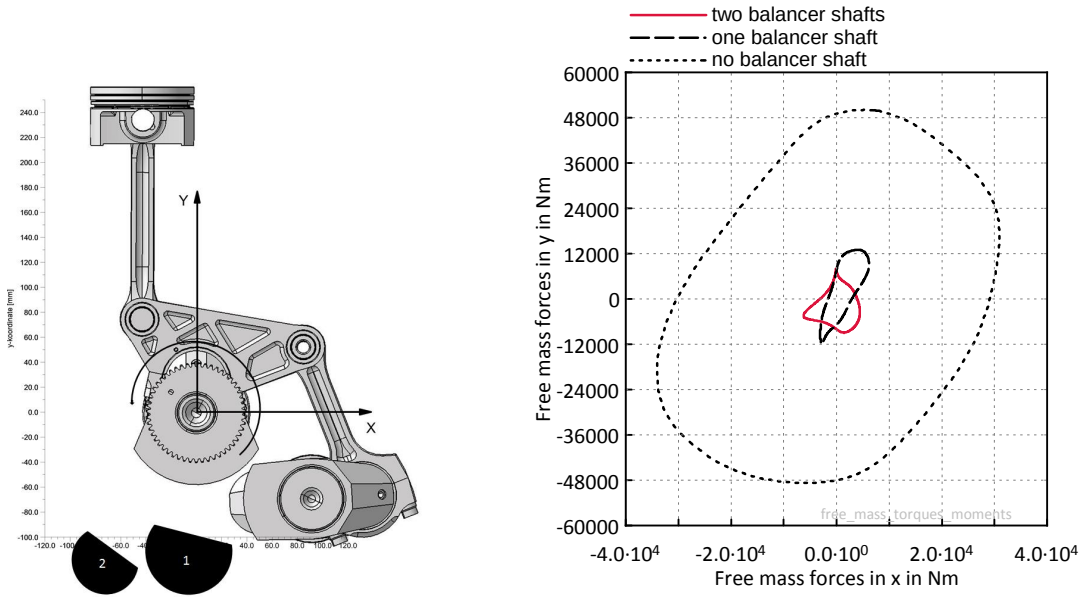

(a) Mass balance

(b) Free mass forces

Figure 4.7: Mass balancing of the technology carrier

The point of origin of the diagram is the rotational axis of the *Crank shaft*. The vertical axis is parallel to the cylinder axis as it is shown in 4.7a. Figure 4.7b represents

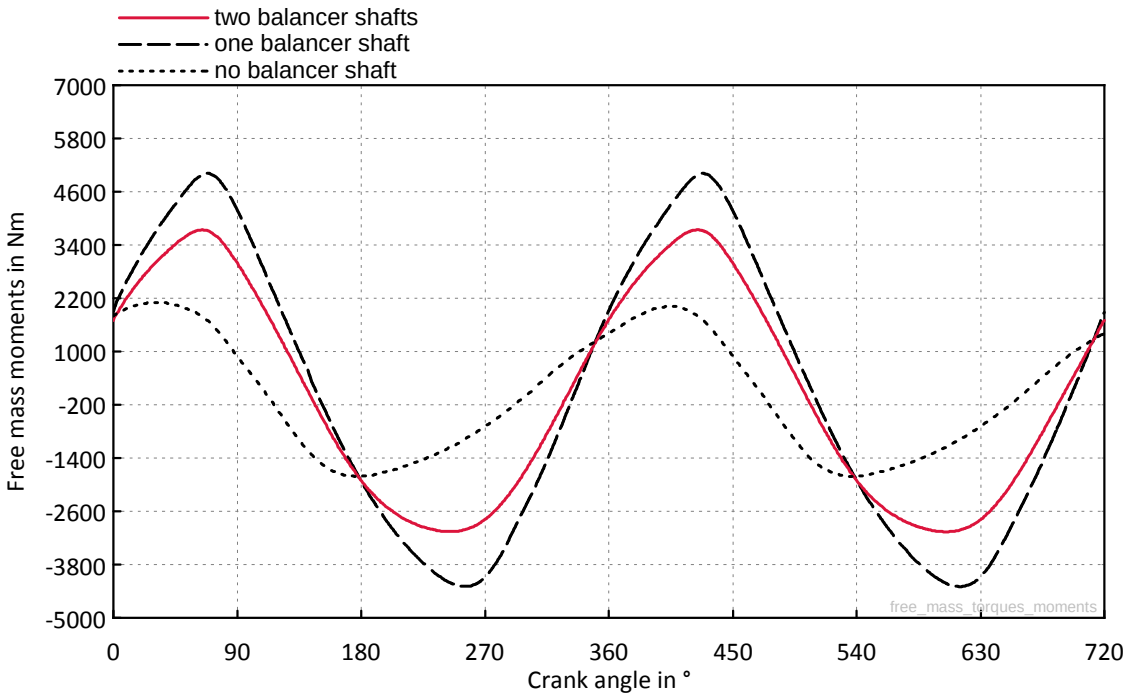

Figure 4.8: Free mass moments of different configurations

the free mass forces with different configurations. The black doted line represents the free mass forces without any mass balancing shafts. The maximum of free mass forces which are reached with this configuration is about 50 kN at 6000 rpm. 6000 rpm is also the maximum speed which can be reached with the technology carrier The black dashed line shows the free mass forces which occur with only one mass balancing shaft, as it is apparent in figure 4.7a with number 1. The maximum of free mass forces are about 14 kN at 6000 rpm. The continuous red line represents the free mass forces which occur if both of the mass balance shafts 1 and 2 are mounted - this is realised at the present case. The maximum amplitude is about 10 kN at 6000 rpm.

Figure 4.8 shows the free mass moments which occur on the *Crank shaft* at different configurations. The black doted line represents the free mass moments due to mass forces without any mass balancing. The black dashed line shows the case with only one balancing shaft (1). The maximum amplitude which occurs is about 5000 Nm at 6000 rpm. The red continuous line represents the case as it is realised at the technology carrier (1 and 2). The maximum amplitude which occurs with both balancing shafts is about 3800 Nm at 6000 rpm.

4.4 Different configurations

The three different pistons which were designed and manufactured can also be used for the technology carrier - apparent in table 4.1. Due to the shorter intake stroke the ε_c is lower compared to the reference engine. The original forged piston figures an ε_c of 9.7 at the technology carrier. Furthermore it ensures a combustion chamber shape which is equal to the combustion chamber shape of the reference engine.

The second type should rise the compression ratio to 12.5 which is similar to the compression ratio of the reference engine. The third type of piston which was made for investigations of the Miller strategy at the reference engine figures an ε_c of 14.9 at the technology carrier. Investigations with an ε_c of 14.9 was not conducted on the technology carrier.

5 Test bench and measurement technique

The investigations of both engines were made on the test bench P4 at the *Institute for Internal Combustion Engines and Thermodynamics*. Both engines was indicated and also the exhaust gas fraction was measured in order to ensure a proper analysis.

Pictures of the test bench design can be seen in figure 5.1a and a more detailed schematic view is visual in figure 5.2.

5.1 Test bench setup

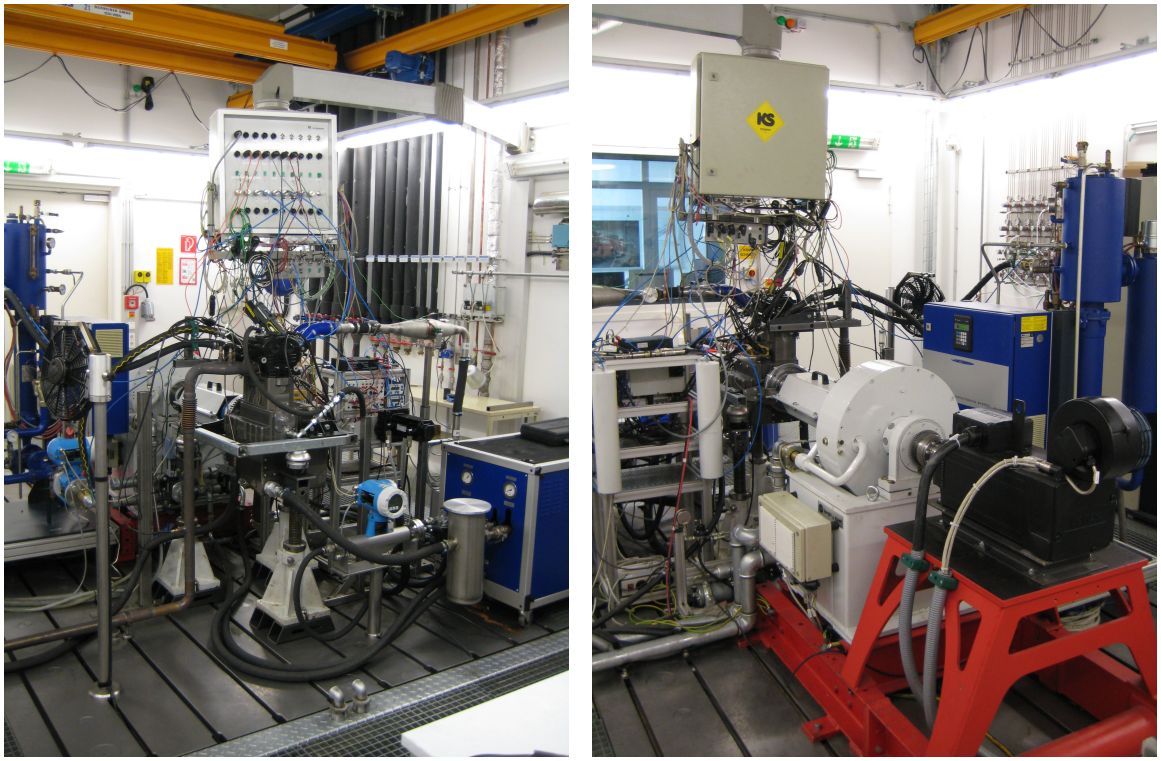

(a) Test bench: front view

(b) Test bench: rear view

Figure 5.1: Test bench

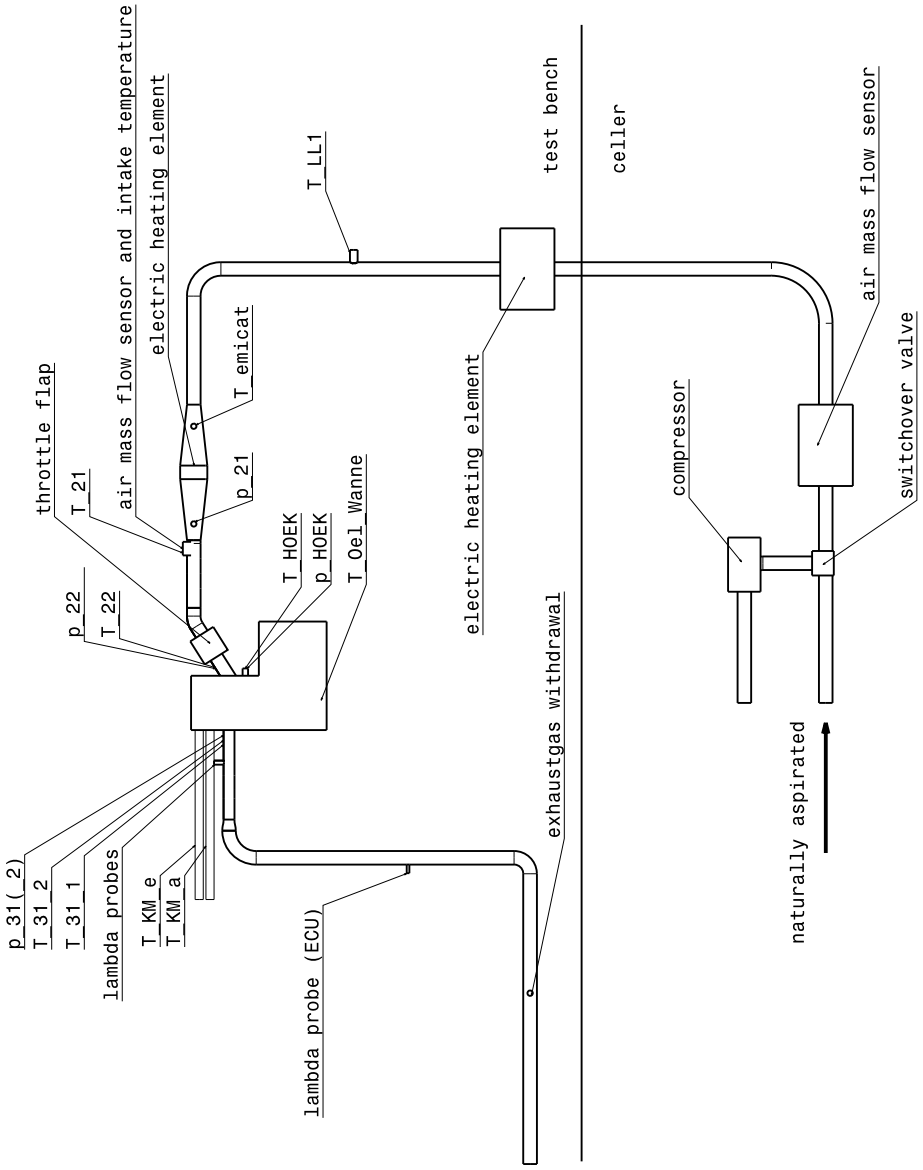

Figure 5.2: Schematic view of the test bench

The eddy current dynamometer which is water cooled was connected to the engine on the one end and on the other end it was connected to the electric motor.

Eddy current dynamometer	
type:	*Borghi & Saveri FE 260S*
maximum torque:	1000 Nm
maximum revolution:	8000 rpm

The use of the electric motor was necessary due to the missing start device at the technology carrier.

Electric motor	
type:	*Lenze asynchronous motor MQA 22P29*
maximum torque:	200 Nm
maximum revolution:	6500 rpm

The torque measurement occurred with a torque flange which was mounted between the cardan shaft and the eddy current dynamometer.

Torque measuring flange	
type:	*HBM T40B*
maximum torque:	1000 Nm
signal transmission:	contactless

The fuel was provided by the building services with a constant pressure of 0.9 bar and the fuel consumption measuring was executed with a Coriolis device of *MicroMotion*. In order to provide a fuel pressure of 3.7 bar before the injection valves between the Coriolis device and the injection valves a fuel conditioning system was installed which regulated the fuel temperature and pressure.

Fuel consumption measurement	
type:	*MicroMotion*
measuring range:	0-50 kg/h
measuring accuracy:	± 0.1 % of measured value

The intervention of the point of ignition and injection mass was executed through a programmable electronic control unit which is also used in racing applications.

Electronic control unit	
type:	*Motec M800*

In order to ensure a closed loop control three wideband lambda probes were installed within the exhaust system. Two lambda probes were installed with a short distance after the exhaust port, one for each cylinder, in order to ensure a cylinder balancing. The third lambda probe was installed with a longer distance to the exhaust port in order to measure the overall lambda. The positions are visual in figure 5.2.

Lambda probes	
type:	*Bosch LSU 4.2*
Lambda range:	0.7-32
maximum temp.:	930 °C/1030 °C(10min.)

Due to the used electronic control unit which has no output stage a spark-plug connector with integrated ignition coils of *BERU ZSE059* was used.

An exhaust gas analyser of *AVL*, model *CEB*, measured CO_2, CO, THC, NO_x and O_2.

The required air was delivered by the building services. On the way to the engine the air flows through a rotary displacement meter which measured the volume flow. Including the information of pressure and temperature the mass flow could be calculated. By operating a switch-over valve in the celler compressed air could be delivered by a screw compressor of *ATLAS COPCO, GA-30*.

The cooling was ensured through an external conditioning system at which the temperature and the mass flow could be adjusted. The cooling system is apparent on the left part of figure 5.1a. Since the technology carrier has no integrated oil supply it was connected with an external oil conditioning system of *AVL*, which is apparent on the right part in figure 5.1a.

The actuation of the throttle flap was executed through a synchronous servo motor of *Lenze*.

5.2 Indication/Pressure measurement

Between the output shaft of the engine and the cardan shaft was an optical angle encoder mounted. The crank angle resolution is 0.5 deg which is recommended by *AVL* at engines with high oscillations or racing applications.

Angle Encoder	
type:	*AVL 365X ANGLE ENCODER*
maximum revolution:	28000 rpm
angle resolution:	0.5 deg

The cylinder indication was carried out in both of the cylinders with cylinder pressure sensors of *AVL* without cooling, which operate according to the piezoelectric principle. The use of these specific sensors is due to the high precision and little required space. In order to get an access into the combustion chamber a hole was drilled into the cylinder head in which an adapter was fixed and sealed against cooling water.

High pressure indication	
type:	*AVL GH 14 D*
measuring range:	0-250 bar
linearity:	$\pm$ 0.3 % FSO
temp. range:	-40...400 °C

The pressure course of the intake and exhaust port was also measured with sensors of *AVL*. The sensor which was mounted on the exhaust pipe was water cooled.

Low pressure indication	
type:	*AVL GH 21 C*
measuring range:	0-250 bar
linearity:	$\pm$ 0.3 % FSO
temp. range:	-40...400°C

5.3 TDC adjustment

The exact determination of the TDC is necessary to shift the unconventional volume course to the right position. A little deviation to the real volume course causes uncertainties during the further calculation. The determination of the TDC position by using the pressure course allows only a rough determination due to several losses which occur near to TDC.

Due to leakage losses and heat transfer during the compression the position of TDC is not equal to the position of the peak pressure. Therefore the position of peak pressure is before TDC. Furthermore the construction is not ideally rigid and the static determination of TDC can lead to uncertainties at calculation. The determination of TDC position was performed by means of a capacitive sensor of *AVL* while the motored operation.

TDC determinationt	
type:	*AVL OT-SENSOR 428*
maximum revolution:	6000 rpm
angle resolution:	± 0.1 deg

As mentioned before the adjustment of the TDC was performed with a capacitive probe of *AVL*. The capacitive probe is mounted at the thread which is made for the spark plug. After the conditioning of oil and cooling water the engine was motored at 3000 rpm through the electric motor. The surface of the probe together with the piston surface form an electrical capacitor. The smaller the distance between the sensor and the piston the higher the output voltage which is recorded vs. crank angle. The voltage signal was recorder over several cycles. At the post processing the voltage signal was averaged over all cycles. Figure 5.3 shows the output signal.

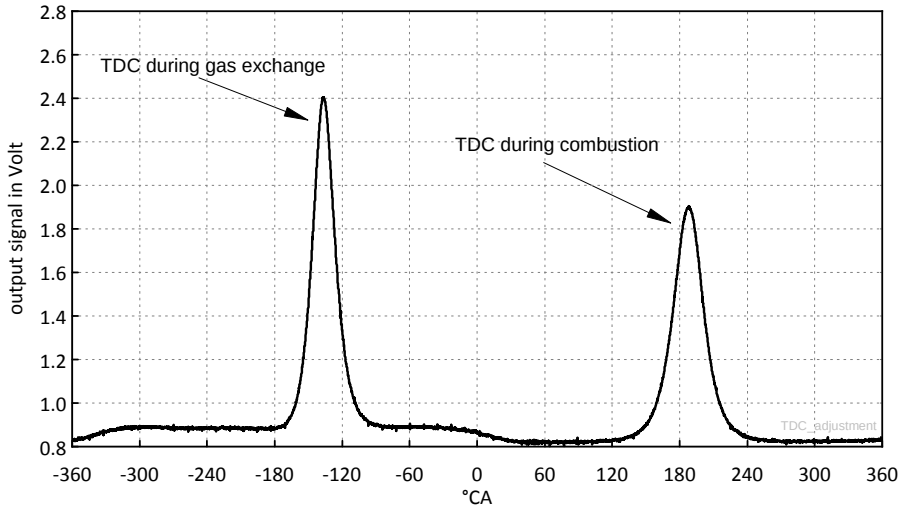

Figure 5.3: Output signal

5.4 Pressure Calibration

In order to ensure a precise cylinder pressure measurement the high-pressure sensors were calibrated after each assembling of the engine. A hydraulic pressure balance was used to carry out a multipoint calibration. The pressure sensor reacts only on pressure jumps and not on constant pressure. A specific pressure which was also monitored at the pressure balance was adjusted. In order to ensure a yield of electric charge of the sensor a pressure jump was applied and the calculated sensitivity was introduced into the indication software. In order to avoid inner friction of the pressure balance it was necessary to ensure a rotation of the weight before the pressure jump. The calibration was performed in steps of 20 bar until 100 bar. The design of the pressure balance can be seen in figure 5.4

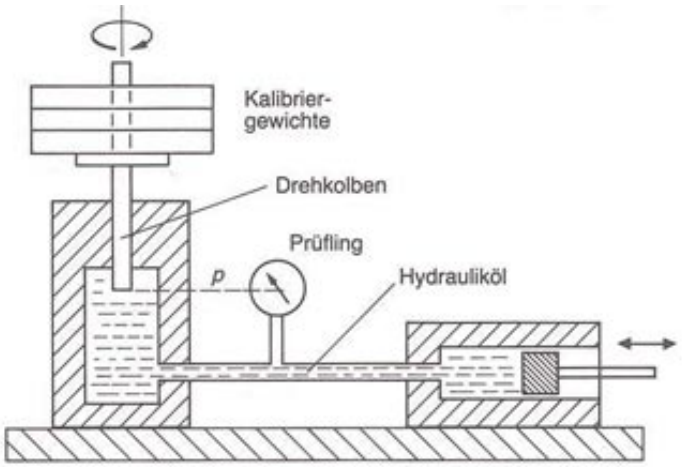

Figure 5.4: Pressure balance [21]

5.5 Vibrations on the test bench

Torsional vibrations and oscillations have been one of the biggest problems since the beginning of the test bench run. In some speed ranges it was not possible to run the extended expansion engine due to the high oscillations. At the beginning of the test bench phase the engine and the eddy current dynamometer were connected through a cardan shaft with a torsional stiffness of 23000 Nm/rad. This configuration leads to high torque deflections within the entire drive train and to destruction of some measurement installations and mountings. In figure 5.5 the fluctuations are clearly visible. This figure shows the shape of torque at 3000 rpm and full load.

In order to minimise these fluctuations the cardan shaft was replaced by a torsional shaft with an over all torsional stiffness of 215 Nm/rad. The red line represents the shape of torque with the cardan shaft and the black line represents the torsional shaft. The used shafts are shown in the figure 5.6.

5.5.1 Theoretical model

In order to understand the physical effects on the test bench the issue was assessed with a simplified model. The moment of inertia from eddy current dynamometer and the asynchronous machine were adopted from technical data sheets. The inertia moment from the engine was adopted from a simplified CAD model. The torsional stiffness was extracted out of technical data sheets. The simplified model contains a three-mass coupled oscillator and is apparent in figure 5.7.

J_1 is the engine with an averaged moment of inertia of 0.1 kgm^2, J_2 includes the moment of inertia of the eddy current dynamometer, which is 0.175 kgm^2 and the moment of inertia of the shafts which are connected to the engine and the electric motor. The overall moment of inertia of the eddy current dynamometer and the shafts

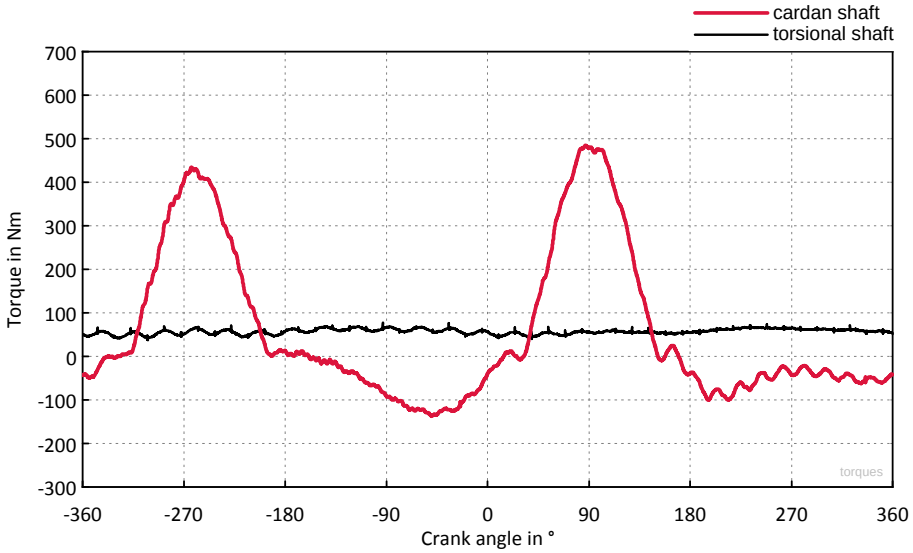

Figure 5.5: Output torque with different configurations

(a) cardan shaft

(b) torsional shaft

Figure 5.6: Figures of the cardan shaft and torsional shaft

is about $0.2\,\mathrm{kgm}^2$. The last component is the electric motor with a moment of inertia of $0.05\,\mathrm{kgm}^2$. c_1 is the torsional stiffness of the cardan shaft and c_2 contains a claw coupling with damping elements out of plastic. The applied method is called Holzer's methode and it is not able to calculate eigenfrequencies with damping. Therefore the damping was neglected in order to make a calculation with this method possible.

The process of the calculation is listed in table 5.1 and is based on newton's axiom. The torque equilibrium was solved with the aid of an iterative process.

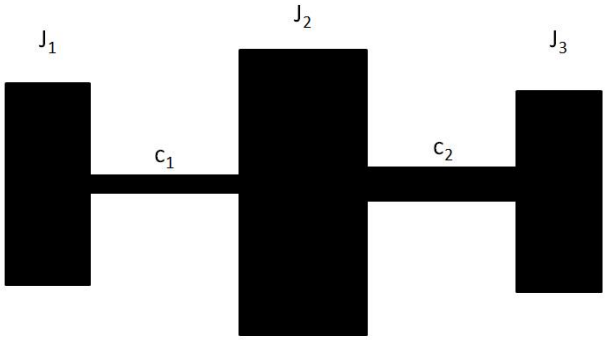

Figure 5.7: Simplified model of the drive train

Table 5.1: Determination of the eigenfrequency using the Holzer's methode

θ	$\theta \cdot \omega^2$	ϕ	$\theta \cdot \omega^2 \cdot \phi$	$\sum(\theta \cdot \omega^2 \cdot \phi)$	c	$1/c \cdot \sum(\theta \cdot \omega^2 \cdot \phi)$
0.1	44474.68	1	4447.47	4447.47	23000	0.1933
0.2	88949.37	0.8066	71749.39	76196.86	18000	4.2331
0.05	22237.34	-3.4265	-76196.86	0	-	-

θ states the moment of inertia of the single masses. ϕ states the deflection compared to the first mass. In this case the left (and the right) end of this system are not clamped and for the same reason the term $\sum(\theta * \omega^2 * \phi)$ must be zero at the third mass. If this system would have a clamped end on the right side ϕ must be zero there. At the beginning of the calculation ω was set to any value. Afterwards ω was varied with a solver until the term $\sum(\theta * \omega^2 * \phi)$ in the fifth row, respectively the torque at ω_3 became zero. The solution was a eigenfrequency at 106 Hz.

In order to shift the eigenfrequency to lower speeds a torsional shaft was mounted. After using the torsional shaft the torque deflection at 3000 rpm was eliminated. With the current drive train the eigenfrequency lies at about 24 Hz which corresponds to a speed of 1440 rpm. This measure lowers the eigenfrequency by a quarter and additionally increases the damping of the entire drive train.

It is assumed that the excitation torque was caused by the engine and/or by the electric motor which has a frequency converter. After a research of problems with oscillations at drive trains the following citation was found.

> *Every electrical machine in the United States that is powered by 60 Hz line frequency gives off a mechanical vibration at 120 Hz. This includes all*

> *as motors and power transformators. This is normal and is called* magnetostriction*. ... In other parts of the world, where the line frequency is 50 Hz, the mechanical vibration emanating from motors and transformers are at 100Hz.* [22].

Whether this problem can be solely explained by this citation is not clear!

6 Calculations and Methods

At the beginning of the measurements with the technology carrier the calculation of the $ROHR$ was not possible since the standard routine was not able to make a calculation with an unconventional volume course. Furthermore the determination of $IMEP_{\mathrm{LPC}}$ was difficult since the low pressure cycle is not ambiguously closed. For this reason several routines were written and introduced into the test bench and evaluation software.

6.1 Calculation of the rate of heat release ($ROHR$)

The rate of heat release is an appropriate measure in order to determine the quality of the combustion. The outcome of the course of the rate of heat release is e.g. ignition delay, centre of heat release and burning duration.

Using the first law of thermodynamics which states that energy is a conserved quantity the energy which is released within the cylinder can be determined. The first law of thermodynamics in its most common form can be written as follows:

$$\mathrm{d}W_{\mathrm{t}} + \mathrm{d}Q_{\mathrm{h}} + \sum \mathrm{d}m_{\mathrm{i}}(h_{\mathrm{i}} + e_{\mathrm{ai}}) = \mathrm{d}U + \mathrm{d}E_{\mathrm{a}} \tag{6.1}$$

In equation (6.1) the value W defines the work and Q the heat which is transformed across the boundaries. The term $\sum \mathrm{d}m_{\mathrm{i}}(h_{\mathrm{i}} + e_{\mathrm{ai}})$ refers to the amount of energy, respectively the enthalpy and the external energy that leave the system minus the energy which enters the system by crossing its boundaries.

U is called the internal energy and expresses the difference between any two states within the system.

The combustion takes place while the valves are closed and when further the energy of the blow-by gas is neglected the combustion can be considered in a closed process. According to the foregoing definitions:

$$\mathrm{d}W_{\mathrm{t}} + \mathrm{d}Q_{\mathrm{h}} = \mathrm{d}U \tag{6.2}$$

In case of a combustion engine $\mathrm{d}W_{\mathrm{t}}$ defines the work which is done due to the change in volume, $-pdV$. $\mathrm{d}U$ describes the change of the inner energy within the cylinder by using the temperature and gas properties. For the precise determination of the gas properties it would be necessary to develop a model which defines the conversion rate from fuel into combustion products. In addition the combustion only

takes place until the chemical balance. The determination of the chemical balance and the amount of chemical products would be a formidable task. In order to make an approximation of the rate of heat release the internal energy is calculated with the aid of averaged gas properties.

$$\mathrm{d}U = m_{\mathrm{cyl}} \cdot c_v \cdot \mathrm{d}T \tag{6.3}$$

$$\frac{\mathrm{d}Q_{\mathrm{h}}}{\mathrm{d}\varphi} = \frac{m_{\mathrm{cyl}} \cdot c_v \cdot \mathrm{d}T}{\mathrm{d}\varphi} + \frac{\mathrm{d}p_{\mathrm{cyl}} \cdot \mathrm{d}V_{\mathrm{cyl}}}{\mathrm{d}\varphi} \tag{6.4}$$

Furthermore the ideal gas equation is necessary:

$$p_{\mathrm{cyl}} \cdot V_{\mathrm{cyl}} = m_{\mathrm{cyl}} \cdot R \cdot T_{\mathrm{cyl}} \tag{6.5}$$

The derivation of the ideal gas equation which contains unchangeable terms, gives:

$$\mathrm{d}p_{\mathrm{cyl}} \cdot V_{\mathrm{cyl}} + \mathrm{d}V_{\mathrm{cyl}} \cdot p_{\mathrm{cyl}} = \cancel{\mathrm{d}m_{\mathrm{cyl}} \cdot R \cdot T_{\mathrm{cyl}}} + \cancel{\mathrm{d}R \cdot m_{\mathrm{cyl}} \cdot T_{\mathrm{cyl}}} + \mathrm{d}T_{\mathrm{cyl}} \cdot m \cdot R \tag{6.6}$$

Divided by 6.5 gives:

$$\frac{\cancel{p_{\mathrm{cyl}}} \cdot \mathrm{d}V_{\mathrm{cyl}}}{\cancel{p_{\mathrm{cyl}}} \cdot V_{\mathrm{cyl}}} + \frac{\cancel{V_{\mathrm{cyl}}} \cdot \mathrm{d}p_{\mathrm{cyl}}}{p_{\mathrm{cyl}} \cdot \cancel{V_{\mathrm{cyl}}}} = \frac{\mathrm{d}T_{\mathrm{cyl}} \cdot \cancel{m_{\mathrm{cyl}} \cdot R}}{T_{\mathrm{cyl}} \cdot \cancel{m_{\mathrm{cyl}} \cdot R}}$$

$$\frac{\mathrm{d}V_{\mathrm{cyl}}}{V_{\mathrm{cyl}}} + \frac{\mathrm{d}p_{\mathrm{cyl}}}{p_{\mathrm{cyl}}} = \frac{\mathrm{d}T_{\mathrm{cyl}}}{T_{\mathrm{cyl}}} \tag{6.7}$$

The gas constant and the adiabatic exponent are defined as:

$$\kappa = \frac{\mathrm{c}_p}{\mathrm{c}_v} \tag{6.8}$$

$$R = \mathrm{c}_p - \mathrm{c}_v \tag{6.9}$$

Equations 6.4, 6.5, 6.7, 6.8 and together with 6.9 give an equation for the approximation of the rate of heat release during the combustion.

$$\frac{\mathrm{d}Q_{\mathrm{h}}}{\mathrm{d}\varphi} = \frac{1}{\kappa - 1} \cdot \left[\frac{\kappa \cdot \mathrm{d}p_{\mathrm{cyl}} \cdot \mathrm{d}V_{\mathrm{cyl}}}{\mathrm{d}\varphi} + \frac{V_{\mathrm{cyl}} \cdot \mathrm{d}p}{\mathrm{d}\varphi} \right] \tag{6.10}$$

For a simple use of this equation the differential equation is replaced by a discrete approximation. It is common practice to use the central difference quotient. The central difference quotient applied on equation 6.10 gives:

$$\frac{\Delta Q_{\mathrm{h}}}{\Delta\varphi} = \frac{1}{\kappa - 1} \cdot \left[\frac{\kappa \cdot \mathrm{d}p_{\mathrm{cyl}} \cdot (V_{\mathrm{i}+1} - V_{\mathrm{i}-1})}{\varphi_{\mathrm{i}+1} - \varphi_{\mathrm{i}-1}} + \frac{\mathrm{V} \cdot (p_{\mathrm{i}+1} - p_{\mathrm{i}-1})}{\varphi_{\mathrm{i}+1} - \varphi_{\mathrm{i}-1}} \right] \tag{6.11}$$

In case of an engine with manifold fuel injection κ is assumed constant with 1.32.

6.2 Calculation of the efficiency due to the unburned fuel within the exhaust gas

At several investigations the residual gas emissions consist out of a big fraction of hydrocarbon and carbon monoxide. This high amount of emissions can be explained by high scavenging losses and the uncompleted combustion. This fraction of fuel could be mainly converted into indicated work within the cylinder if the combustion would occur with a better efficiency. This approach would rise the efficiency of the engine. Due to the following calculations the efficiency due to a better combustion can be assessed.

6.2.1 Air requirement

First of all the stoichiometric air-to-fuel ratio needs to be determined. The mass fractions of the fuel were determined by means of a fuel analysis. The used petrol has the following mass fraction which are related to 1 kg of fuel:

- carbon fraction of 84.07 %
- hydrogen fraction of 13.22 %
- oxygen fraction of 2.71 %

In order to obtain the mole fraction the mass fraction have to be divided by the molar mass M_x of each species.

$$\mathrm{C} = \frac{\mathrm{c_m}}{M_\mathrm{C}} = \frac{0.8407}{12} \frac{\frac{\mathrm{kg_C}}{\mathrm{kg_{fuel}}}}{\frac{\mathrm{kg_C}}{\mathrm{kmol_C}}} = 0.07 \frac{\mathrm{kmol_C}}{\mathrm{kg_{fuel}}} \tag{6.12}$$

$$\mathrm{H} = \frac{\mathrm{h_m}}{M_\mathrm{H}} = \frac{0.1322}{1.008} \frac{\frac{\mathrm{kg_H}}{\mathrm{kg_{fuel}}}}{\frac{\mathrm{kg_H}}{\mathrm{kmol_H}}} = 0.13115 \frac{\mathrm{kmol_H}}{\mathrm{kg_{fuel}}} \tag{6.13}$$

$$\mathrm{O} = \frac{o_\mathrm{m}}{M_\mathrm{O}} = \frac{0.1322}{1.008} \frac{\frac{\mathrm{kg_O}}{\mathrm{kg_{fuel}}}}{\frac{\mathrm{kg_O}}{\mathrm{kmol_O}}} = 0.001693 \frac{\mathrm{kmol_O}}{\mathrm{kg_{fuel}}} \tag{6.14}$$

The fractions is related to carbon.

$$\frac{\mathrm{H}}{\mathrm{C}} = 1.874 \frac{\mathrm{kmol_H}}{\mathrm{kmol_C}}$$

$$\frac{\mathrm{O}}{\mathrm{C}} = 0.02418 \frac{\mathrm{kmol_O}}{\mathrm{kmol_C}}$$

The chemical composition of the fuel can be written as $C_1H_{1.874}O_{0.02418}$. Allowing for the chemical composition of the fuel the chemical equation may be written as follows:

$$C_1H_{1.874}O_{0.024185} + O_{2_{min}} \overbrace{\left(1 + \frac{1.874}{4} - \frac{0.0242}{2}\right)}^{O_{2_{min}}=1.4564} = CO_2 + \frac{1.874}{2}H_2O \tag{6.15}$$

Due to the oxygen demand which is apparent in equation 6.15, the air demand can be calculated through a division by 0.21 because of the fact that the fraction of oxygen within the air amounts 21%.

$$L_{min}^{mol} = \frac{O_{2_{min}}}{0.21} = \frac{1.4564}{0.21} \frac{\frac{kmol_{O2}}{kmol_{fuel}}}{\frac{kmol_{O_2}}{kmol_{air}}} = 6.9352 \frac{kmol_{air}}{kmol_{fuel}} \tag{6.16}$$

The molar mass of the fuel can be calculated using the volume fraction of every single species.

$$M_{fuel} = 1 \cdot M_C + 1.872 \cdot M_H + 0.0242 \cdot M_{O_2} = 14.26 \frac{kg_{fuel}}{kmol_{fuel}} \tag{6.17}$$

In order to ensure an easier handling of the air demand it is related to fuel mass. Together with the molar mass of technical air,

$$M_{air} = 28.84 \frac{kg_{air}}{kmol_{air}}$$

the air demand amounts:

$$L_{min} = L_{min}^{mol} \frac{M_{air}}{M_{fuel}} = 6.9352 \frac{kmol_{air}}{kmol_{fuel}} \frac{28.84}{14.26} \frac{\frac{kg_{air}}{kmol_{air}}}{\frac{kg_{fuel}}{kmol_{fuel}}} = 14.026 \frac{kg_{air}}{kg_{fuel}} \tag{6.18}$$

6.2.2 Amount of exhaust gas

Dry atmospheric air consists out of 21% oxygen, 78% nitrogen and 1% of other gases. However for this thermodynamic approach the portion of 1% of other gases is replaced by an equal amount of nitrogen. Thus, within this computation atmospheric air consist of 21% oxygen and 79% nitrogen. Due to this fact the amount of nitrogen can be calculated according the following equation

$$n_{N_2} = L_{min}^{mol} \cdot 0.79 = 5.479 \frac{kmol_{N_2}}{kmol_{fuel}} \tag{6.19}$$

In order to obtain the overall moist exhaust gas the other fractions like water steam and carbon dioxide have to be considered. Water steam and carbon dioxide are the

results of equation 6.15. In operating points with air excess an additional term have to be considered. This calculations are performed without air excess.

$$n_{\mathrm{ae}} = L_{\mathrm{min}}^{\mathrm{mol}} \cdot (\lambda - 1)$$

$$n_{\mathrm{ex_m}} = n_{\mathrm{N_2}} + n_{\mathrm{CO_2}} + n_{\mathrm{H_2O}} + n_{\mathrm{ae}}$$
$$= 5.479 \frac{\mathrm{kmol_{N_2}}}{\mathrm{kmol_{fuel}}} + 1 \frac{\mathrm{kmol_{CO_2}}}{\mathrm{kmol_{fuel}}} + \frac{1.874}{2} \frac{\mathrm{kmol_{H_2}}}{\mathrm{kmol_{fuel}}} + 0 \frac{\mathrm{kmol_{ae}}}{\mathrm{kmol_{fuel}}} = 7.416 \frac{\mathrm{kmol_{sg_m}}}{\mathrm{kmol_{fuel}}} \quad (6.20)$$

For the calculation of the residual heat within the exhaust gas, the amount of dry exhaust gas is necessary. The determination of hydrocarbon emissions takes place through an analyser which cool down the exhaust gas until steam is condensed.

$$n_{\mathrm{ex_m}} = n_{\mathrm{N_2}} + n_{\mathrm{CO_2}} = 5.479 \frac{\mathrm{kmol_{N_2}}}{\mathrm{kmol_{fuel}}} + 1 \frac{\mathrm{kmol_{CO_2}}}{\mathrm{kmol_{fuel}}} + 0 \frac{\mathrm{kmol_{ae}}}{\mathrm{kmol_{fuel}}} = 6.479 \frac{\mathrm{kmol_{sg_d}}}{\mathrm{kmol_{fuel}}} \quad (6.21)$$

6.2.3 Residual heat within the exhaust gas

The fractions within the exhaust gas which include a certain amount of residual heat are CO, HC and H_2. During the investigations H_2 was not considered, due to the fact that the analyser did not exist.

$$Q_{\mathrm{CO}} = CO_{\mathrm{ppm}} \cdot n_{\mathrm{exg_d}} \cdot M_{\mathrm{CO}} \cdot H_{\mathrm{CO}} \quad (6.22)$$

In equation 6.22, CO_{ppm} states the volume fraction of carbon monoxide within the exhaust gas which is delivered from the exhaust gas analyser. CO_{ppm} multiplied by the amount of exhaust gas and M_{CO} which states the molar mass of carbon monoxide, results in the mass fraction of CO. In order to determine the residual heat within the exhaust gas due to CO, the mass fraction has to be multiplied by the caloric value of CO.

$$Q_{\mathrm{HC}} = HC_{\mathrm{ppm}} \cdot n_{\mathrm{exg_m}} \cdot M_{\mathrm{fuel}} \cdot H_{\mathrm{U}} \quad (6.23)$$

The approach to determine the residual heat of HC within the exhaust gas is similar to 6.22 at this consideration, with the difference that the amount of moist exhaust gas has to be considered as mentioned before. Equation 6.23 is an approximation since the exact determination of the composition of the species which includes carbon and hydrogen is a formidable task.

The overall usable energy within the exhaust gas is the sum of Q_{CO} and Q_{HC}.

$$Q_{\mathrm{exg}} = Q_{\mathrm{CO}} + Q_{\mathrm{HC}} \quad (6.24)$$

One assumption in order to determine the amount of H_2 can made with the approximation formula according to Witt. This equation assumes that H_2 corresponds to one third of the amount of CO. This approximation can only be applied at sociometric operating points. [23]

$$Q_{H_2} = \frac{1}{3} \cdot CO_{\text{ppm}} \cdot n_{\text{exg}_\text{m}} \cdot M_{H_2} \cdot H_{H_2} \tag{6.25}$$

This calculation does not include H_2.

6.2.4 Calculation of corrected efficiency

The indicated efficiency is calculated according to the following equation:

$$\eta_\text{i} = \frac{\text{W}_\text{ind}}{\text{m}_\text{fuel} \cdot H_\text{U}} \tag{6.26}$$

In order to determine the amount of unburned fuel a coefficient is defined according the following equation:

$$\eta_\text{cf} = \frac{\eta_\text{i}}{\eta_{\text{i}_\text{corr}}} = \frac{\frac{\text{W}_\text{ind}}{\text{m}_\text{fuel} \cdot H_\text{U}}}{\frac{\text{W}_\text{ind}}{\text{m}_\text{fuel} \cdot H_\text{U} - Q_\text{exg}}} = \frac{\text{m}_\text{fuel} \cdot H_\text{U} - Q_\text{exg}}{\text{m}_\text{fuel} \cdot H_\text{U}} \tag{6.27}$$

η_cf gives a statement about the conversion of the fuel and is called fuel conversion factor.

$\eta_{\text{i}_\text{corr}}$ is calculated by dividing the indicated efficiency by the fuel conversion factor. It is assumed that the residual heat within the exhaust gas can be converted into usable work which is done on the piston with the efficiency of η_i.

$$\eta_{\text{i}_\text{corr}} = \frac{\eta_\text{i}}{\eta_\text{cf}} \tag{6.28}$$

6.3 Calculation of compression work within the supercharged operation

The compressed air at the supercharged operation was provided by the building services. In order to make an useful estimation of the efficiency possible the work which is necessary to compress the air has to be determined.

A process in which the velocities of inflow and outflow are constant with respect to time is called steady-flow process. It is assumed that the velocities and internal energy across the entrance and exit sections are constant. Considering that, the first law of thermodynamics can be written as:

$$w_\text{t} = h_2 - h_1 \tag{6.29}$$

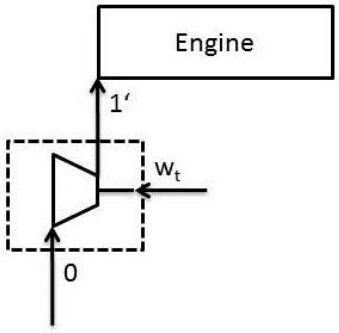

Figure 6.1: Schematic view and boundaries of a compressor

Air is considered as a perfect gas and therefore the enthalpy can be written as:

$$w_{\mathrm{ts}} = \mathrm{c}_p \cdot (T_{2\mathrm{s}} - T_1) = \mathrm{c}_p \cdot T_1 \cdot \left(\frac{T_{2\mathrm{s}}}{T_1} - 1 \right) \tag{6.30}$$

By taking the equations for an isentropic change in status into account it gives

$$w_{\mathrm{ts}} = \mathrm{c}_p \cdot T_1 \cdot \left(\frac{p_2}{p_1}^{\frac{\kappa-1}{\kappa}} - 1 \right) \tag{6.31}$$

By taking the relations of the ideal gas equation into account and consider the relation for the isentropic exponent the equation for the calculation of the isentropic work can be expressed as:

$$w_{\mathrm{ts}} = \frac{\kappa}{\kappa - 1} \cdot T_1 \cdot R \cdot \left(\frac{p_2}{p_1}^{\frac{\kappa-1}{\kappa}} - 1 \right) \tag{6.32}$$

The foregoing equation contains the conditions at the entrance of the system, the pressure ratio between the entrance and exit and the properties of the gas.

The compressor work is calculated by using the isentropic efficiency η_{sc}. The isentropic efficiency is assumed with 0.7.

$$w_{\mathrm{t}} = \frac{w_{\mathrm{ts}}}{\eta_{\mathrm{sc}}} \tag{6.33}$$

The difference of efficiency is calculated according to equation 6.34.

$$\Delta\eta_{\mathrm{c}} = \frac{W_{\mathrm{t}}}{Q_{\mathrm{fuel}}} = \frac{w_{\mathrm{t}} \cdot m_{\mathrm{air}}}{Q_{\mathrm{fuel}}} \tag{6.34}$$

η_{ic} contains the indicated efficiency of the engine subtracted by the efficiency which contains the required work for the compressor.

$$\eta_{\mathrm{ic}} = \eta_{\mathrm{i}} - \Delta\eta_{\mathrm{c}} \qquad \eta_{\mathrm{ec}} = \eta_{\mathrm{e}} - \frac{\Delta\eta_{\mathrm{c}}}{\eta_{mc}}$$

6.4 Methods

The naturally aspirated operating points of the technology carrier and the reference engine contain a loss analysis which was carried out with a simulation software owned by *TU Graz*. Because of the unconventional volume course and therefore different piston velocities during the compression stroke compared to the expansion stroke several routines and approaches needed to be changed. The further section briefly describes some approaches and theoretical models which are changed to be suitable for the use at the technology carrier.

6.4.1 Theoretical models and the approach of the simulation software

One of the major unknown quantities at the extended expansion engine is the heat transfer, respectively the heat transfer coefficient. The used model for the heat transfer is that of Woschni/Huber which was originally developed by Woschni in 1965, especially for diesel engines. The modified version is written as follows:

$$\alpha = 130 \cdot d^{-0.2} \cdot p_{\mathrm{cyl}}^{0.8} \cdot T^{-0.53} \left(\mathrm{C_1} \cdot \mathrm{C_m} \cdot \left(1 + 2 \left(\frac{V_{\mathrm{TDC}}}{V_{\mathrm{cyl}}} \right)^2 \cdot IMEP^{-0.2} \right) \right)^{0.8} \tag{6.35}$$

The equation includes d as the cylinder bore diameter, p_{cyl} represents the cylinder pressure and T is the current temperature within the cylinder. V_{cyl} defines the cylinder volume. $\mathrm{C_1}$ is a dimensionless constant in order to make a description of different engine types possible.

Whereby $\mathrm{C_m}$ defines the averaged piston velocity. Since the analysis software automatically used the expansions volume, respectively the averaged piston velocity during the expansion stroke the wall heat losses were initially to high. An additional factor was implemented into the analysis software in order to make it possible to influence the wall heat factor.

During the compression of the charge mass the behaviour of the extended expansion engine and a conventional engine is similar. Since the piston have to cover nearly double the distance at the expansion the wall heat flow is obviously higher compared to conventional engines.

The great expansion stroke delivers a higher averaged piston velocity during the expansion phase and therefore a higher wall heat factor. Near to the TDC the piston velocity of both engine types is similar and therefore it is unlikely that the heat transfer factor is determined by the averaged piston velocity at the expansion stroke immaterially after TDC. Therefore in the evaluation software a variable heat transfer was implemented which allows a shifting of the heat transfer coefficient at a certain

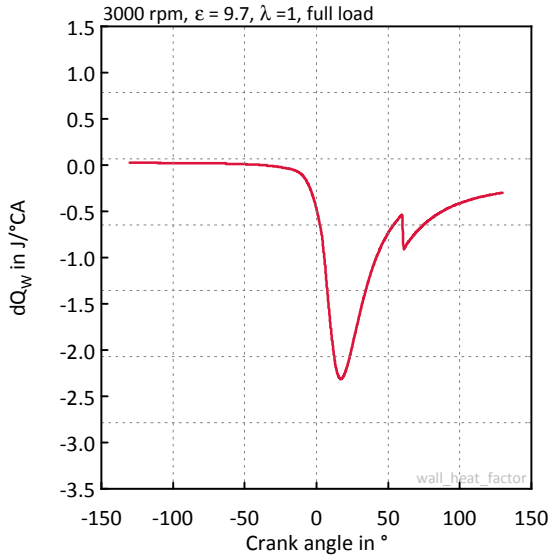

Figure 6.2: Shifting the wall heat coefficient

degree of crank angle. After several simulation results and measurements the description of the wall heat losses shown to be suitable for a shift of the wall heat coefficient at 60 °CA after TDC. This was a great finding during these investigations and is apparent in figure 6.2.

Until the jump in the wall heat factor it is multiplied by 0.574. C_m is the most determining quantity for the wall heat losses and the term ${C_m}^{0.8}$, which can be abstracted from equation 6.35 equates 0.574. Afterwards the wall heat losses was determined by the averaged piston velocity during the expansion stroke.

6.4.2 Determination of the Indicated Mean Effective Pressure during low pressure and high pressure cycle

The low pressure cycle is no more unambiguous closed as at conventional engines. This fact is visual in figure 6.3a. Therefore the following approach was applied in order to make a comparison between a conventional engine and an extended expansion engine possible.

$$W_{\mathrm{ind}} = \oint p_{\mathrm{cyl}} \mathrm{d}V_{\mathrm{cyl}} \tag{6.36}$$

The calculation of the $IMEP_{\mathrm{HPC}}$ as well as $IMEP_{\mathrm{LPC}}$ would include the area form the additional volume to the reference pressure - in this case it is zero bar - apparent as p_{ref} in figure 6.3a. Apparent as the intersection of the light blue area and the hatched area. Since the intake as well as the expansion volume is equal at conventional engines the level of the reference pressure is indifferent.

Therefore the pressure during intake was averaged and defined as the reference pressure for the calculation of $IMEP_{\mathrm{HPC}}$ and $IMEP_{\mathrm{LPC}}$ apparent in figure 6.3b. The calculation of $IMEP_{\mathrm{HPC}}$ and $IMEP_{\mathrm{LPC}}$ is performed according to 6.37.

$$W_{\mathrm{ind}} = \underbrace{\int_{V_1=349}^{V_2=699} (p_{\mathrm{cyl}} - p_{\mathrm{ref}})\,\mathrm{d}V_{\mathrm{cyl}}}_{=IMEP_{\mathrm{HPC}}} + \underbrace{\int_{V_1=699}^{V_2=349} (p_{\mathrm{cyl}} - p_{\mathrm{ref}})\,\mathrm{d}V_{\mathrm{cyl}}}_{=IMEP_{\mathrm{LPC}}} \tag{6.37}$$

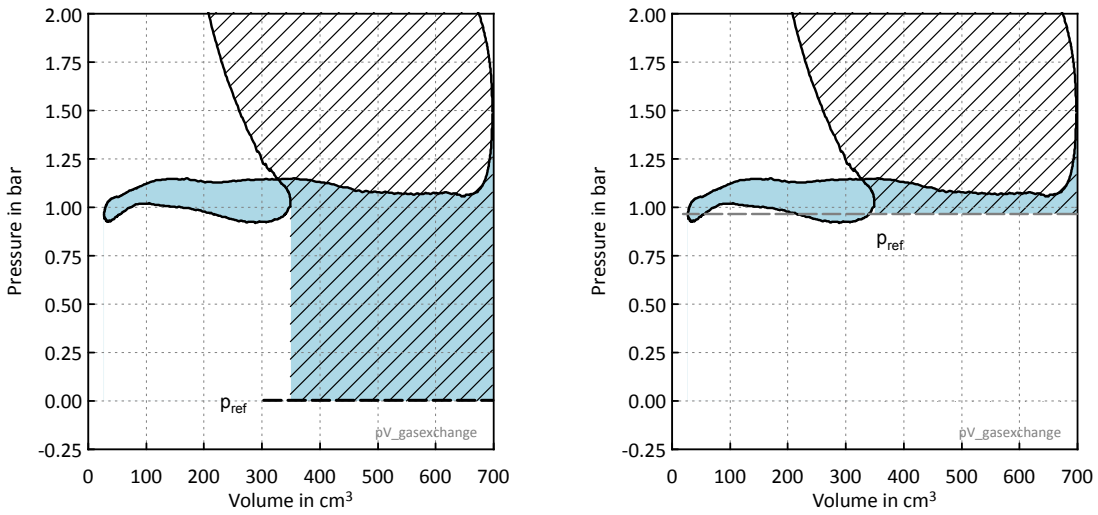

(a) Determination of $IMEP_{\mathrm{HPC}}$ and $IMEP_{\mathrm{LPC}}$ (I)

(b) Determination of $IMEP_{\mathrm{HPC}}$ and $IMEP_{\mathrm{LPC}}$ (II)

Figure 6.3: Determination of $IMEP_{\mathrm{HPC}}$ and $IMEP_{\mathrm{LPC}}$

6.4.3 Loss analysis

The loss analysis is an appropriate measure in order to determine the sources and the amount of different losses. For this purpose the efficiency of the fuel-air cycle with real charge considering the chemical equilibrium is calculated. In this case it would be 47.6 %, apparent by the light blue bar in figure 6.4. The apparent loss analysis is related to the reference engine at 3000 rpm and full load.

The next step includes a calculation of the efficiency allowing for the boundary condition which was made before and furthermore the unburned fuel fractions in the exhaust. The operation of an engine with these boundary conditions would deliver and efficiency of 45.50 %. This efficiency can be seen at the second bar in figure 6.4. The same bar contains the difference which is caused by the additional assumption. At this operating point the consideration of the unburned fuel fraction in the exhaust gas

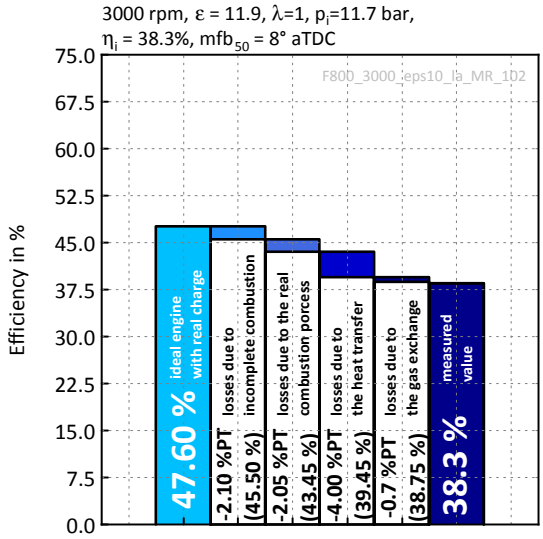

Figure 6.4: Loss analysis

compared to the fuel-air cycle with real charge considering the chemical equilibrium reduces the efficiency of about 2.10 %PT. The coloured area above shows the amount of the current loss related to the efficiency which was reached before.

The third bar contains all losses considered before and in addition allowing for the real combustion process which would deliver an efficiency of 43.45 % on the ideal engine. The difference between the second and the third bar is 2.05 %PT.

39.45 % is the efficiency which can be achieved when the heat transfer of the ideal engine is equal to the real engine. The achievable efficiency is furthermore reduced by 4.00 %PT due to the heat transfer.

38.75 % defines the efficiency where all losses before and the gas exchange losses are considered.

38.3 % is the real measured value.

The deviation results in 0.45 %PT between the real measured value, 38.3% and the efficiency which is calculated by the the loss analysis software, 38.75%.

7 Results of measurements

This chapter contains the results and analysis of the measurements.

Two different engines, each in various hardware configurations, were used to carry out investigations of several topics concerning extended expansion. An overview of the discussed engines, configurations and measurement numbers gives table 7.1.

Within this chapter the discussion of each topic is complemented with an overview plot on the page before (e.g. figure 7.1 for section 7.1. *Reference Engine*) which shows the most important measurement results. The results related to the actual discussion are always plotted in red continuous lines. For comparison each overview plot contains also suitable other results, depending on the actual content. Please refer to table 7.1 for the page reference of the overview plots.

Table 7.1: Results of measurements

Engine	Speed	Compression ratio	Description	Page/MR
F800	3000	11.9	Original configuration, WOT	68/111
	3000	11.9	Filling cam shaft, WOT	68/102
	3000	11.9	Miller, WOT	72/113
	3000	11.9	Miller-Supercharged	94/115-118
	3000	11.9	Tumblesheet	100/146
	3000	17.7	Miller	86/133
	3000	17.7	Miller-Supercharged	90/137-139
	3000	17.7	Miller-λ-Variation	97/136
Technology carrier	3000	9.7	WOT	76/167
	3000	9.7	Supercharged	90/175-178
	3000	9.7	λ-Variation	97/174
	3000	9.7	Coolant temperature of $100°C$	103/172
	3000	12.45	WOT	86/191
	3000	12.45	Supercharged	90/187-189
	3000	12.45	λ-Variation	97/185
	3000	12.45	Tumblesheet	101/184
	3000	12.45	Coolant temperature of $100°C$	104/193

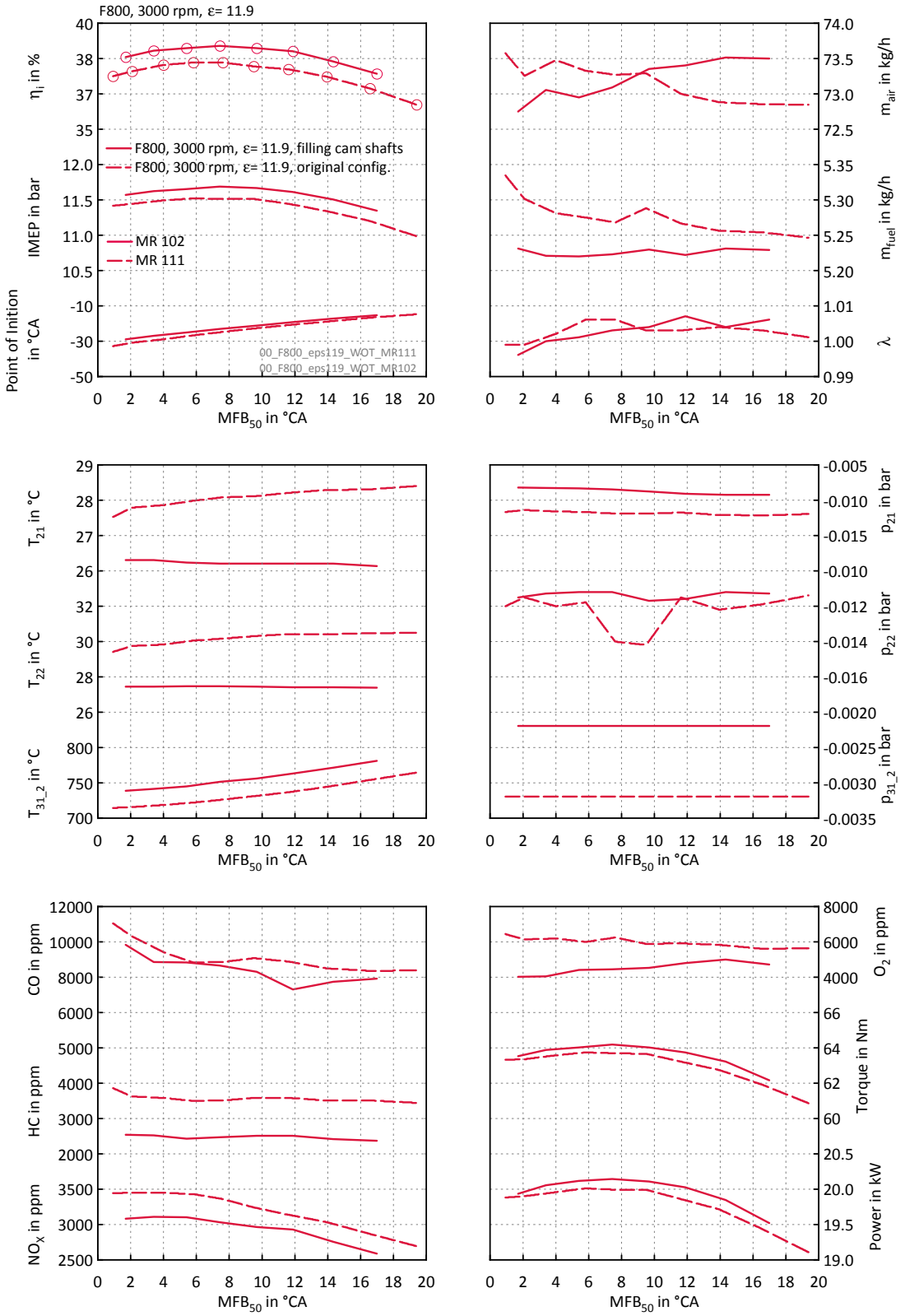

Figure 7.1: F800, 3000 rpm, ε=11.9, WOT, Original configuration and filling cam shaft

7.1 Reference engine

(Result overview see figure 7.1)

The reference engine which is also used in mass production was measured within a wide map region. The target was finding the point with the highest efficiency at several speeds to make a comparison between the reference engine and the technology carrier possible. The most important operating point was the highest efficiency at 3000 rpm and full load

In mass production the cylinder head is used in a motorcycle and it is designed for a maximum of charge, without any in-cylinder gas motion. It is assumed that the high hydrogen and carbon monoxide emissions occur due to the incomplete combustion and/or due to scavenging losses.

7.1.1 Naturally aspirated

The following section shows the comparison of two different configurations of the reference engine.

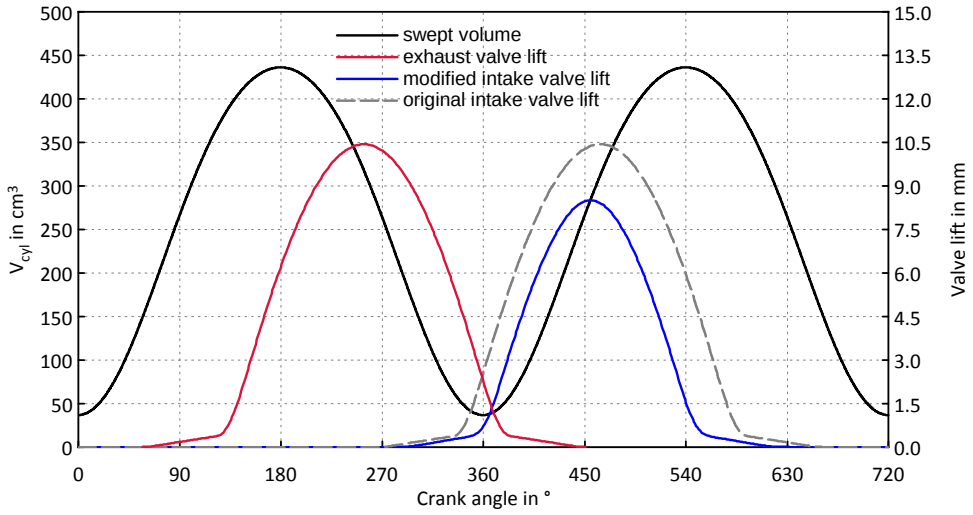

Figure 7.2: Valve lift curves of the reference engine

Firstly the reference engine with the valve timing which is also used in mass production, visible as the dashed grey line in figure 7.2 and secondly the valve timing which is specifically made for these investigations, visible as the continuous blue line. Only the intake cam shaft is modified in order to increase the efficiency at 3000 rpm.

Both configurations are apparent in figure 7.2. Furthermore the intake cam shaft was also used at the technology carrier. From now on only the reference engine with the filling cam shaft serves for the comparison.
Figure 7.3 shows the $IMEP$ vs. Mass fraction burned (MFB_{50}). The highest indicated efficiency which can be reached with the original configuration is about 37.8 %. By means of a modified intake cam shaft an efficiency can be achieved which is 0.5 %PT higher than the efficiency with the original configuration - visual in figure 7.3a. This full load curve differs to the full load curve of the series application due to the fact that during these investigations the engine was operated stoichiometric. In general petrol engines operate rich at full load in order to protect the components or avoid knocking. Furthermore the highest torque can also be reached due to a rich operation.

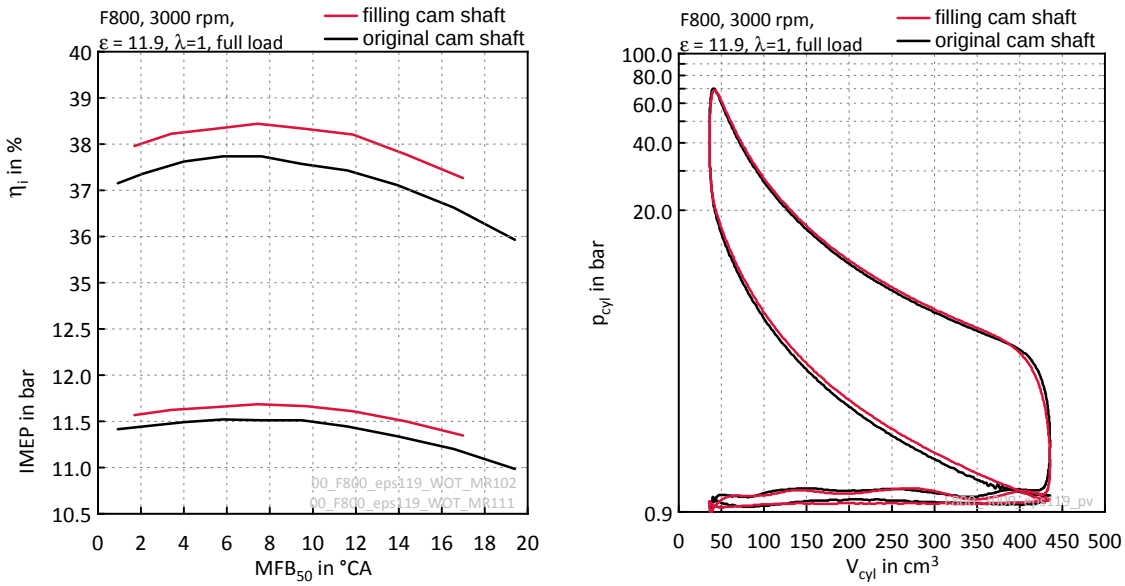

(a) $IMEP$ vs. MFB_{50} and efficiency (b) pV-diagram

Figure 7.3: Reference engine with different configurations, ε=11.9

Figure 7.3b shows the pressure-volume diagram of both configurations. As it is clearly apparent the pressure level of the engine with the modified valve timing is higher during the compression and expansion, compared to the original configuration. A lower amount of residual gas and the higher volumetric efficiency positively influence the efficiency.

The amount of air at both configurations is nearly equal at the highest efficiency but the O_2 emissions are higher at the original configuration which let assume that the scavenging losses are higher (see figure 7.1).

The higher NO_x level at the original configuration, which goes along with higher combustion temperatures let suppose that the amount of residual gas is higher com-

pared to the modified configuration. Also the higher temperature after the throttle flap at the original configuration could be an effect of back expelling of residual gas.

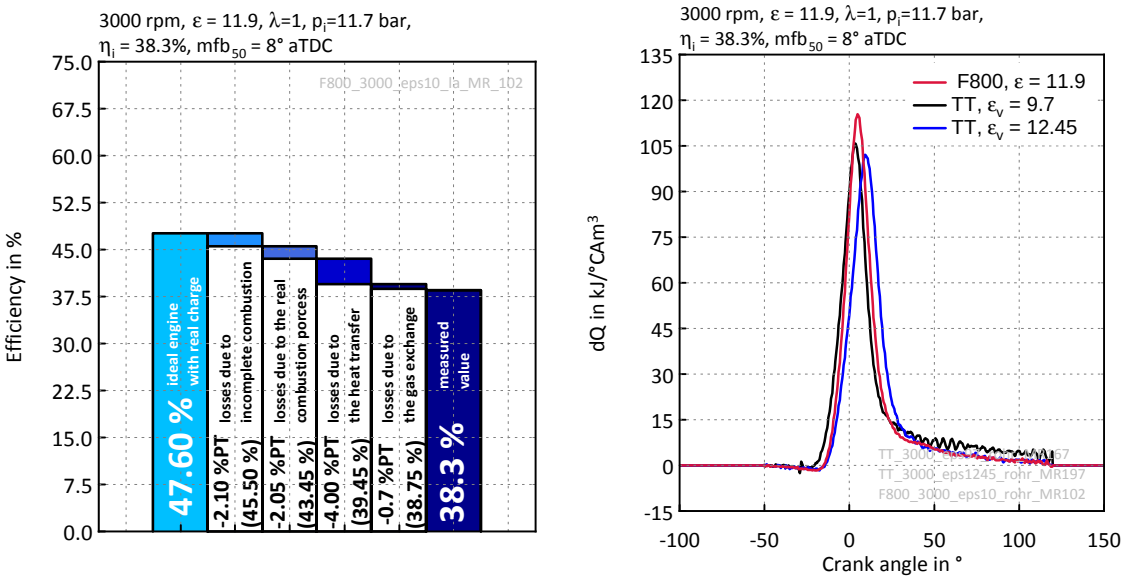

(a) Loss analysis

(b) $ROHR$ vs. °CA

Figure 7.4: Loss analysis and $ROHR$

Figure 7.4a shows the loss analysis of the reference engine with the highest efficiency. The deviation results in 0.45 %PT between the measured value and the efficiency which is calculated by the the loss analysis software.

Between the ideal and the real engine is a difference of 9.3 %PT. The biggest losses occur due to the wall heat losses as it is apparent in figure 7.4a. The fraction of the wall heat losses is more than 40 % of the entire losses. Figure 7.4b shows the $ROHR$ of the reference engine and for comparison the $ROHR$ of the technology carrier with different compression ratios. The pressure increase at the beginning of the combustion occurs much faster at the reference engine compared to the technology carrier.

The combustion duration between MFB_{05} and MFB_{90} at the reference engine is about 40 °CA. The combustion duration at the technology carrier needs up to 60 °CA.

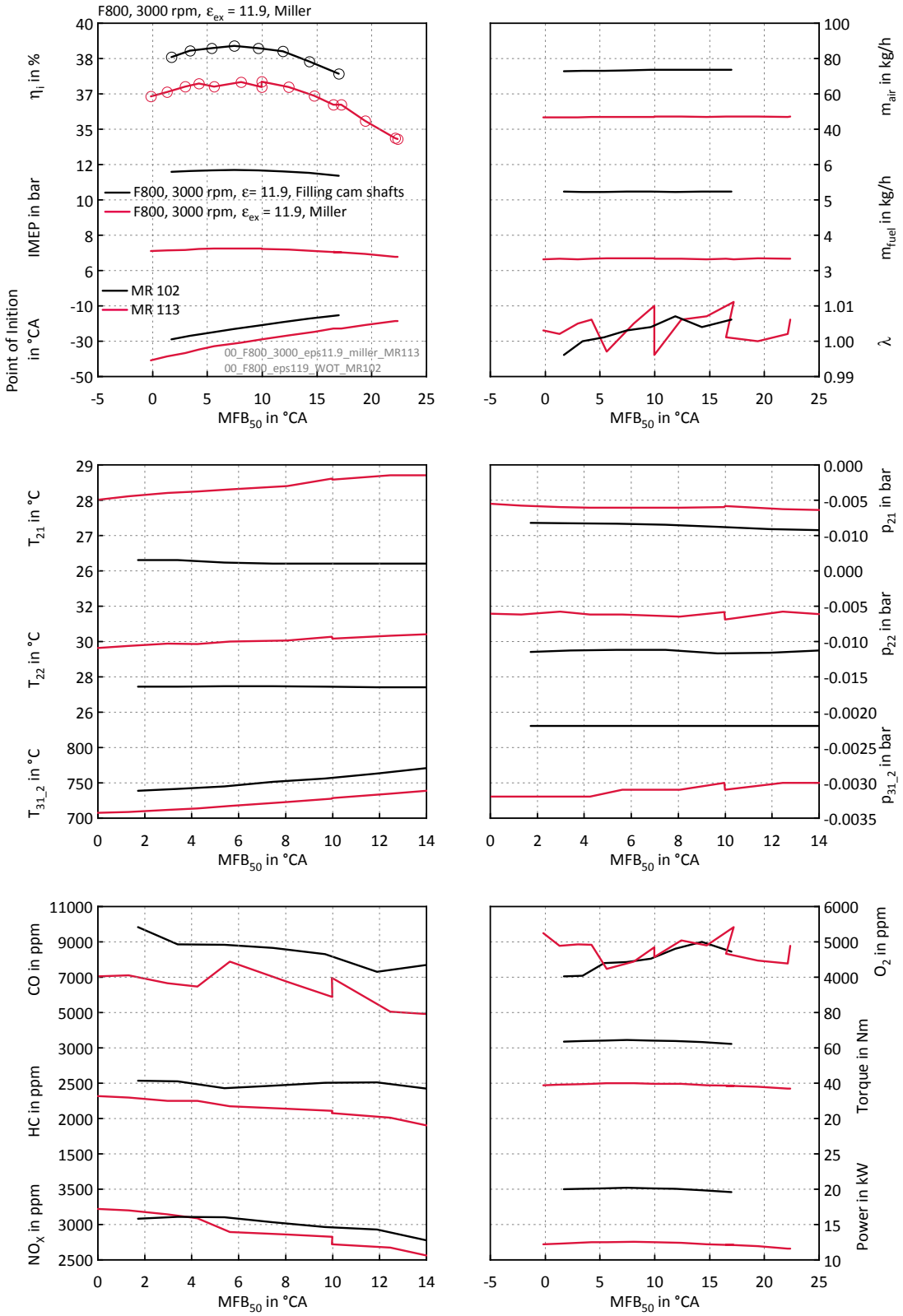

Figure 7.5: F800, 3000 rpm, ε=11.9, Miller and filling cam shaft

7.2 Miller vs. reference engine - Miller as a strategy to reduce gas exchange losses

(Result overview see figure 7.5)

In order to determine the potential of the Miller strategy compared to the conventional concept the reference engine was fitted with an intake cam shaft which was specifically made for these investigations. The valve lift curves related to crank angle can be seen in figure 7.6. The red continuous line represents the exhaust valve lift curve which is unchanged to the original configuration. The blue continuous line represents the valve lift curve of the Miller cam shaft. The grey broken line represents the intake valve lift curve of the conventional engine. The ε_c is unchanged for these Miller investigations with 11.9.

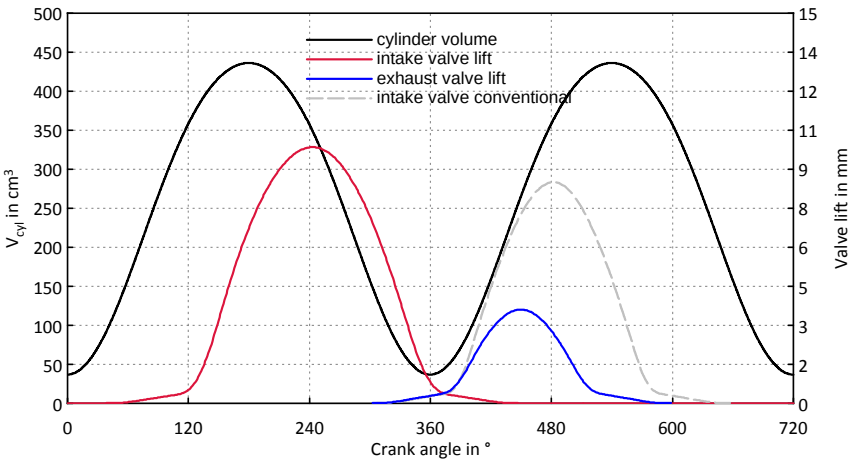

Figure 7.6: Valve timing at Miller strategy

Due to the shorter intake valve opening the charge mass within the cylinder at full load is lower compared to full load at conventional valve timing. Thus the lower amount of charge mass delivers a lower load point compared to the conventional engine.

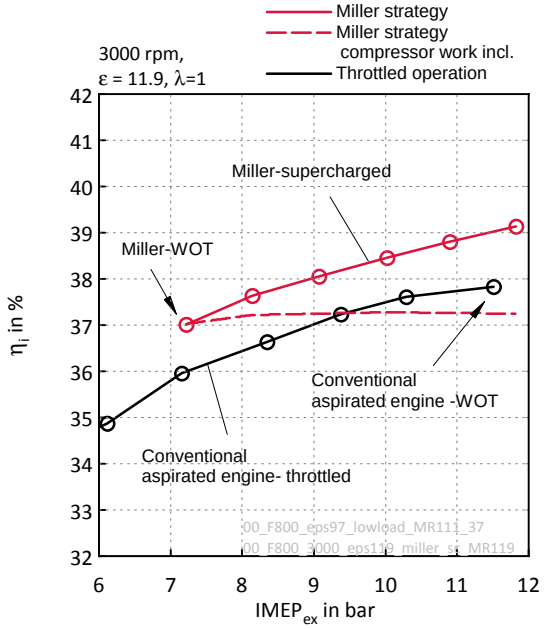

(a) $IMEP$ vs. MFB_{50} and efficiency - throttled operation and Miller strategy

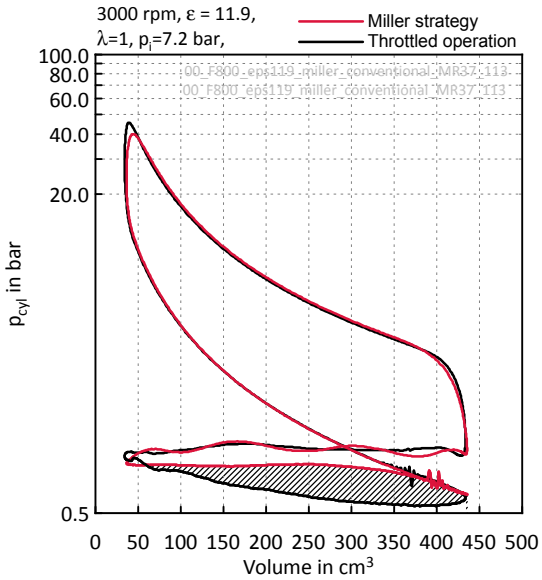

(b) pV-diagram - throttled operation and Miller strategy

Figure 7.7: Throttled operation and Miller strategy, ε_c=11.9

Figure 7.7a shows the course of the efficiency. The red line represents the Miller strategy and the red dashed line includes the work which is necessary for the compression of the charge mass due to the supercharger. For a more detail description at supercharged operating points see section 7.6.

In figure 7.7b the pressure course related to the cylinder volume can be seen. At the end of the intake stroke firstly the expansion until BDC takes place and secondly the compression. Using the valve timing which is shown in figure 7.6 an $IMEP_{ex}$ of about 7.2 bar can be reached at full load. The engine fitted with the conventional valve timing reaches an $IMEP$ of 11.7 bar at full load.

It is clearly apparent that the gas exchange losses at the Miller strategy are significantly lower compared to the conventional concept - visual by the hatched area in figure 7.7b.

At conventional spark ignition engines the pressure gradient between ambient pressure and the pressure in the cylinder during the aspiration at throttled operating points produces losses. Unlike the conventional engine at the Miller strategy the low load operating points are reached due to the valve timing. The earlier intake closure limits the fresh charge within the cylinder and therefore the load point. The closure of the intake valve begins about 270 cm^3 and ends at 370 cm^3. After the intake valve is closed the expansion begins, until BDC is reached. Afterwards the compres-

sion begins. Due to the lower temperature at BDC at the Miller strategy the peak temperature and pressure is much lower at the same MFB_{50}.

Due to the reduced gas exchange losses and the lower heat capacity of the gas mixture within the cylinder at lower peak temperatures, the efficiency increases. Furthermore the NO_x formation can be reduced due to the lower temperature level.

The difference of efficiency between the conventional approach and the Miller strategy at an $IMEP_{ex}$ of 7.2 bar is about 1 %PT.

In order to increase the load point the charge mass must be increased. In this case it was performed by supercharging. Since the required work for the compression of the charge mass strongly rises, the overall efficiency of the Miller strategy drops down under the efficiency of the engine with the conventional approach - visual by the dashed line in figure 7.7a Using the Miller strategy for the entire load control with the main target to rise the efficiency at the entire map a variable valve timing system is necessary. The difference of efficiency between the conventional approach and the Miller strategy at the same $IMEP_{ex}$ rises with decreasing load. The course of the efficiency would be similar to the course which can be seen in figure 2.4.

This investigations was performed without a variable valve system and therefore the potential of the Miller strategy as a load control strategy can only be shown for one load point - 7.2 bar.

Without a variable compression ratio the highest achievable efficiency of the Miller strategy is lower compared to the highest efficiency at the conventional approach at full load. This fact is also visual in figure 2.4. The maximum potential of the Miller strategy can only be reached by a variable compression ratio. Investigations on the engine with Miller strategy and a higher compression ratio can be seen in section 7.5.

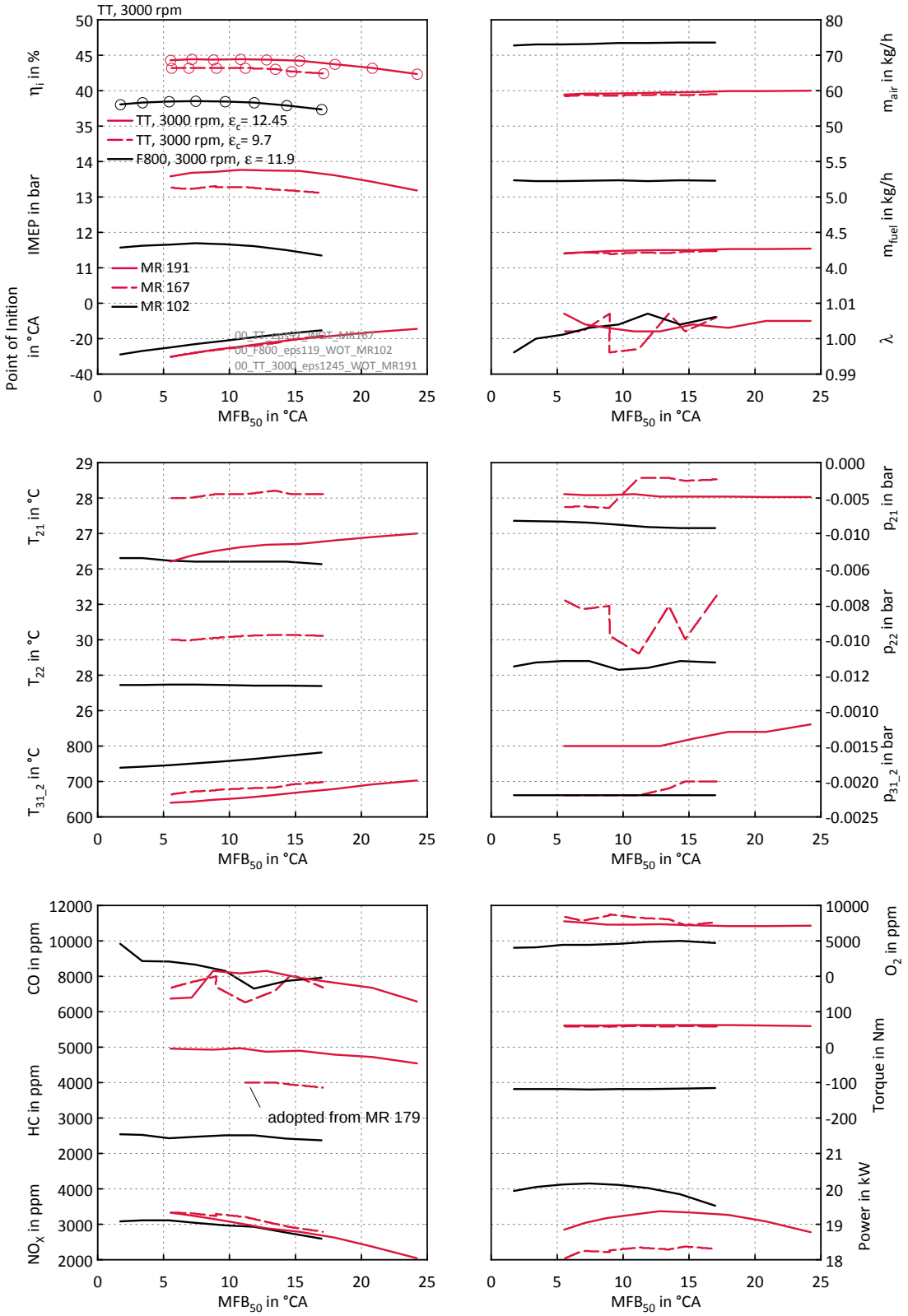

Figure 7.8: TT, 3000 rpm

7.3 Technology carrier

(Result overview see figure 7.8)

The following section shows measurements at 3000 rpm which is the most important comparative speed to the reference engine. The technology carrier was fitted with the valve timing which is apparent in figure 7.9. The adjustment of the valve timing was used for the naturally aspirated as well as for the supercharged operating points. The shifted valve lift curves compared to the conventional concept are due to the overlapping of both oscillations. The position of TDC during the gas exchange is shifted about 360 + 35 degrees compared to the position of TDC during the combustion.

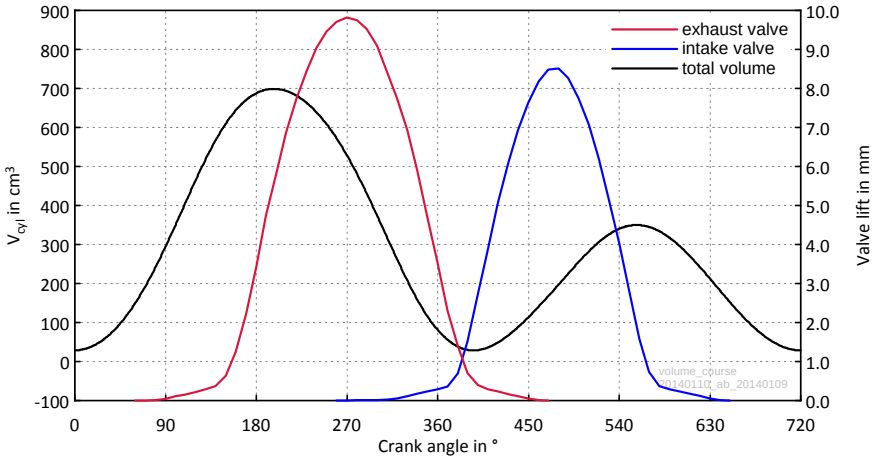

Figure 7.9: Valve timing at the technology carrier

Firstly the technology carrier was operated with an ε_c of 9.7 and afterwards measurements was carried out with an ε_c of 12.45. Figures 7.11a and 7.11b contains a comparison of the extended expansion engine with an ε_c of 9.7 and 12.45. The points with the highest efficiency of both compression ratios are described afterwards in more detail by means of a loss analysis and the *ROHR*.

Additional Information

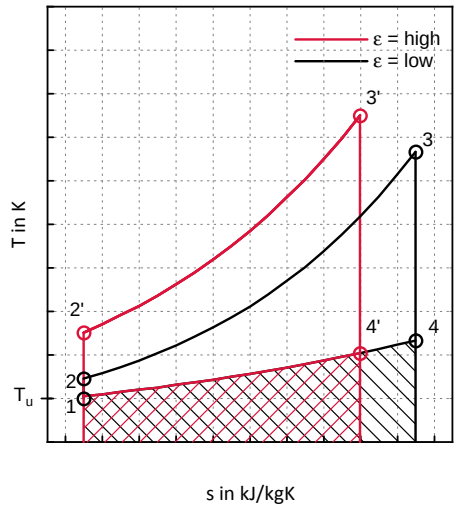

Figure 7.10: Ts-diagram of the idealised process

Figure 7.10 should briefly explain the reason for the rising efficiency at rising values of ε at a conventional engine. The added fuel heat which is equal to the area under the state points from 2 to 3 at an ε of 10 and the area from 2' to 3' at an ε of 12 is the same for both processes. In case of lower values of ε the removed heat from state point 4 to 1, respectively the black hatched area is higher compared to higher values of ε. At an ε of 12 the removed heat is equal to the red hatched area. A lower amount of removed heat at the same added fuel heat rises the efficiency. The higher peak temperature and pressure at the same MFB_{50} can be also seen at the real engine in figure 7.11b.

The point in which the engine was operated with the highest efficiency with an ε_c of 9.7 and naturally aspirated was 43.2 % at a MFB_{50} of about 9 °after Top Dead Centre (aTDC). The highest efficiency with an ε_c of 12.45 is about 44.4 % and the MFB_{50} is shifted to 10° aTDC.

Compared to the conventional engine with the filling cam shaft the rise of indicated efficiency is about 6.1 %PT. Whereby it has to be considered that the ε_c of the technology carrier is half a unit higher compared to the conventional engine.

In figure 7.11b both pressure curves are visible. The process starts with the compression and the combustion peak pressure is higher since a lower combustion chamber volume is available at the same added fuel heat. The pressure drop at the expansion at higher values of ε_c goes much faster related to piston position compared to lower values of ε_c since the expansion volume is comparatively higher at the same piston position due to the lower combustion chamber volume. Hence, the red line is below the black line at the phase of expansion.

During the expansion work is done on the piston which rises the $IMEP_c$. With an ε_c of 9.7 an $IMEP_c$ of 13.3 bar can be reached. The use of an ε_c of 12.45 can furthermore rise the $IMEP_c$ to 13.8 bar, which is substantial more compared to the reference engine with an $IMEP$ of 11.7 at an ε_c of 11.9. The rise of the $IMEP$ equates nearly 18 % between the reference engine and the technology carrier with an ε_c of 12.45.

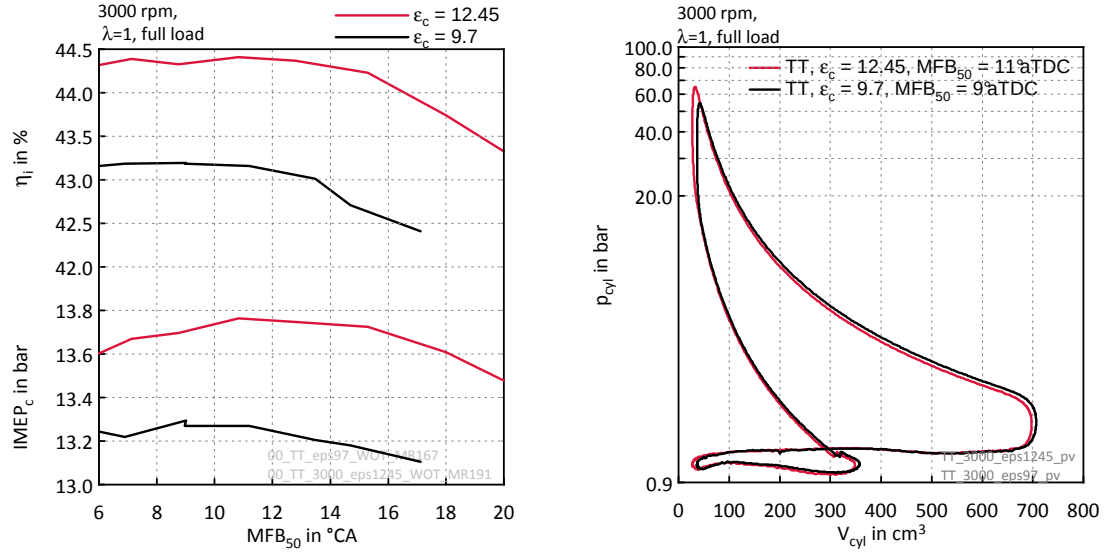

(a) $IMEP_c$ vs. MFB_{50} and efficiency

(b) pV-diagram

Figure 7.11: Comparison of the technology carrier at different compression ratios

A noticeable fact is the dependency of the efficiency from the MFB_{50} which is flatter compared to conventional engines. This fact is better visible in figure 7.12b. The red dashed line represents the drop in efficiency related to the MFB_{50} of the technology carrier. The black dashed line represents the reference engine. Since the reference engine achieves its best efficiency at earlier values of MFB_{50} the original efficiency is shifted about 3 degree in order to ensure a better comparison.

It is clearly visible that the relative level of the efficiency at the technology carrier is always higher compared to the reference engine. The reason for this phenomenon is better explained in section 7.3.1.

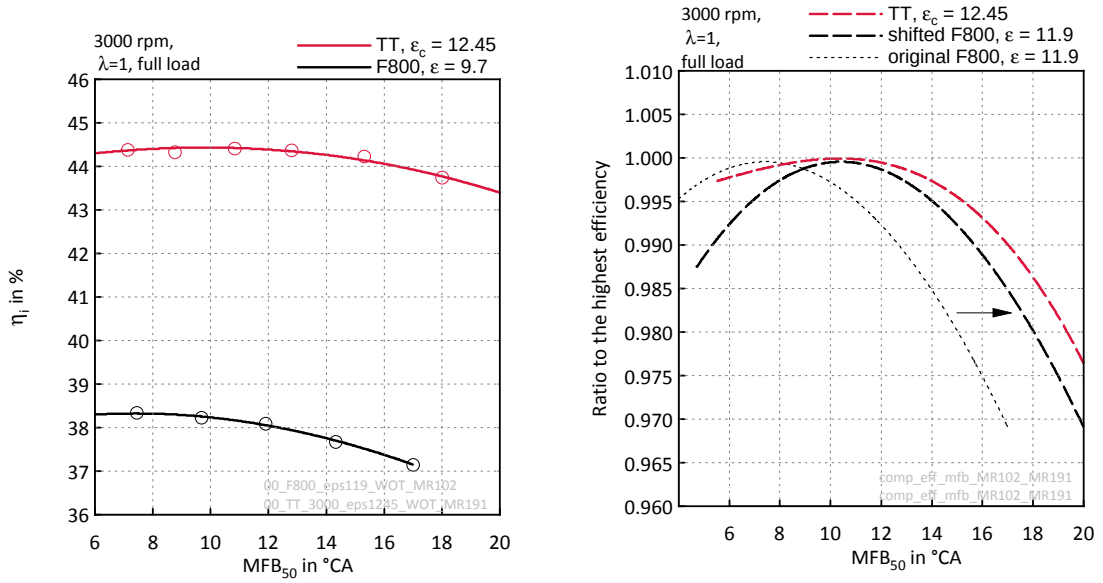

(a) Technology carrier and reference engine

(b) Comparison of the efficiency drop vs. MFB_{50}

Figure 7.12: Comparison of the technology carrier and the reference engine related to the efficiency drop vs. MFB_{50}

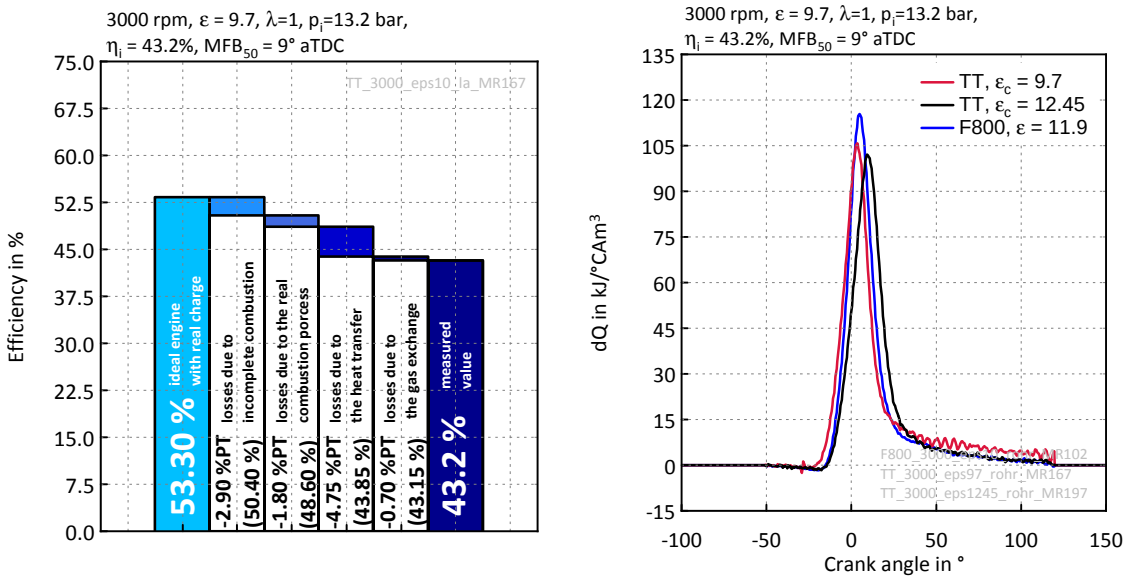

(a) Loss analysis

(b) $ROHR$ vs. °CA

Figure 7.13: Technology carrier, 3000 rpm, λ=1, ε_c = 9.7

The loss analysis is apparent in figure 7.13a. The boundary conditions are 7900 ppm CO and 3600 ppm HC, respectively 5.5 % of unburned fuel, which equates 54 J per cycle. The heat factor related to the expansion volume was shifted to 60 °CA in order to achieve a energy balance of 100.6 %. The end of combustion is defined by 70 °CA. The deviation between the measured and the calculated pressure curve is about 0.05 %PT.

The following figures 7.14 show the measurement result at 3000 rpm and ε_c=12.45 and a more detailed description of the operating point with the highest efficiency.

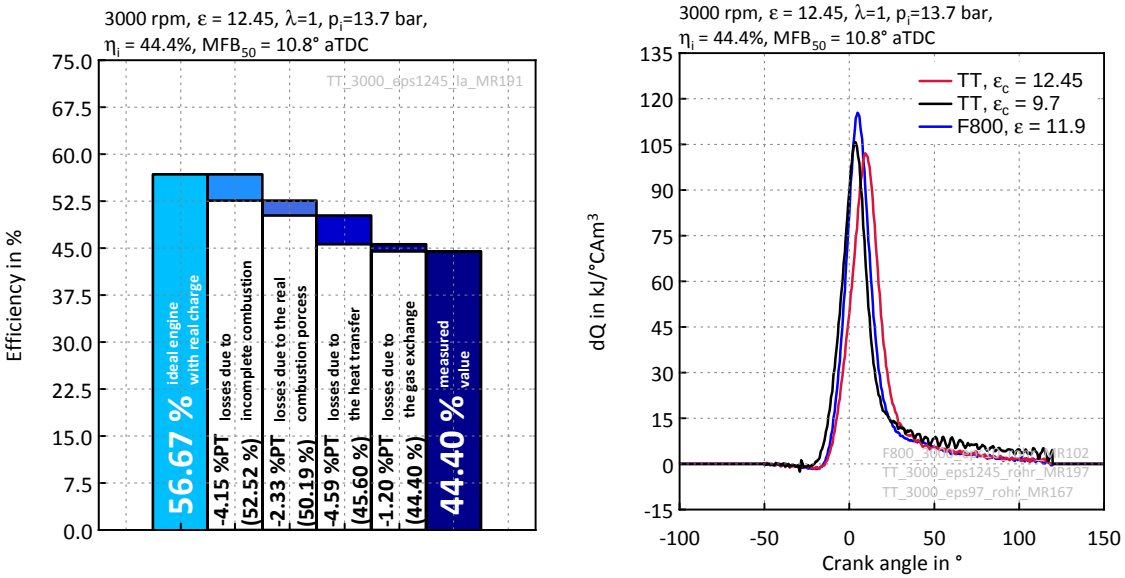

(a) Loss analysis

(b) $ROHR$ vs. °CA

Figure 7.14: Technology carrier, 3000 rpm, ε=12.45, $\lambda = 1$

In figure 7.14a the loss analysis of the operating point with the highest efficiency is apparent. The basis for this loss analysis was a fraction of unburned fuel of about 4900 ppm CO and 8300 ppm HC, respectively 8.5 % which equates an energy of 78 J per cycle. The heat transfer factor related to the expansion volume was shifted to 60 °CA in order to achieve a deviation of 0 %PT. This operating point reached an energy balance of only 96.2 %.

7.3.1 The influence of the point of ignition on the efficiency

At conventional engines a late combustion reduces the efficiency from converting the added fuel heat into work done on the piston, due to the fact that the combustion turns away from the ideal constant-volume combustion. An essential finding was the behaviour of the technology carrier in terms of the efficiency by changing the point

of ignition. At an engine with an elongated expansion stroke the losses through the late combustion near to the TDC becomes partly compensated through the higher pressure in the following expansion process.

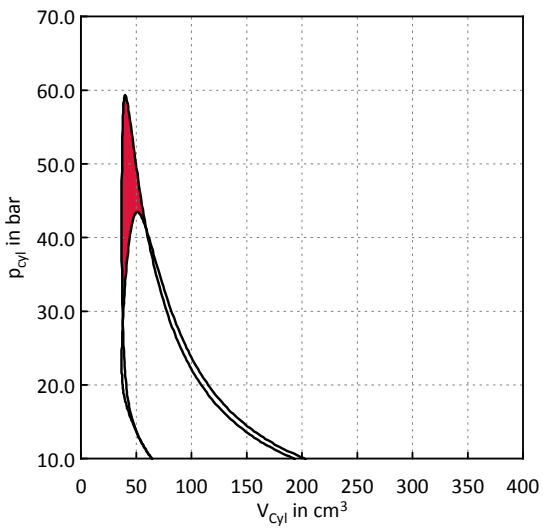

(a) pV-diagram; influence of the ignition point (I)

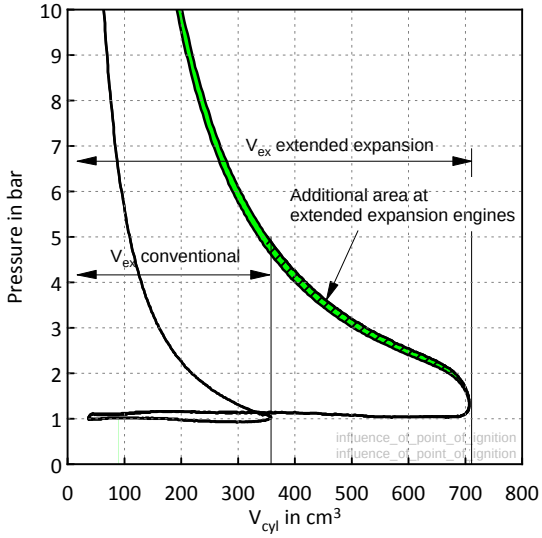

(b) pV-diagram; influence of the ignition point(II)

Figure 7.15: influence of the point of ignition at extended expansion engines

Figure 7.15 shows this issue. Within this figure are two pressure lines apparent. The pressure line which reaches the highest peak pressure of 60 bar is also this one with the highest efficiency and a MFB_{50} of 10 °aTDC. The second one which reaches only 43 bar peak pressure is an operating point with late combustion and a MFB_{50} of 17 °aTDC. In figure 7.15a the red coloured area is the energy which is more done on the piston near to the TDC compared to the pressure curve of the other operating point. Within the expansion stroke the pressure curve of the operating point with late combustion is higher compared the pressure curve with earlier combustion. Due to this issue a substantial part of the loss which was made near to the TDC can be compensated. The green area in figure 7.15b displays this proportion. Within conventional engines it is only possible to use the green area until the intake displacement is reached, due to a γ of 1. In figure 7.15b this would be 350 cm^3. Since the expansion at extended expansion engines is enlarged the whole green part in figure 7.15b can compensate a big part of the loss which was made near to the TDC. The additional part compared to a conventional engine is represented by the hatched area. Due to this issue the influence of the point of ignition on the efficiency is little within a wide range.

7.4 Conventional engine vs. Extended expansion engine

(Result overview see figure 7.8)

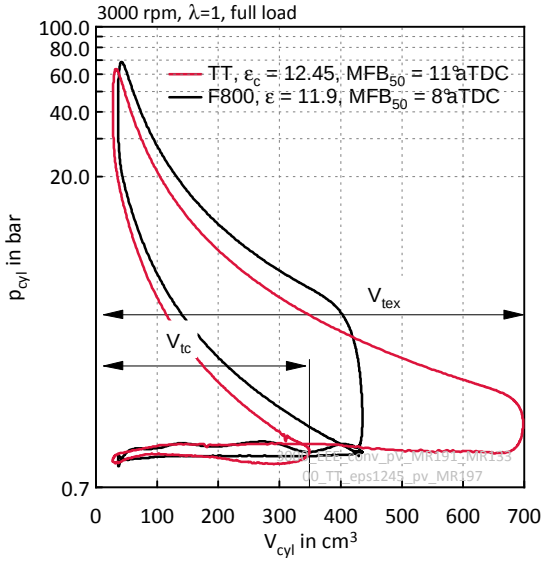

Figure 7.16: Extended expansion engine vs. Conventional engine - pV-diagram

Figure 7.16 shows a comparison of the conventional engine with filling cam shaft and the technology carrier. Both operating points were at 3000 rpm, full load and at the point of ignition with the highest efficiency. The extended high pressure cycle due to the unconventional crank train is clearly visual.

Figure 7.17a shows the efficiency difference between both concepts. Furthermore the $IMEP$ and points of ignition are shown. A striking tendency shows the extended expansion engine in terms of the points of ignition related to MFB_{50}. In order to achieve the same MFB_{50} at the technology carrier, the point of ignition is 5 degrees earlier compared to the reference engine.

In figure 7.17b the exhaust gas temperature is visual. The exhaust gas temperature (T_3) is about 100 K lower compared to the reference engine. Torque and power are slightly lower at the technology carrier since the intake volume is only 643 cm^3 - the reference engine has an intake volume of 798 cm^3. Therefore the difference of the theoretical charge mass, at a volumetric efficiency of 1 is nearly 25 %. Since the extended expansion engine has a higher overall efficiency the difference in torque and power is only about 4.3 %.

In figure 7.18a both $ROHR$ are shown. It is clearly apparent that the pressure rise at the beginning of the combustion at the reference engine occurs much fast compared to the technology carrier.

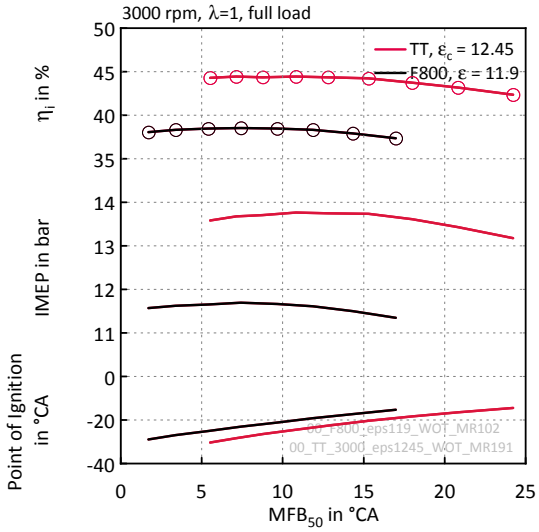

(a) Extended expansion engine vs. Conventional engine - IMEP vs. MFB_{50} and efficiency

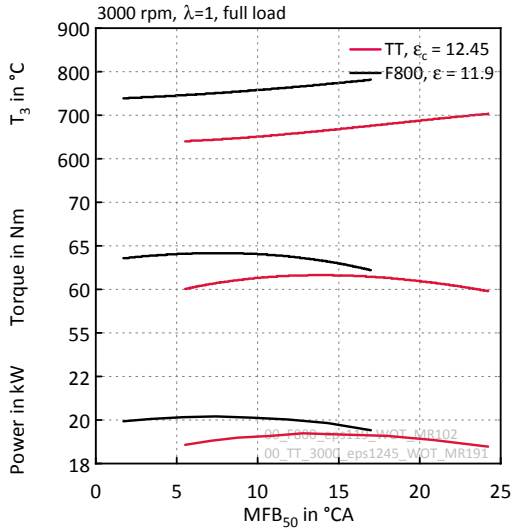

(b) Extended expansion engine vs. Conventional engine - Exhaust temperature, Power, Torque

Figure 7.17: Extended expansion engine vs. Conventional engine

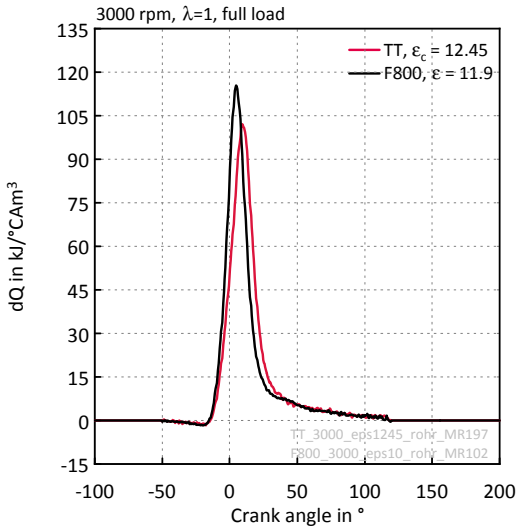

(a) Extended expansion engine vs. Conventional engine - $ROHR$

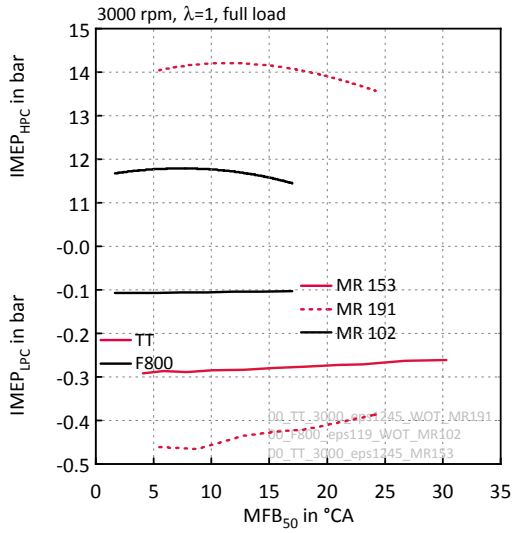

(b) Extended expansion engine vs. Conventional engine - $IMEP$

Figure 7.18: Extended expansion engine vs. Conventional engine

Figure 7.18b shows the comparison of the $IMEP_{\mathrm{HPC}}$ and furthermore the $IMEP_{\mathrm{LPC}}$.

The measurement showed an $IMEP_{\mathrm{LPC}}$ that is obviously to low - apparent by the dashed line in figure 7.18b The cause for that error could not be explained so far. The result of a measurement series with similar boundary conditions is added to the plot to enable a proper comparison (MR 153).

The required work for the gas exchange is higher at the technology carrier. The higher gas exchange work is firstly caused due to the higher exhaustion volume. Related to this fact the gas exchange work would be twice compared to the reference engine.

The gas exchange work additionally rises due to the higher cylinder mass after the blow-down process. The lower pressure difference at the beginning of exhaust valve opening, compared to a conventional engine, causes a higher remaining exhaust gas mass and rises the work for the expelling.

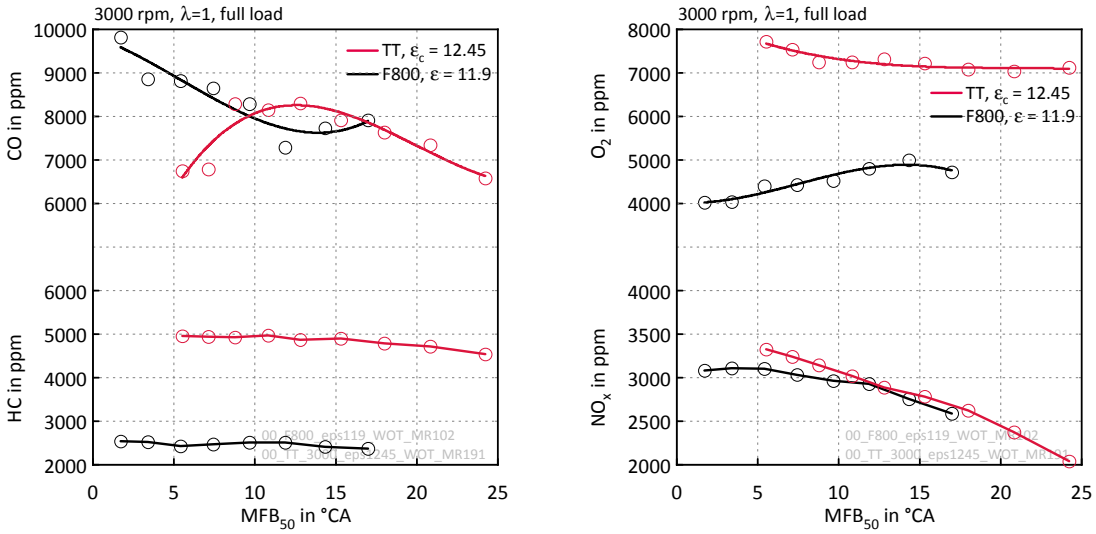

(a) Extended expansion engine vs. Conventional engine - HC/CO emissions

(b) Extended expansion engine vs. Conventional engine - O_2/NO_x emissions

Figure 7.19: Extended expansion engine vs. Conventional engine

Figure 7.19 shows the comparison of the emissions of both concepts. The results let assume that the reason for this high hydrocarbon and oxygen emissions at the technology carrier is due to the scavenging losses and/or due to an inefficient burning. The highest carbon monoxide emissions near to the operating point with the highest efficiency let assume that the combustion becomes more and more inefficient near to point with the highest efficiency.

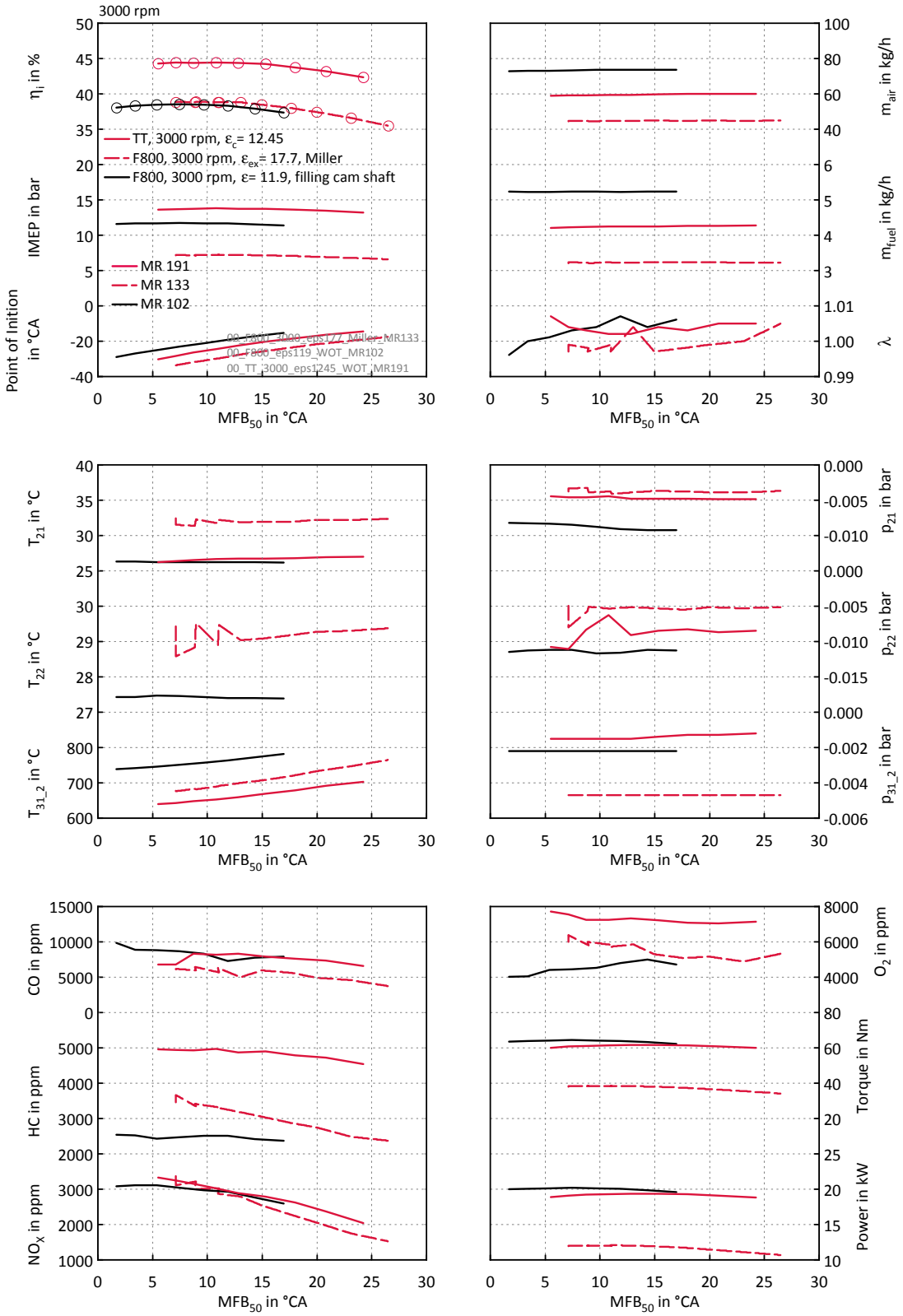

Figure 7.20: Extended expansion engine vs. Miller, 3000 rpm

7.5 Miller vs. Extended expansion - Miller as a strategy to realise extended expansion

(Result overview see figure 7.20)

The foregoing Miller investigations (see 7.2) were performed with an ε_c of 11.9. The reduced intake volume due to the valve timing at the same combustion volume reduces the overall ε which furthermore reduce the overall efficiency at rising γ. In order to exploit the maximum potential of the Miller strategy the reference engine was fitted with pistons which realise an ε_{ex} of 17.7. The following figures concern the comparison of Miller strategy vs. Extended expansion. In order to make a comparison between both concepts possible, W_{ind} is related to the expansion volume. Since the determination of the effective intake cylinder volume at the Miller strategy is a formidable task, both $IMEP$s are related to the expansion volume. The $IMEP_{ex}$ which is shown in figure 7.21a do not corresponds with the $IMEP_c$ in figure 7.11a since at other approaches W_{ind} is related to the intake cylinder volume.

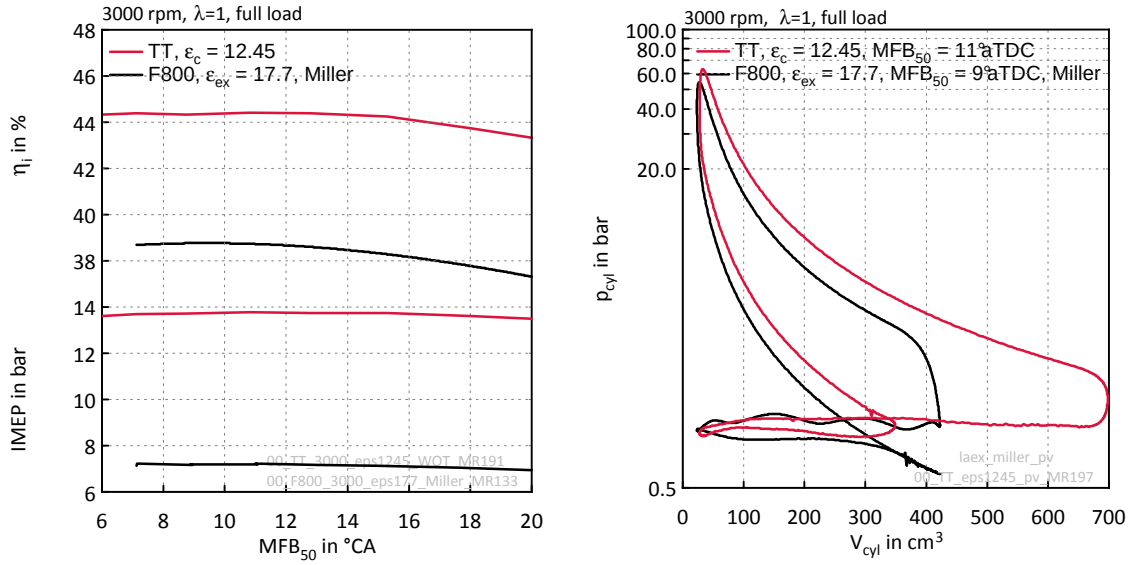

(a) Extended expansion vs. Miller strategy - $IMEP$ vs. MFB_{50} and efficiency

(b) Extended expansion vs. Miller strategy -pV-diagram

Figure 7.21: Extended expansion vs. Miller strategy

The reference engine reached its highest efficiency of 38.9 % at a MFB_{50} of 9 °aTDC. The technology carrier reached 44.4 % at a MFB_{50} of 11 °aTDC.

At these investigations the engine with Miller strategy delivered not the full potential of this concept since the crank train is not designed for this strategy. An engine with a valve train which is designed for Miller strategy could ensure higher efficiencies

as it is shown at this investigation. According to the simulation the engine with the Miller strategy and a suitable valve train could reach an efficiency which is 3%PT lower compared to the extended expansion engine. The valve lift at this Miller strategy is only 3.3 mm which causes much gas exchange work. In addition a part of the big difference in efficiency can be explained by the lower γ at the reference engine with Miller strategy. Moreover the inefficient combustion is a further reason for the low efficiency.

This investigations was definitely in favour of the extended expansion engine.

The determination of γ at the Miller strategy is difficult, due to the fact that the γ varies with different point of views. The simplest way to determine the γ would be the ratio of the volumes at valve closing compared to the volume at BDC.

At this approach the different valve lift curves and as a consequence the different charge masses are not considered. However they are mostly responsible for the lower level of charge mass and as a result for the load point. Furthermore the flow losses are neglected. Due to the finite valve closing velocity at the end of the intake stroke the flow losses rise while the piston moves downwards. The piston covers quite a long distance despite the little increase of charge mass. Thus valves with different valve lift curves and closing velocities at the same valve timing would result in the same γ although the charge mass within the cylinder would be different.

$$\gamma_{\mathrm{V}} = \frac{\mathrm{V_{tc}}}{\mathrm{V_{tMiller}}} \tag{7.1}$$

Equation 7.1 compares the $\mathrm{V_{tc}}$ which represents the cylinder volume at BDC and $\mathrm{V_{tMiller}}$ which is the cylinder volume at a specific valve timing, respectively Miller level.

Another approach for the determination of γ would be to define the γ as the ratio between the volumetric efficiencies. The volumetric efficiency which can be reached by the conventional engine at full load and this speed would be VE_{γ_1}. The volumetric efficiency which can be reached at the Miller strategy would be $\mathrm{VE_{Miller}}$. VE_{γ_1} related to $\mathrm{VE_{Miller}}$ would determine γ_{VE}.

$$\gamma_{\mathrm{VE}} = \frac{\mathrm{VE}_{\gamma_1}}{\mathrm{VE_{Miller}}} \tag{7.2}$$

At this approach the point of the inlet valve closure is not considered and as a consequence the effective compression ratio is difficult to determine.

A suitable approach for the determination of γ is to determine the cylinder volume, at the compression, where the manifold pressure is reached. The cylinder volume at BDC compared to the volume mentioned before equates the Miller level.

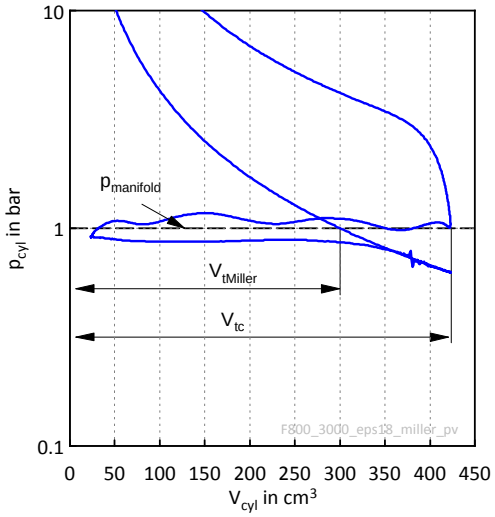

Figure 7.22: Determination of the Miller level

Both volumes in figure 7.22, 300 cm^3 where the manifold pressure is reached and 422 cm^3 as the total cylinder volume at BDC, put into equation 7.1 equates a γ of 1.40 at the reference engine with an ε_c of 17.7 and the Miller cam shaft.

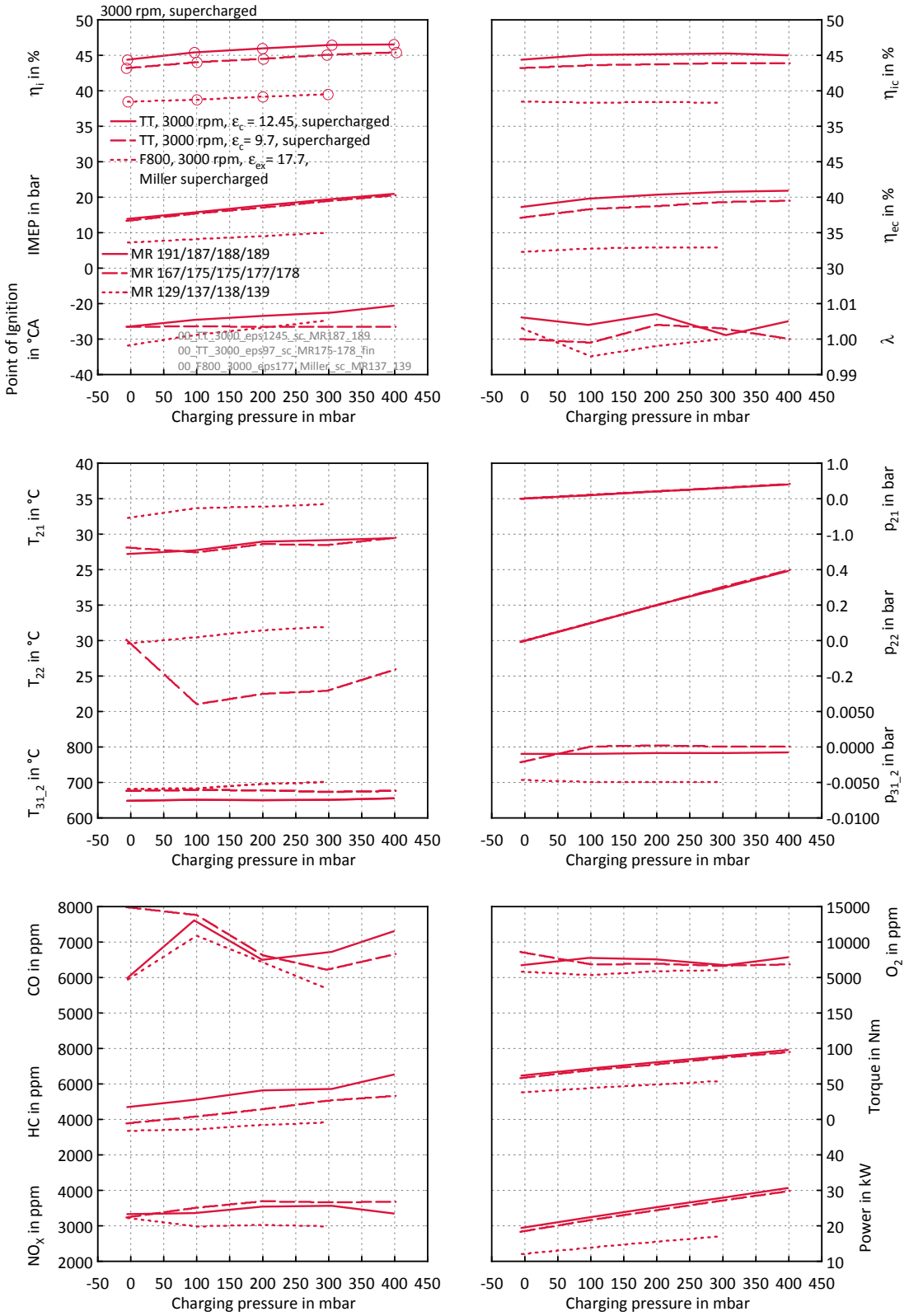

Figure 7.23: 3000 rpm, supercharged

7.6 Supercharged operation

7.6.1 Technology carrier - supercharged

(Result overview see figure 7.23)

The charging pressure was adjusted to p_{22} which is positioned after the throttle flap in order to take the losses through the intake system into account and to ensure a specified pressure after the throttle flap.

The first operating point at the supercharged operation was at 3000 rpm and 100 mbar charging pressure. The charging pressure was varied up to 400 mbar in steps of 100 mbar. Afterwards a variation of the ignition point was carried out at λ of 1.

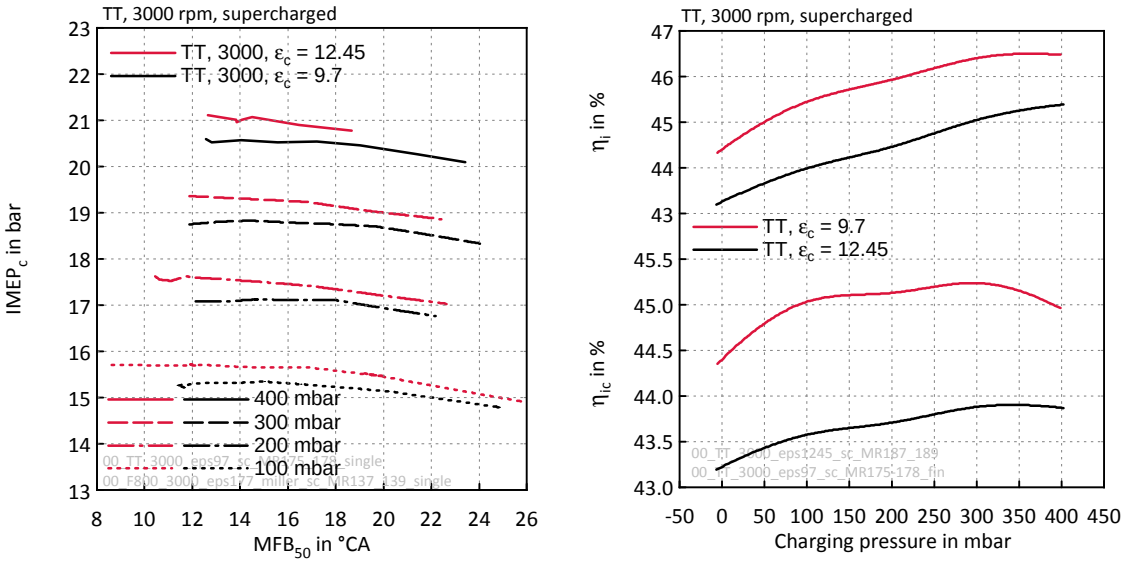

(a) $IMEP_c$ vs. MFB_{50}

(b) η_i and η_ic vs. MFB_{50}

Figure 7.24: Supercharged operation

Figure 7.24a shows the $IMEP_c$ vs. MFB_{50}. Since the combustion peak pressure reached nearly 110 bar late points of ignition was necessary in order to avoid any harm on the cylinder head. Figure 7.24b displays the indicated efficiency vs. MFB_{50}. The isentropic efficiency is assumed by 0.7 for the compressor. The highest efficiency was reached with an ε_c of 12.45 and a charging pressure of 300 mbar. The indicated efficiency is about 46.4 % and with consideration of the work which is necessary for the compression of the charge mass an efficiency of 45.2 % is possible. At 400 mbar later points of ignition was necessary due to the peak pressure and therefore η_ic is lower. At an ε_c of 9.7 the point with the highest efficiency is reached at 400 mbar.

Earlier measurement series showed lower efficiencies at the same operating points due to high emissions, as it is apparent in figure 7.26 by the dashed line. It is obvious

that the reason for the high rise of unburned fuel could be found within the scavenging losses.

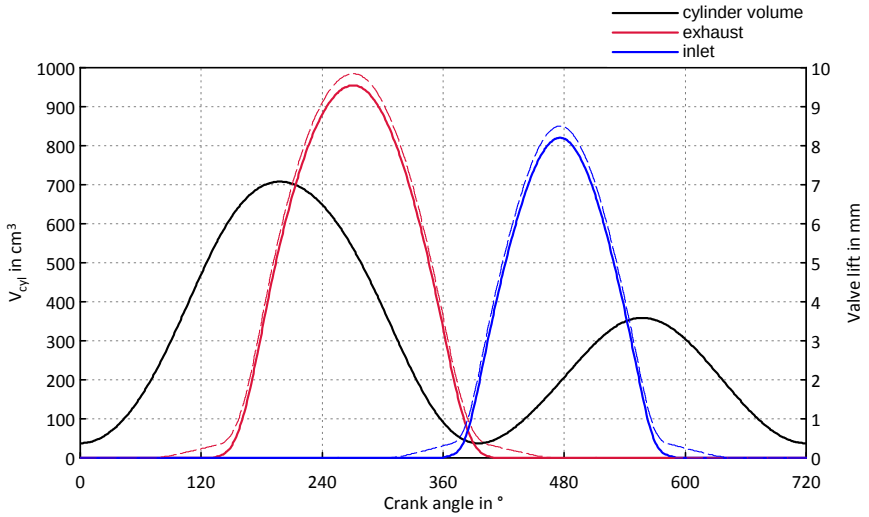

Figure 7.25: Valve lift curves

The dashed lines in figure 7.25 contains the real measured valve lift curves which are put into action through the cam. The continuous lines are the valve lift curves realised by the cam reduced by the valve clearance. The black line shows the cylinder volume. This figure shows that the valve clearance mainly influences the scavenging losses. The simulation shows that the valve clearance which was adjusted under ambient conditions results in 0.35 % of scavenging losses.

Considering this value, the amount of unburned fuel can not be explained. A further simulation with the assumption that the valve clearance would be zero was undertaken, which corresponds to the dashed valve lift curves. The result of this simulation showed that the scavenging losses would be approximately ten the time as before. This issue is shown in figure 7.27. Due to this simulation the big influence of the scavenging losses because of the valve clearance was shown. Due to the solution of the simulation a big part of the unburned fuel can be explained. Thus, slight shifted valve timing was adjusted in order to reduce the emission output and rise the indicated efficiency. Another reason for the rising unburned fuel rate with rising charging pressure can be explained by the incomplete combustion due to the low in-cylinder motion.

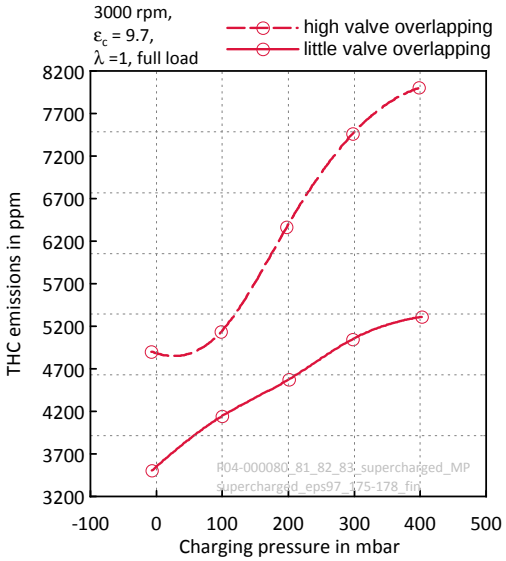

Figure 7.26: Total hydrocarbon emissions vs. charging pressure, n=3000 rpm, ε_c=9.7

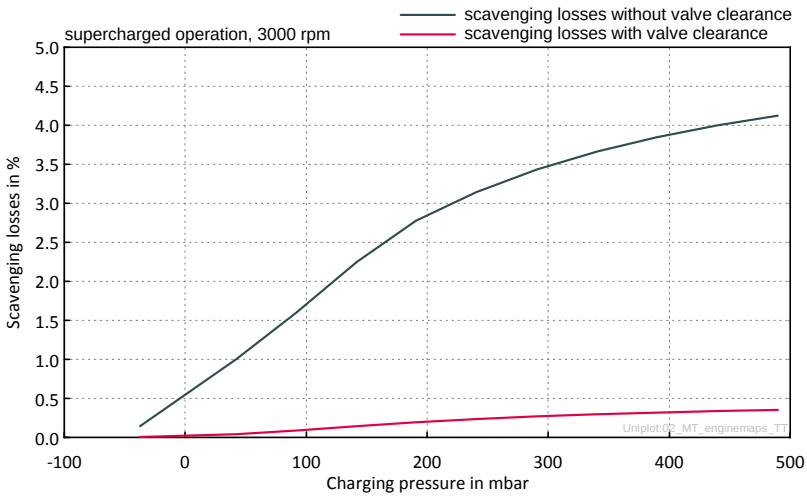

Figure 7.27: Scavenging losses (Simulation)

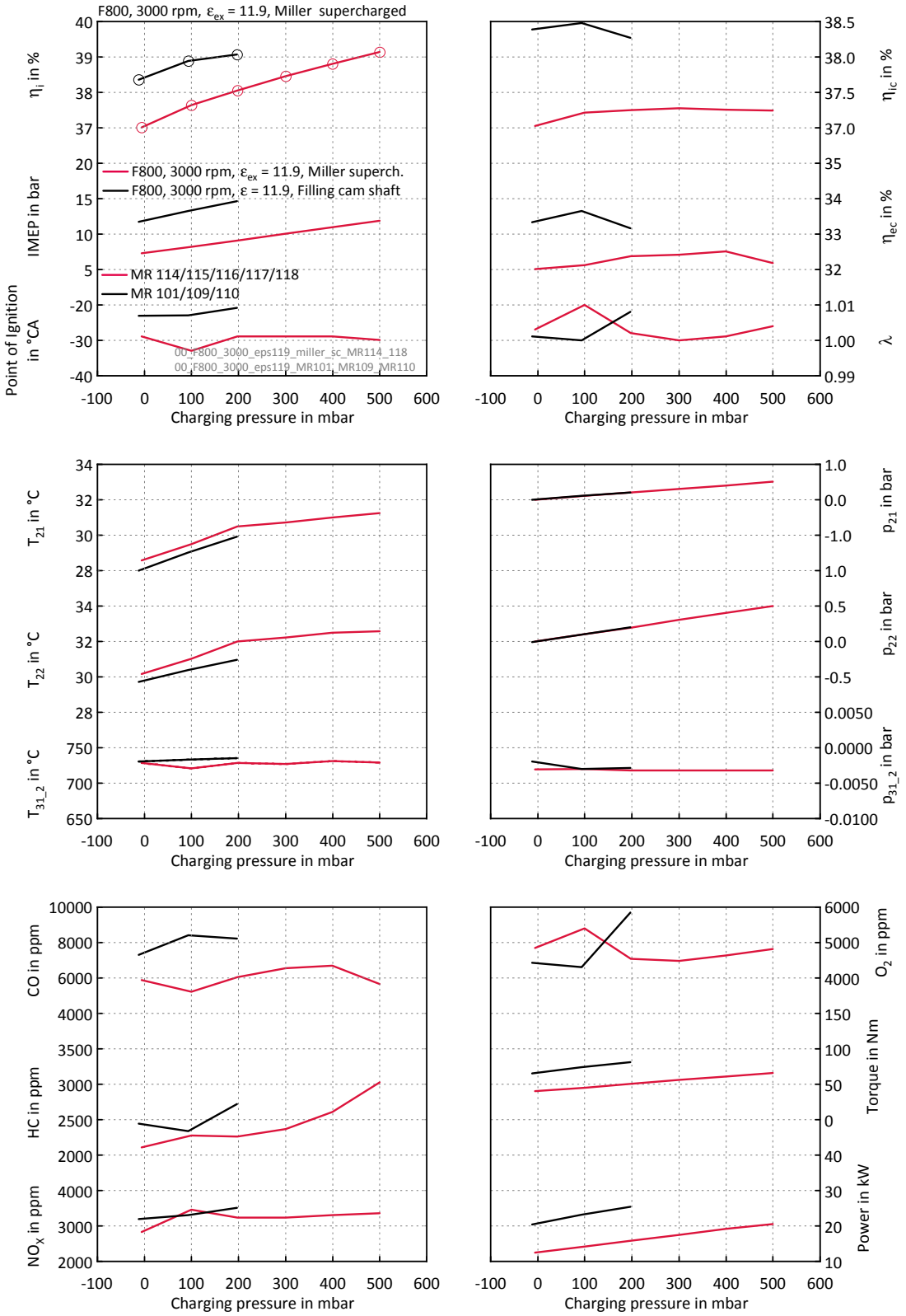

Figure 7.28: F800, 3000 rpm, Miller supercharged

7.6.2 Miller supercharged

(Result overview see figure 7.28)

In order to ensure higher load points despite the Miller strategy the charging pressure needs to be increased. Figure 7.29a shows the $IMEP_{\text{ex}}$ vs. MFB_{50} and efficiency. The isentropic efficiency of the compressor is assumed with 0.7.

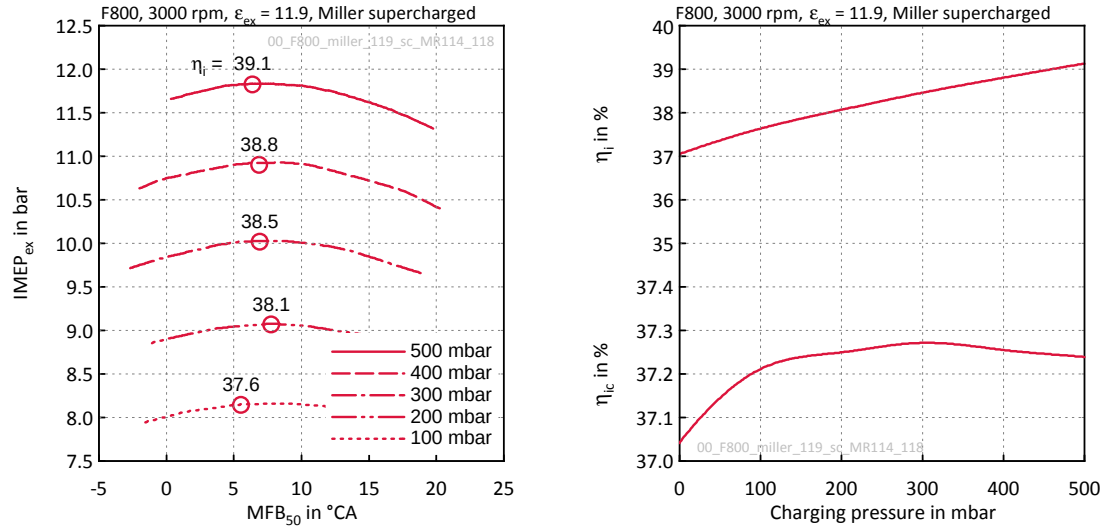

(a) $IMEP_{\text{ex}}$ vs. MFB_{50} and efficiency (b) $IMEP_{\text{ex}}$ vs. MFB_{50} and efficiency

Figure 7.29: Supercharged operation with Miller

Without any supercharging the Miller strategy reaches better efficiencies in the low load regions compared to the conventional engine. The supercharging ensures a pre-compression of the charge mass, which furthermore rises the effective compression ratio. But the required work of the compression of the charge mass is higher than the advantage due to the pre-compression. Furthermore the gas mass is throttled due to the low valve lift at Miller strategy. Therefore the Miller strategy reaches an efficiency of 37.2 % at 11.8 bar, apparent in figure 7.29b. The conventional engine reaches an efficiency of 38.3 % at 11.9 bar without supercharging. Therefore in order to rise the load the most efficient approach is to decrease the Miller lever instead the supercharging.

At the conventional concept the efficiency rises with rising load due to the de-throttling. Therefore by means of the Miller strategy a rise in efficiency compared to the conventional concept can only be reached in low load regions as it was shown in figure 2.4. By the way, the Miller level has to be increased for lower load points in order to ensure better efficiency and this is only possible with a variable valve timing.

7.6.3 Miller vs. Extended expansion - supercharged operation

(Result overview see figure 7.28)

In order to ensure higher load points the reference engine with Miller strategy and an ε_c of 17.7 was supercharged. Also the technology carrier was supercharged in order to make a comparison possible. Figure 7.30a shows the $IMEP_{ex}$ vs. MFB_{50} and efficiency. Since the knocking limit was reached at the Miller strategy at 300 mbar, earlier points of ignition were not possible. For the determination of the $IMEP_{ex}$ again the expansion volume of both concepts is used. The technology carrier was supercharged up to 400 mbar. A higher charging pressure was not possible due to the peak pressure limit of 110 bar.

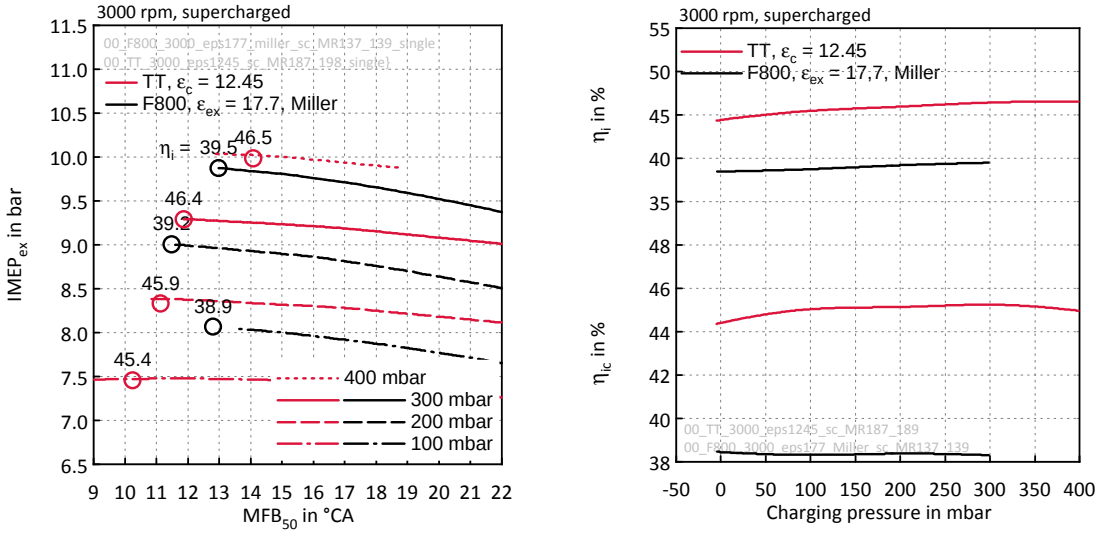

(a) $IMEP_{ex}$ vs. MFB_{50} and efficiency

(b) Efficiency vs. MFB_{50}

Figure 7.30: Extended expansion engine vs. Miller

In figure 7.30a all curves of the supercharged operation are apparent. In figure 7.30b η_i and η_{ic} are apparent. The difference between both efficiencies is the work for the compression of the charge mass related to the added fuel heat - $\Delta\eta_c$.

The maximum indicated efficiency which is reached by the Miller strategy is about 39.5 %, without consideration of the compression work. Whereas, the engine with extended expansion reaches an efficiency of about 46.5 %. This is also the highest indicated efficiency which was ever reached by the technology carrier. This results in a difference of about 7 %PT. The difference of η_{ic} of both concepts is about 6.7 %PT. The technology carrier reaches 45.2 % and the reference engine with the Miller strategy reaches about 38.4 %.

$\Delta\eta_c$ is equal for both strategies, since the technology carrier has a higher indicated efficiency the percentage value is lower.

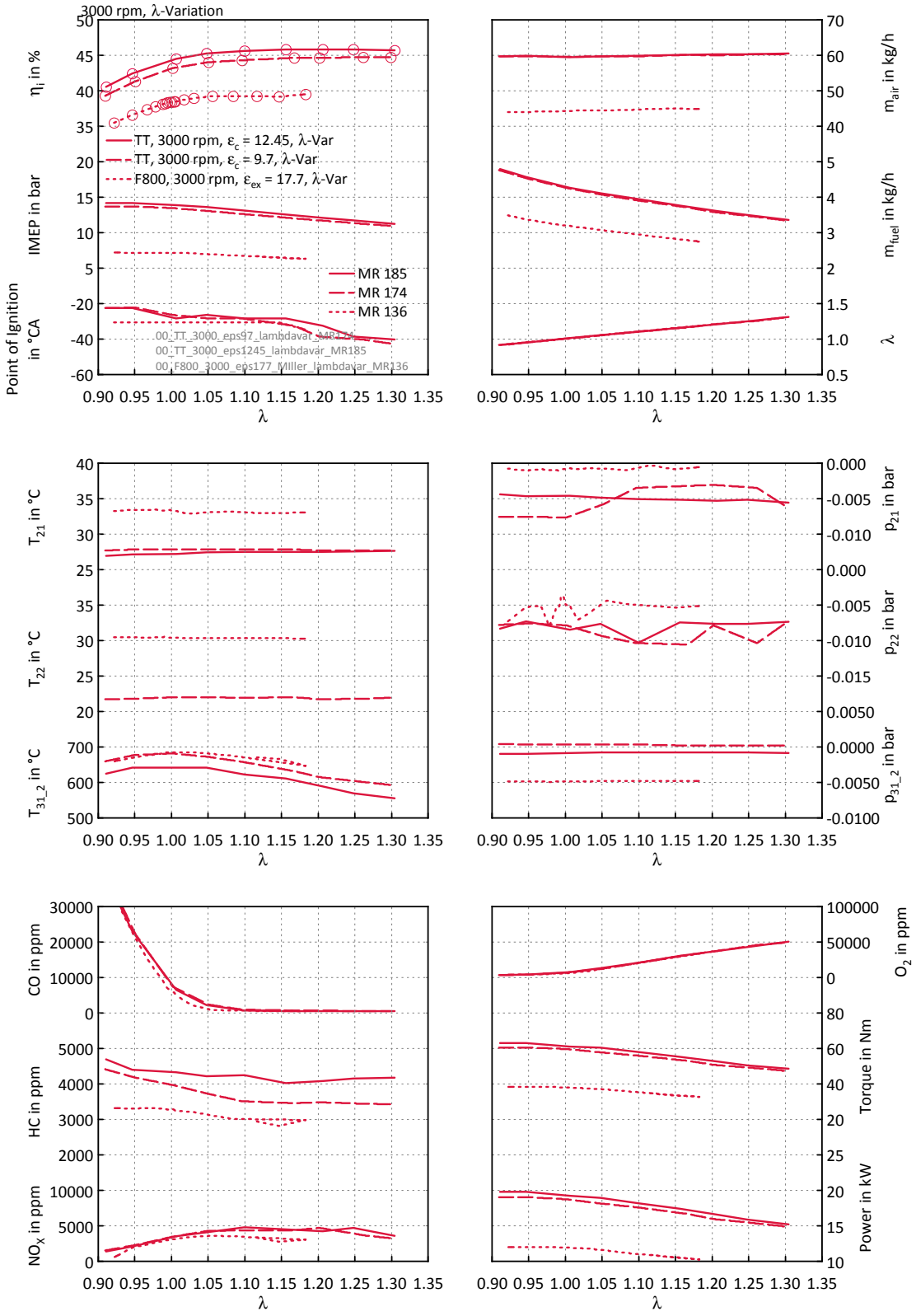

Figure 7.31: λ-Variation, 3000 rpm

7.7 Miller vs. Extended expansion - lean operation

(Result overview see figure 7.31)

In order to determine the influence of λ on the efficiency the extended expansion engine as well as the reference engine with the Miller strategy was operated with lean combustion. Figure 7.32 shows the curve of the efficiency vs. λ.

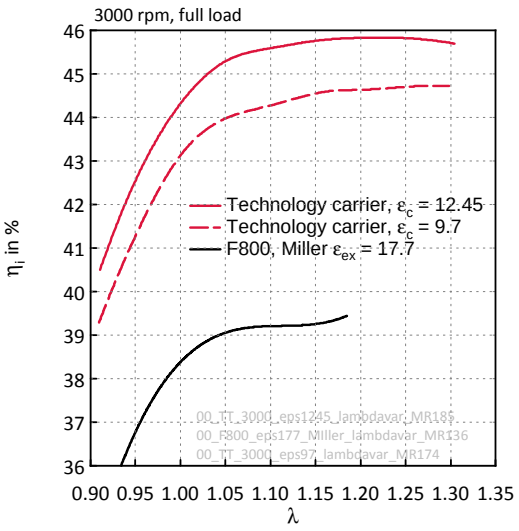

Figure 7.32: Efficiency vs. λ

As it is visual in figure 7.32 the technology carrier reached an efficiency of 45.8 % at a λ of 1.2 and ε_c of 12.45. The highest reached efficiency at an ε_c of 9.7 is about 44.7 % at a λ of 1.3. The reference engine reached its highest efficiency at a λ of 1.17 with 39.3%. The difference between the reference engine and the technology carrier with an ε_c of 12.45 is about 6.5 %PT.

At mass production the lean operation is seldom used at petrol engines due to the effort of the after treatment system, in order to be within the emission standards.

Additional Information

One reason for the rising efficiency at lean combustion are the gas properties, which influence the process in a positive way. Since air is a diatomic gas and therefore the heat for rising the temperature is lower compared to gases with more than two atoms. That fact is also apparent due to κ which rises from 1.32 at a λ of 1 to 1.4 - at ambient temperature - if a petrol engine would be operated with an infinite λ. In addition at the real engine the rise of efficiency is due to the rising fraction of air which reduces wall heat losses. Moreover a lower amount of fuel has to heat up more amount of air compared to λ of 1 which decreases the combustion temperature.

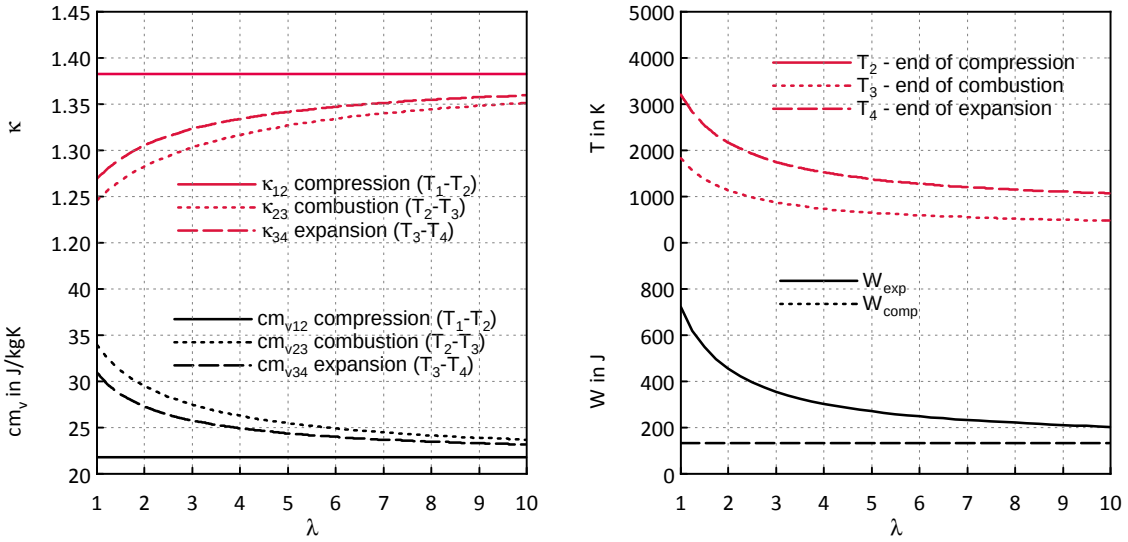

(a) Influence of λ on the gas properties I

(b) Influence of λ on the gas properties II

Figure 7.33: Influence of λ on the gas properties

In figures 7.33 is assumed that the intake and the compression process occur with atmospheric air, κ, c_{mv} and W_{comp} are therefore constant at every single lambda.

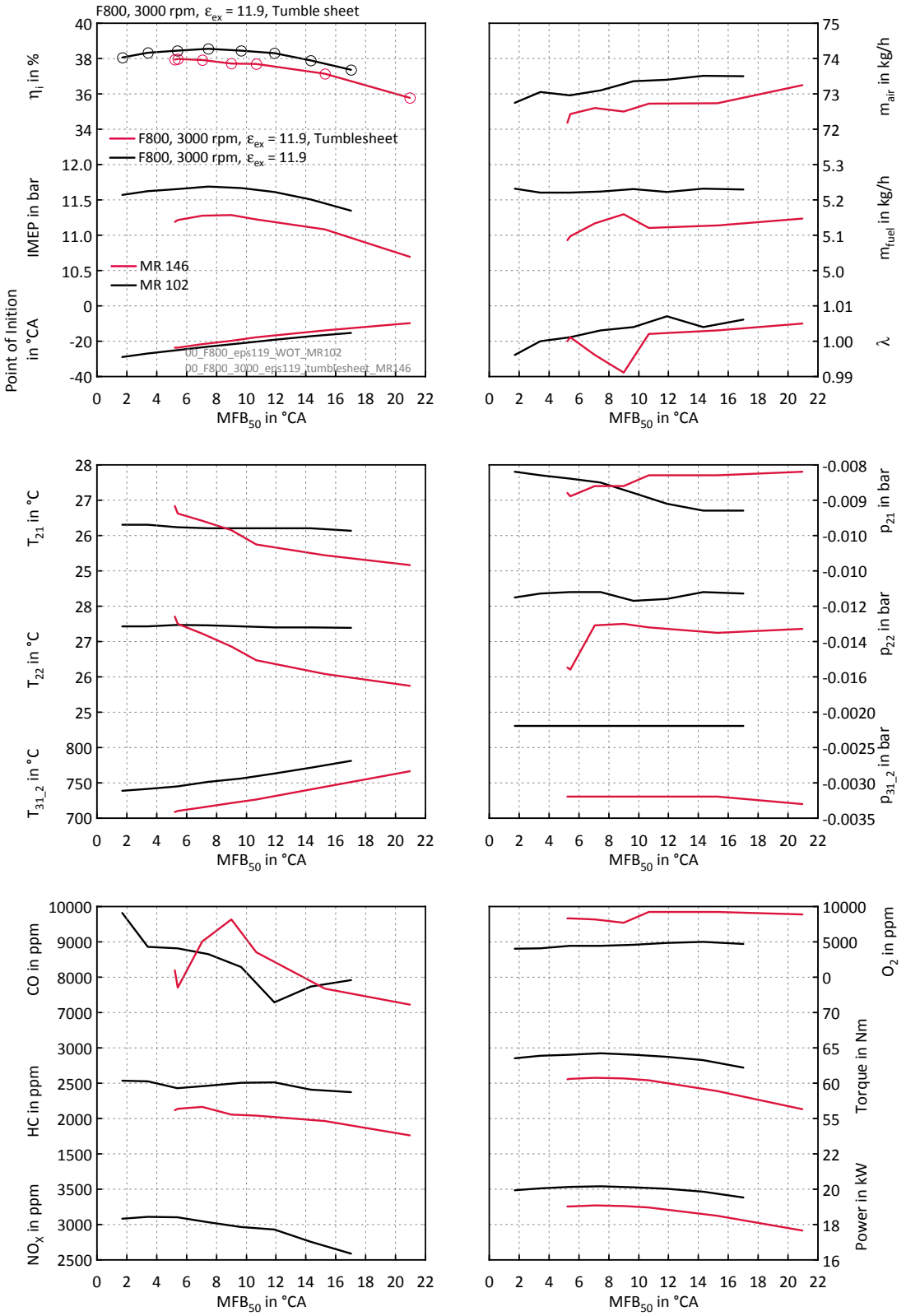

Figure 7.34: F800, 3000 rpm, ε_c=11.9, Tumble sheet

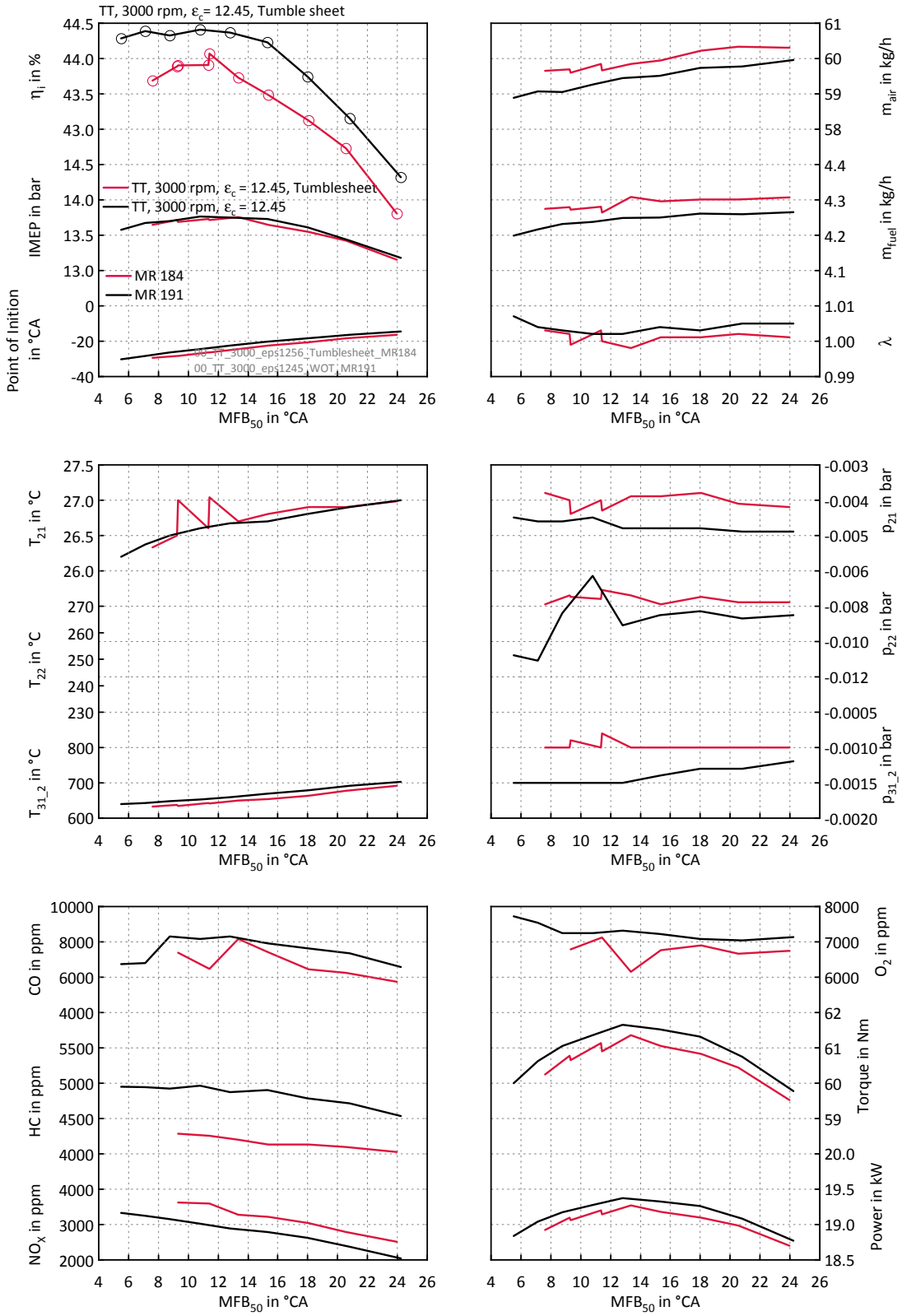

Figure 7.35: TT, 3000 rpm, ε_c=12.45, Tumble sheet

7.8 Additional measurements

7.8.1 Measurements with a higher in-cylinder charge motion

(Result overview see figure 7.34 and 7.35)

In order to make an appraisal how an in-cylinder motion could enhance the combustion a tumble sheet was designed and manufactured.

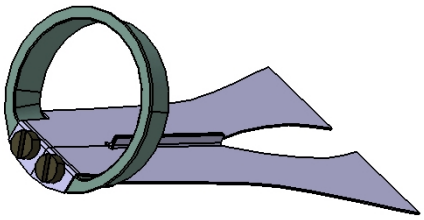

Figure 7.36: Tumble sheet

By means of this tumble sheet an in-cylinder motion which is parallel to the axis of the crank shaft should be ensured. This kind of motion is also called tumble - visual in figure 7.37a. On the left side of figure 7.37b, the unmodified intake port is apparent. On the right side the intake port is apparent in which the tumble sheet is installed.

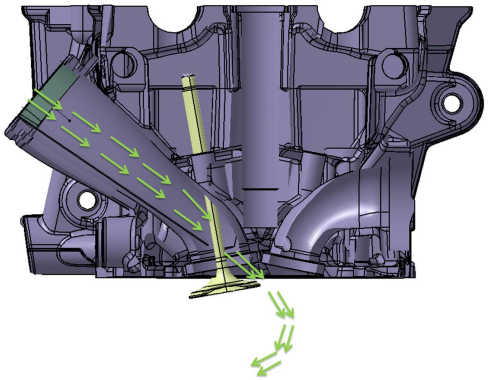

(a) Tumble sheet (I)

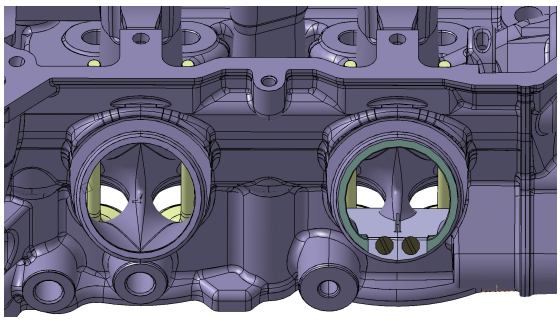

(b) Tumble sheet (II)

Figure 7.37: Different views of the tumble sheet

The hoped low-emission output did not occur, despite this measure. The overall emission output with the aid of this measure did not decrease. The efficiency has even decreased due to the tumble sheet. After this measure no more actions was attempt in order to reduce the output of hydrogen and carbon monoxide emissions.

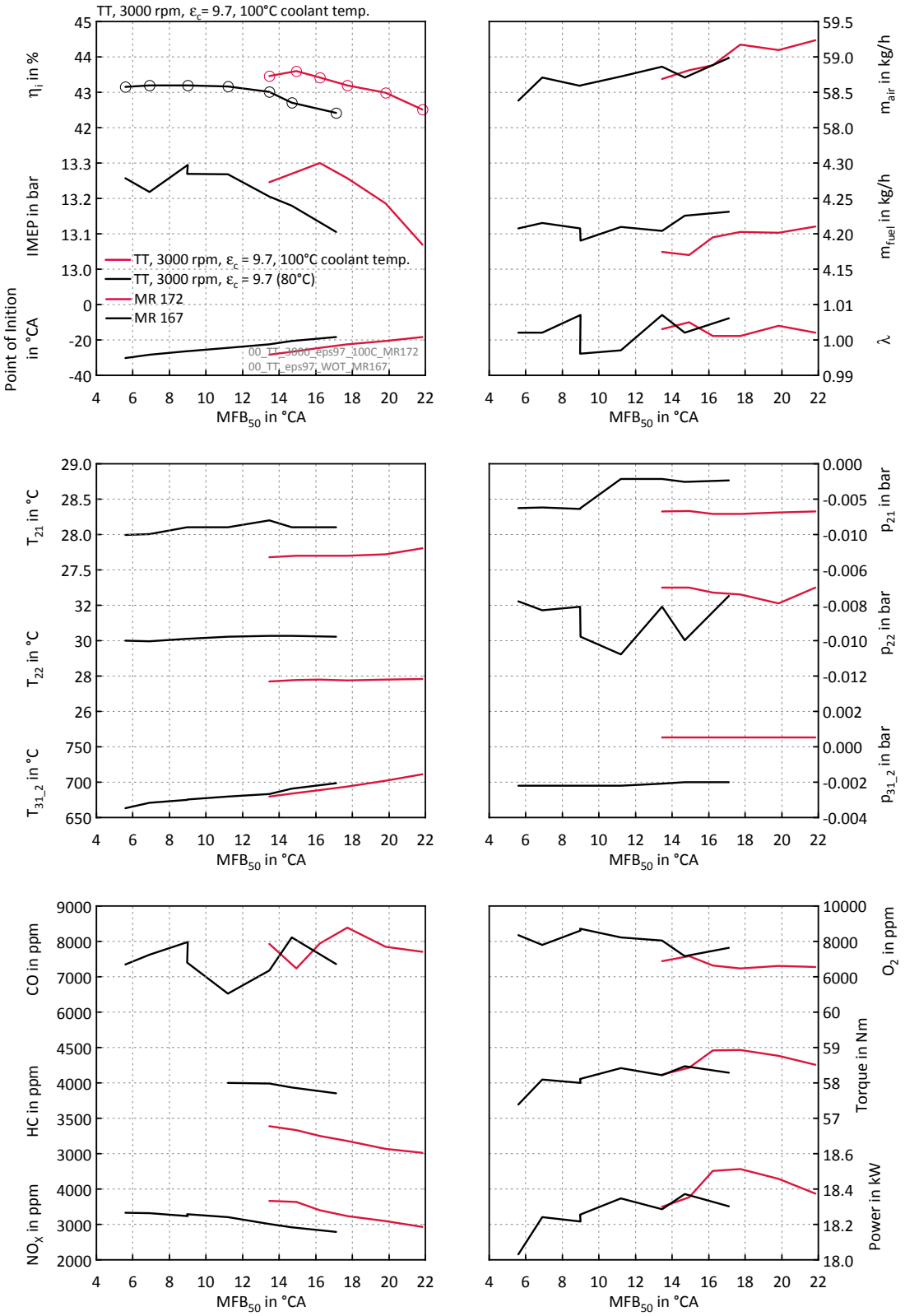

Figure 7.38: TT, 3000 rpm, ε_c=9.7, 100°C

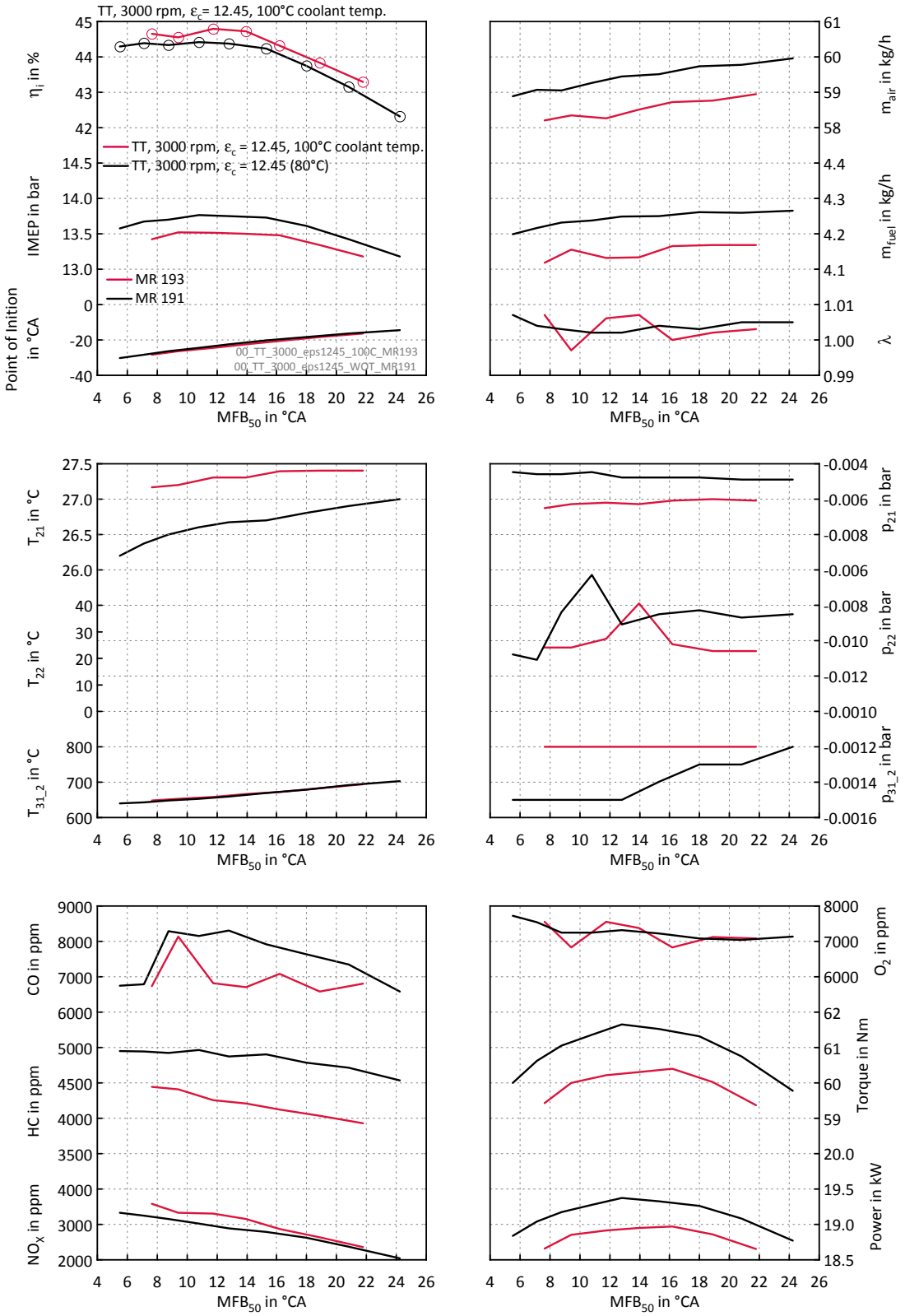

Figure 7.39: TT, 3000 rpm, ε_c=12.45, 100°C

7.8.2 Measurements with elevated coolant temperature

(Result overview see figure 7.38 and 7.39)

This operating points should show the influence of the coolant temperature on the efficiency not only for this concept but in general. Investigations which concern the influence of an elevated coolant temperature at conventional engines was not conducted. As it is apparent in figure 7.40a the rise in efficiency is about 0.8 %PT at an ε_c of 9.6 and similar MFB_{50} which is surprisingly much for this little effort. Of course due to this approach the tendency for knocking increases which was also the reason for later points of ignition. Figure 7.40b shows the behaviour of the technology carrier with an ε_c of 12.45 in terms of an elevated coolant temperature. The rise in efficiency is lower compared to an ε_c of 9.7 and is about 0.2 to 0.3 %PT.

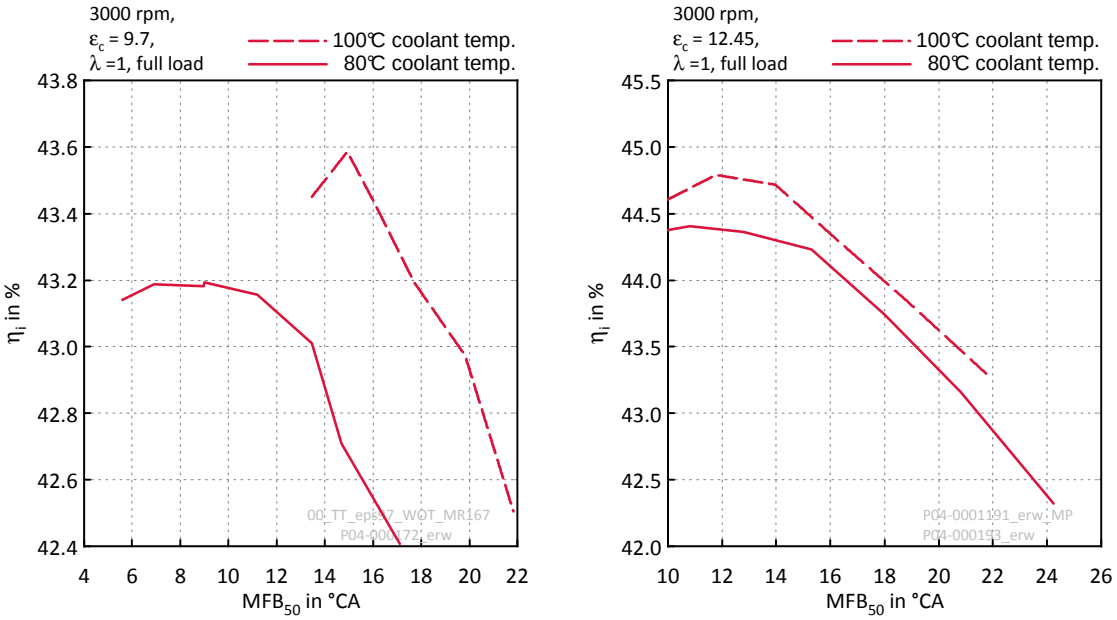

(a) Efficiency vs. MFB_{50}, $\varepsilon_c = 9.7$

(b) Efficiency vs. MFB_{50}, $\varepsilon_c = 12.45$

Figure 7.40: Technology carrier with elevated coolant temperature

7.8.3 Reduced coolant temperature at supercharged operation

In order to ensure earlier MFB_{50} than 15 °aTDC the coolant temperature at 400 mbar charging pressure was reduced to 60 °C.

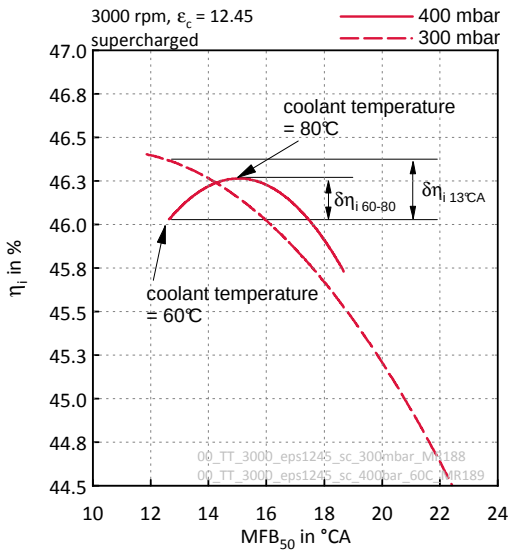

Figure 7.41: Reduced coolant temperature at supercharged operation

Noticeable is the significant influence of the coolant temperature. $\delta\eta_{i60-80}$ shows the difference of efficiency between a MFB_{50} at 15 °CA and a coolant temperature of 80 °C, and the efficiency which is reached at a MFB_{50} at 13 °CA at a coolant temperature of 60 °C. The difference is about 0.3 %PT.

$\delta\eta_{i13°CA}$ shows the difference of efficiency between a supercharging pressure of 300 mbar and 400 mbar at a MFB_{50} of 13 °CA. The difference is about 0.4 %PT.

7.8.4 Friction of the crank mechanism

This section deals with the friction of the used engines. The quantity in order to make a statement about the friction within an engine is called Friction Mean Effective Pressure ($FMEP$) and is defined as follows:

$$FMEP_c = IMEP_c - BMEP_c \tag{7.3}$$

$BMEP_c$ defines the measured torque related to the intake cylinder volume.

Since the extended expansion engine is fitted with two rotational shafts and several additional parts the amount of friction is obviously higher compared to conventional engines. The friction during the fired as well as the motored operation amounts approximately 1.8 bar at 3000 rpm and 2.0 bar at 3500 rpm. The engine features an η_e of 38.8 % at 3000 rpm, full load and an ε_c of 12.45 - η_i is 44.4 %. Despite the complex crank train the difference of effective efficiency compared to the reference engine at 3000 rpm and full load is about 5.5 %PT. The $FMEP_c$ of the technology carrier in figure 7.42a seems to be comparable high because a conventional engine with this configuration has a little bit more than 1 bar. This fact occurs since the $FMEP_c$ is related to the short intake stroke.

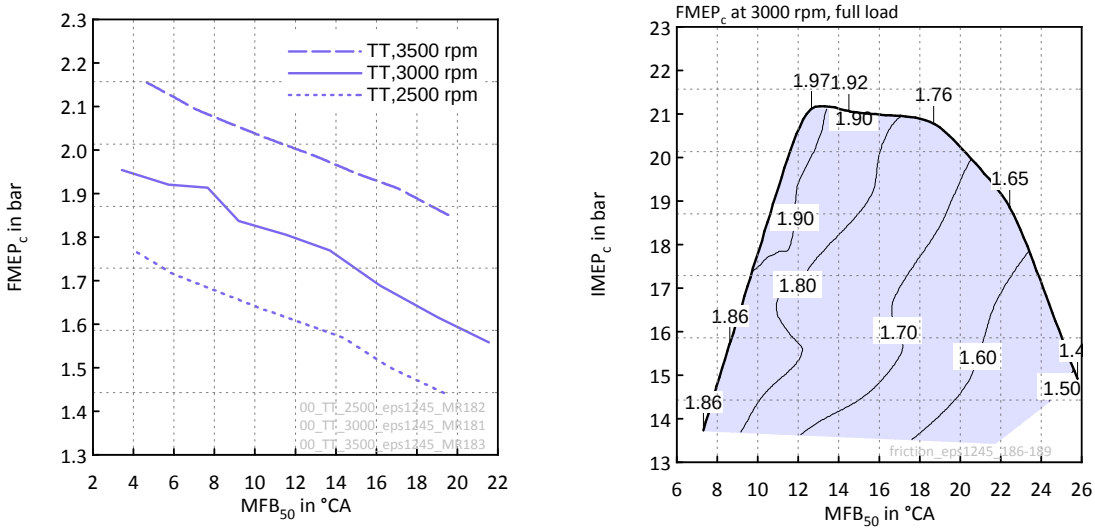

(a) $FMEP_c$ at different revolutions

(b) Friction map at 3000 rpm

Figure 7.42: Overview of the fraction of friction at the technology carrier

Noticeable are the $FMEP_c$ vs. MFB_{50} at the technology carrier - visual in figure 7.42a. At the technology carrier the friction becomes lower with later MFB_{50}.

Figure 7.42b shows the $FMEP_c$ at the supercharged operation. An $IMEP_c$ of 21 bar is reached at 400 mbar charging pressure. At this operating point and near to the point with the highest efficiency the $FMEP_c$ is about 2 bar.

8 Conclusion

With the aid of these measurements the behaviour of the extended expansion engine which was simulated in a previous project could be demonstrated. The simulated potential of the extended expansion engine compared to the reference engine was predicted by 7 %PT at 3000 rpm and an ε_c of 12.5. The real extended expansion engine shows an indicated efficiency of 44.4 % at an ε_c of 12.45. This results in a difference of efficiency of 6.1 %PT compared to the reference engine which delivered an efficiency of 38.3 %. Furthermore an $IMEP_c$ of nearly 13.8 bar is a noticeable value compared to conventional existing naturally aspirated engines. The results of measurements clearly show the potential of an extended expansion engine. For implementation of this concept in mass production a lot of challenges have to be met. Since the concept reaches these high efficiencies only at high load operating points the field of operation is limited - visual in figure 8.1.

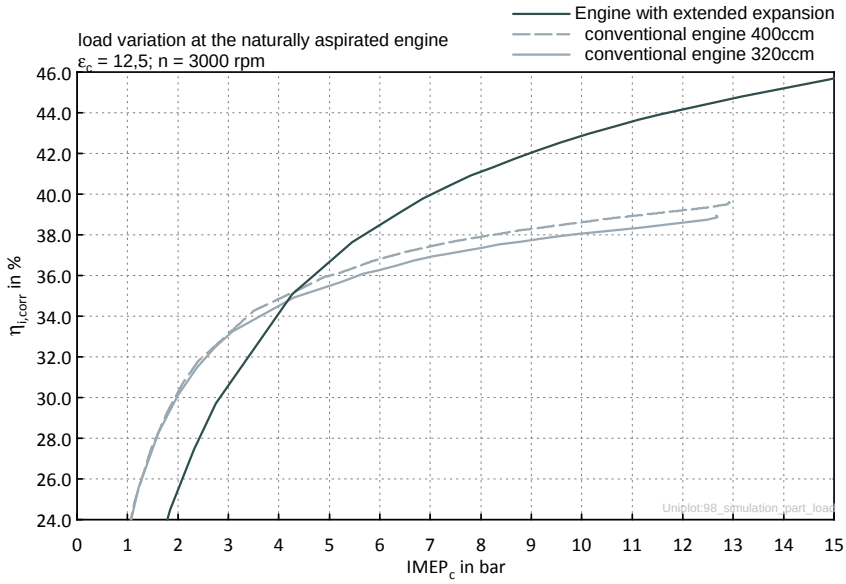

Figure 8.1: Conventional engine compared to extended expansion engine (Simulation) [24]

One imaginable concept could be in combination with hybridisation in order to ensure high load points within the whole operation. A use as primary propulsive power prove difficult. The engine might have at least a variable exhaust valve timing

in order to compensate the decreasing efficiency in low load regions as it is shown in figure 8.1. Furthermore a formidable task is to handle the mass balancing since the occurring oscillations are different to a conventional engine. Since the main target of this investigation was to show the indicated efficiency, the effective efficiency played a subordinate role.

The investigation also show the potential of the Miller strategy for low load operating points. The efficiency rose about 1%PT at 7.2 bar compared to the conventional approach.

The potential of an engine with Miller strategy in order to realise extended expansion could not be shown. The simulation of the Miller strategy showed that no advantage of efficiency can be reached with the used configuration and in particular with this valve train, which was also demonstrated. Due to the valve train and little valve lift of 3.3 mm a lot of losses occur during the gas exchange which was responsible for this low efficiency. The simulation showed that the reference engine equipped with a modified valve train and valve lift curve could reach an efficiency which is 3 %PT lower than the efficiency of the technology carrier.

The highest achievable efficiency with Miller strategy is lower than the efficiency which can be reached with the technology carrier. One reason is the non isentropic expansion and compression after the earlier intake valve closure which lead to rising temperatures at the actual compression. In order to avoid knocking the ε must be reduced which additionally reduces the efficiency.

Another reason for the lower efficiency at the Miller strategy compared to the extended expansion engine is the gas dynamics. At the extended expansion engine the piston covers only a little distance at BDC and due to the gas dynamics the charge mass and pressure rise within the cylinder without an increase in gas exchange work. Due to the earlier intake valve closure at the Miller strategy the gas dynamic effects can not be used.

Bibliography

[1] The international council on clean transportation. *EU CO 2 EMISSION STANDARDS FOR PASSENGER CARS AND LIGHT-COMMERCIAL VEHICLES*. http://theicct.org/sites/default/files/publications/, accessed on 07.07.2014.

[2] A.P. Roskilly R. Mikalsen, Y.D. Wang. *A comparison of Miller and Otto cycle natural gas engines for small scale CHP applications*. http://www.sciencedirect.com/science/article/pii/S0306261908002456, 2009.

[3] Matthias Kratzsch Michael Guenther Martin Scheidt, Christoph Brands. *Combined Miller/Atkinson strategy for future downsizing concepts*. MTZ worldwide, 2014.

[4] I. Vlaskos E. Codan. *Turbocharging medium speed diesel engines with extreme Miller timing*. http://www.temperaturblog.de/lehrbuch/Fehlerquellen.htm, accessed on 18.06.2014.

[5] Eberhard Schutting et. al. *Miller-and Atkinson-Cycle on a Tubrocharged Diesel Engine*. MTZ worldwide, 2007.

[6] Carl Nelson. *Variable stroke engine*. patent specification US 4517931 A, 21. Mai 1985.

[7] Honda. *Performing more work with less fuel-EXlink*. http://world.honda.com/powerproducts-technology/exlink/.

[8] Vaillant. *mikro-BHKW ecoPOWER 1.0*. http://www.vaillant.de/Produkte/Kraft-Waerme-Kopplung/Blockheizkraftwerke/, accessed on 07.07.2014.

[9] A. Abis S. Schmidt; R. Kirchberger P. Pertl, A. Trattner. *Expansion to Higher Efficiency - Investigations of the Atkinson Cycle in Small Combustion Engines*. *SAE*, 2012.

[10] Walter M. Austin. *Variable Stroke Internal Combustion Engine*. patent specification US 1 278 563, 10.09.1918.

[11] Gerhard Schmitz. *Five-stroke internal combustion engine*. patent specification US 6553977 B2, 29. April 2003.

[12] Ilmor Engineering. *5 Stroke Engine*. http://www.ilmor.co.uk/capabilities/5-stroke-engine?/, accessed on 19.06.2014.

[13] Gerhard Schmitz. *5-Takt Motor*. http://www.5-takt-motor.com/de/Entwicklung.html, accessed on 07.07.2014.

[14] Michael Wensing Markus Bauer. *Potenziale von Ottomotoren mit einem zusaetzlichen Expansionszylinder*. Ladungswechsel im Verbrennungsmotor, 5. MTZ Fachtagung, 2012.

[15] heat2power SARL. *Heat to power conversion benchmark*. http://www.heat2power.net/en contactus.php, accessed on 07.07.2014.

[16] John B. Heywood. *Internal Combustion engine fundamentals*. McGraw-Hill, Inc., 1988.

[17] Rudolf Pischinger et. al. *Thermodynamik der Verbrennungskraftmaschine*. Springer-Verlag, 2009.

[18] Charles Fayette Taylor. *The Internal Combustion Engine in Theory and Practice*. MIT press, 1986.

[19] Dipl.-Ing. Michael Gumpesberger et. al. *The Drive of the New F800*. MTZ, June 2006.

[20] BMW-Motorrad. *F 800 R*. http://www.bmw-motorrad.com, accessed on 12.06.2014.

[21] Hans Traenkler. *Taschenbuch der Messtechnik mit Schwerpunkt Sensortechnik*. Oldenbourg, 1992.

[22] Victor Wowk. *Machinery Vibrations-Measurement and Analysis*. McGraw Hill Inc., 1991.

[23] Andreas Witt. *Analyse der thermodynamischen Verluste eines Ottomotors unter den Randbedingungen variabler Steuerzeiten*. TU Graz, 1999.

[24] Georg Kellermayr. *Simulation eines 2-Zylindermotors mit langer Expansion*. Institute for internal combustion engines and thermodynamics, TU Graz, 2013.